High-Pressure Synthesis, Crystal Structure and Physical Properties of Gallium Oxonitride

Vom Fachbereich Material- und Geowissenschaften
der Technischen Universität Darmstadt
zur Erlangung des akademischen Grades
Doctor rerum naturalium
(Dr. rer. nat.)
genehmigte Dissertation von

Carmen Elena Zvorişte
aus Iaşi, România

Berichter: Prof. Dr. Ralf Riedel
Mitbericht: Prof. Dr. Wolfgang Donner

Tag der Einreichung: 14.12.2010
Tag der mündlichen Prüfung: 09.03.2011

Darmstadt 2011
D17

Abstract

This thesis is concerned with the synthesis and properties of the high-pressure, high-temperature (HP/HT) phase of gallium oxonitride, which has a spinel-type structure. Since this material is an analogue of γ-alon (spinel-aluminium oxonitride), which is known to be an important material with a wide range of applications, the spinel-structured gallium oxonitride is an attractive material with the potential for tailoring its composition and tuning its electronic properties, i.e. for optoelectronic applications. The research reported in this thesis is focused on two main aspects: firstly the HP/HT synthesis of the spinel phase using different starting materials and employing different high-pressure devices, and secondly a detailed characterisation of the HP material.

For the synthesis of the spinel-structured gallium oxonitride, different starting materials have been used. For a systematic investigation of the pressure-temperature relation in the Ga-O-N system, different molar ratios of the w-GaN and β-Ga_2O_3 were tested for the HP/HT syntheses. Large-volume presses provided higher amounts of samples for further investigations of the spinel phase. Diamond anvil cells (DACs) loaded with same powder mixtures provided valuable insights for the formation of the spinel phase.

A different starting material also employed for the HP/HT syntheses was a precursor-derived gallium oxonitride (GaON) ceramic. In order to obtain the GaON ceramic, gallium tris(t-butoxide)-dimethylamine adduct, $Ga(O^tBu)_3.HNMe_2$, was synthesised and heat treated in an ammonia flow. The obtained ceramics were x-ray amorphous and stable up to around 1000 K. The HP/HT experiments using the (GaON) ceramics revealed a phase transition from the amorphous phase to a spinel-structured gallium oxonitride at 0.7 GPa and 1600 K. The use of the single source precursor GaON resulted in the formation of the spinel phase at much lower pressures than in the syntheses performed using different mixtures of GaN and Ga_2O_3. Hence, a piston cylinder press has been used to provide larger amounts of the spinel phase from the (GaON) ceramic for different *ex situ* investigations.

A third starting material for the syntheses of the spinel gallium oxonitride was metastable cubic γ-Ga_2O_3. When loaded in a DAC with nitrogen gas under pressure, the oxide reacted with nitrogen, forming the spinel-type gallium oxonitride at pressures of 4.2 GPa and temperatures between 1500 and 1800 K.

The second part of this thesis deals with the structural characterisation of the spinel gallium oxonitride and an investigation of its properties. A single crystal structure investigation of the HP/HT phase of gallium oxonitride has revealed a spinel structure within the space group $Fd\bar{3}m$ (No. 227) with the lattice parameter a_0 = 8.2782 Å. Electron Energy-Loss Spectroscopy (EELS) has enabled the relative amounts of nitrogen and oxygen to be quantified for structural refinement. The structure analyses revealed that for the spinel phase, the composition is $Ga_{2.79}\square_{0.21}(O_{3.05}N_{0.76}\square_{0.19})$ (with □ = vacancy) with vacancies on both anionic and cationic sites.

The elasto-mechanical properties investigated for the spinel-structured gallium oxonitride yielded a bulk modulus K = 216(7) GPa, an estimated indentation hardness H = 10 GPa and a reduced elastic modulus E_r = 130 GPa. The thermal behaviour of the HP/HT phase was also studied. The powder x-ray diffraction patterns showed that the spinel phase is stable up to 1170 K. No decomposition or cell distortions were found up to this temperature. The thermal expansion coefficient was shown to increase from 1.3×10^{-6} K^{-1} at 300 K to 4.7×10^{-6} K^{-1} at 1100 K.

Soft X-ray Spectroscopy (SXS) supported by *ab initio* DFT calculations has been applied to study the electronic structure and band gap of the spinel-type gallium oxonitride. The HP phase was found to have a direct band gap of 4.39 ± 0.10 eV, which confirms that the system has a potential application in optoelectronic devices.

Zusammenfassung

Diese Arbeit behandelt die Synthese und Eigenschaften der Hochdruck- und Hochtemperaturphase (HD/HT-Phase) von Galliumoxonitrid mit Spinellstruktur (Ga_3O_3N). Dieses Material ist ein Analogon zu γ-Alon (Spinellaluminiumoxonitrid) , welches für eine Reihe von Anwendungen bekannt ist. Galliumoxonitrid mit Spinellstruktur ist daher ein attraktives Material mit der Möglichkeit, die elementare Zusammensetzung anzupassen und die elektronischen Eigenschaften zum Beispiel für optoelektronische Anwendungen zu optimieren. Die Forschung im Umfang dieser Arbeit konzentriert sich auf zwei Hauptaspekte: Erstens die Synthese der HD/HT-Spinellphase unter Verwendung verschiedener Ausgangsstoffe und unterschiedlichen Hochtemperaturapparaturen und zweitens einer detaillierten Charakterisierung der HD-Phase.

Zur Synthese von Galliumoxonitrid mit Spinellstruktur wurden unterschiedliche Ausgangsstoffe verwendet. Für die systematische Untersuchung des Zusammenhanges zwischen Druck und Temperatur bei der Synthese von Verbindungen im Ga-O-N-System wurden verschiedene molare Verhältnisse von w-GaN und β-Ga_2O_3 als Ausgangsstoffe eingesetzt. Druckzellen mit großem Probenvolumen lieferten eine größere Menge an Proben für weitere Untersuchungen der Spinellphase. Mit gleichen Pulvermischungen geladene Diamantstempelzellen (DACn) erbrachten wertvolle Einblicke in die Entstehung der Spinellphase.

Ein anderer Ausgangsstoff für die HD/HP-Synthese war eine als Vorstufe entwickelte Galliumoxonitridkeramik (GaON). Um die (GaON)-Keramik zu erhalten wurde das Addukt Galliumtris(t-butoxid)dimethylamin, $Ga(O^tBu)_3.HNMe_2$, synthetisiert und in einem Ammoniakstorm hitzebehandelt. Die erhaltenen Keramiken waren amorph mit nanokristallinen Einschlüssen und stabil bis ca. 1000 K. Die HD/HT Experimente unter Verwendung der (GaON)-Keramiken zeigten einen Phasenübergang von der amorphen zur Spinellphase von Galliumoxonitrid bei 0,7 GPa und 1600 K. Unter Verwendung der Vorstufe GaON als einziger Ausgangsstoff bildete sich die Spinellstruktur bei deutlich niedrigeren Drücken als bei der Synthese unter Verwendung verschiedener Mischungen aus GaN und Ga_2O_3. Um größere Mengen

der Spinellphase aus der (GaON)-Keramik für unterschiedliche ex situ Untersuchungen zu erhalten, wurde eine Zylinderkolbenpresse verwendet.

Ein dritter Ausgangsstoff für die Spinellgalliumoxonitridsynthese war das metastabile kubische γ-Ga_2O_3. Beim Laden in die DAC mit Stickstoff unter Druck reagierte das Oxid mit Stickstoff, sodass sich Galliumoxonitrid mit Spinellstruktur bei einem Druck von 4.2 GPa und Temperaturen zwischen 1500 und 1800 K bildete.

Der Zweite Teil dieser Arbeit behandelt die Strukturcharakterisierung von Spinellgalliumoxonitrid und die Untersuchung seiner Eigenschaften. Eine Einkristallstrukturanalyse ergab das Vorliegen einer Spinellstruktur der Raumgruppe $Fd\bar{3}m$ (No. 227) mit dem Gitterparameter a_0 = 8.2782 Å. Elektronenenergieverlustspektroskopie (EELS) ermöglichte eine Quantifizierung der relativen Mengen an Stickstoff und Sauerstoff für die Strukturfeinanalyse. Die Strukturanalyse ergab die Zusammensetzung $Ga_{2.79}\square_{0.21}(O_{3.05}N_{0.76}\square_{0.19})$ (mit □ = Leerstelle) mit Leerstellen auf der anionischen und kationischen Seite.

Die für Galliumoxonitrid mit Spinellstruktur untersuchten elastischen und mechanischen Eigenschaften ergaben ein Kompressionsmodul K = 216(7) GPa, eine Eindruckshärte H = 10 GPa und ein reduziertes Elastizitätsmodul E_r = 130 GPa. Das thermische Verhalten der HD/HT-Pahse wurde ebenfalls untersucht. Die Diffraktogramme nach dem Debye-Scherrer-Verfahren zeigten, dass die Spinellphase bis zu 1170 K stabil ist. Bis zu dieser Temperatur wurde keine Zelldistorsion order Zersetzung gefunden. Es konnte gezeigt werden, dass der thermische Ausdehnungskoeffizient von 1.3×10^{-6} K^{-1} bei 300 K auf 4.7×10^{-6} K^{-1} bei 1100 K ansteigt.

Die elektronische Struktur und die Bandlücken des Galliumoxonitrides mit Spinellstruktur wurden mit weicher Röntgenspektroskopie (SXS) untersucht, untermauert mit *ab initio* DFT-Rechnungen. In der HD-Phase wurde eine direkte Bandlücke von 4.39 ± 0.10 eV ermittelt, womit dieses System ein hohes Potential für Anwendungen in optoelektronischen Bauteilen aufweist.

Contents

List of Figures

List of Tables

1 Introduction and motivation

1.1 General remarks

Materials science is to an extensive part concerned with the relationship between the structure and properties of materials. Experience shows that the properties and phenomena associated with a material are intimately related to its composition and structure at all levels, including which atoms are present and how the atoms are arranged in the material, and that this structure is the result of synthesis and processing. The final material is designed to perform a given task and must be both economical and safe.

Materials science unites applications from many scientific disciplines such as chemistry, physics, biology, geochemistry and geophysics, which all contribute to the development of new materials. New materials, new structures, and new manufacturing tools have enabled the development of novel high performance devices. In other words it can be said that the field of material science and engineering is defined by the strong interrelationship between synthesis/processing, structure/composition, properties and performance.

This thesis deals with the synthesis and properties of gallium oxonitride, and in order to put this work into context, it is informative to learn about other examples of technologically interesting materials. In the remainder of Section 1.1, an overview of some different examples of related compounds is provided, such as oxonitride compounds, nitride semiconductors used in electronic and optoelectronic devices, and high-pressure materials.

By understanding more about the research area from which this project has grown, the motivation which has driven this project will become clear.

1.1.1 The oxonitride family

The oxonitrides constitute a vast class of solids which was shown to provide new or improved properties to those of oxides or nitrides.

Oxygen and nitrogen have similar chemical, structural, and electronic properties such as polarizability, electronegativity [1], coordination numbers and ionic radii [2], form similar structure types when combined with cations, and substitute for each other in the same sites to form solid solutions. Oxonitrides have been reported with different structures, such as perovskites [3], spinels [4], pyrochlores [5], baddeleyites [6], scheelites [7], apatites [8], etc., often showing nitrogen non-stoichiometries and in some cases wide ranges of N/O solid solutions. By changing the N/O ratio it is possible to change the oxidation state of the cations modifying the physical properties. Nitrogen is less electronegative than oxygen so the optical gap between the valence band and the conduction band decreases as oxygen is substituted by nitrogen. On the other hand N^{3-} ions have a higher electrical charge which leads to a larger crystal field splitting in nitride materials.

The nitride-based materials are relatively less explored with respect to the oxides due to their lower stability. The bond energy of a N_2 molecule is about twice that of O_2 (945 kJ mol^{-1} for N≡N and 498 kJ mol^{-1} for O=O) [9]. Another main factor which makes the energy of formation for nitrides smaller than for oxides is that the energy to form a N^{3-} ion is higher than that for oxides to form oxygen anions (1736 kJ mol^{-1} for $N \rightarrow N^{3-}$ compared with 601 kJ mol^{-1} for $O \rightarrow O^{2-}$) [10].

The differences between the two anions are reflected in the variation of properties of oxonitride compounds, for example in the nitridation of oxides, the photocatalytical activity is shifted towards visible light [11, 12]. The difference is also highlighted in the colour of the inorganic pigments, as the perovskites $Ca_{1-x}La_xTaO_{2-x}N_{1+x}$ can be tuned by adjusting the Ca/La and O/N ratio [13]. In addition, the magnetoresistance can be varied in the europium oxonitride perovskites $EuMO_{2-x}N_{1+x}$ (M = Nb, W) by adjusting the nitrogen content [14, 15]. Another example is in the emission wavelength of the phosphor Eu^{2+}-doped $SrSi_2O_2N_2$ which is shifted to low energy with respect to oxide based luminescent materials [16]. Hence, the design of new oxonitrides is a useful tool for exploring and/or modifying a wide variety of physical properties, either by synthesizing completely new phases or solid solutions.

A significant breakthrough in materials science and industry was the discovery of the spinel-type aluminium oxynitride (γ-AlON) in the 1970s [17]. Using a constant anion model, which assumes a constant number of 32 anions in a spinel unit cell (space group $Fd\bar{3}m$, No. 227), the γ-AlON is described by the following formula: $Al_{(64+x)/3}\square_{(8-x)/3}O_{(32-x)}N_x$ (with □=vacancy) [18].

After the fabrication of a translucent AlON material in 1979 [17], intense world-wide research was undertaken making the material a widespread commercial product. Subsequently, the Raytheon Company further developed AlON into a highly transparent material (ALON^{TM}). High optical transparency, high hardness and oxidation resistance up to high-temperatures are only few of the properties which made the AlON materials extensively and continually investigated over the years [19, 20].

This product has found many applications including military aircraft and missile domes, transparent armour, IR windows, hyper-hemispherical domes, laser windows, military aircraft lenses, semi-conductor processing applications, and scanner windows (point of sale (POS) windows) [19-21]. Amorphous aluminium oxynitride (AlON) films possess the unique properties of high dielectric strength, high resistivity, high decomposition temperature, chemical inertness and good thermal conductivity. These properties make these films encouraging for use in manufacturing high energy density capacitors for pulse power and other extreme environment applications [22].

Another example of oxonitride materials which have been of great interest for the researchers and engineers are the sialon phases in the Si-Al-O-N system. They are derived from silicon nitrides and oxonitrides by simultaneous replacement of silicon and nitrogen by aluminium and oxygen respectively. Their structure is built up from tetrahedral [(Si, Al)$(O,N)_4$] structural units [23]. The metallurgical applications of some of the sialons for holding and conveying molten metals are of great importance. The sialon ceramics are being explored for their thermal, mechanical, chemical and electrical properties [23]. A spinel-structured sialon was synthesized under high-pressure, high-temperature for which a hardness value of 27.5 GPa was determined [24]. This result qualifies these materials as good candidates for cutting or abrasive applications.

1.1.2 Nitrogen based semiconductors

Another example of a scientific field in which the application of a material has led to a crucial breakthrough is in the field of electronic and optoelectronic devices. Research advances in group III-nitride semiconductor materials have led to an exponential increase in activity directed towards electronic and optoelectronic applications.

Semiconductor materials are defined as insulators at absolute zero temperature but conduct electricity at room temperature. They are characterised by an energy band gap between the valence and conduction bands, which can be direct (when the minimal energy state in the conduction band has the same momentum as the maximal energy state in the valence band) or indirect (the maximum and minimum have different momentum). The direct gap semiconductors are particularly important in optoelectronics because they are much more efficient as light emitters than the indirect gap materials. Another important characteristic of semiconductor materials is the width of the band gap. Wide band gap materials are semiconductors with electronic band gaps larger then one or two electron Volts (eV). These materials allow the operation of power devices at high-temperatures and give lower thermal noise to low power devices at room temperature. In optoelectronic devices, the wide band gap materials can be used to create light throughout the visible spectrum (390 – 750 nm).

Because of the application of semiconductors in devices such as transistors (and therefore computers), light emitting diodes (LEDs), laser diodes, photodiodes, the interest in improving specific properties of these materials is an important field of study in materials science.

One of the most studied and used semiconductors for optical devices is gallium nitride which is a wide direct band gap semiconductor [25]. The early work of Pankove and co-workers in the 1970s yielded a metal-insulator-semiconductor GaN light-emitting diode (LED). In the late 1980s and early 1990s, Akasaki and co-workers and Nakamura and co-workers developed the p-type doping in GaN and demonstrated the use of nitride-based LEDs at visible wavelengths. These advances were followed by the successful fabrication and commercialization of nitride blue laser diodes. Another potentially large application of GaN is in the fabrication of blue laser diodes (LDs) for high-density optical storage systems. Various optoelectronic devices have been

developed using GaN and have been fabricated by depositing GaN films on different substrates. Single crystals of GaN are the ideal substrates for homoepitaxial growth of high quality GaN films, as any residual strain introduced by a different substrate is thereby avoided.

The AlN-GaN-InN system of material semiconductors has been extensively studied for fabricating light emitting devices for wavelengths shorter than green light (below 510 nm). A feature of LEDs based on nitrides is the possibility of fabricating heterostructures[1] with large band discontinuities using AlGaN and AlInGaN. These structures are used in heterostructural field effect transistors (HFETs), which can be driven at large current densities [26]. A metal-oxide-semiconductor field effect transistor (MOSFET) based on β-Ga_2O_3/GaN has also been reported [27].

Another material used in optical devices is ZnSe, which is widely recognised as being an excellent material for fabricating blue-green LEDs and laser diodes. It is used as an infrared optical material with a wide transmission wavelength range (450–21500 nm) [28]. SiC and diamond are also important wide band gap semiconductors, SiC p-n junctions being used for fabricating blue LEDs which operate in the 460-470 nm wavelength range. One drawback for SiC LEDs is the poor emissivity efficiency[2] which is more than two orders of magnitude less than that of GaN [29].

Nitride semiconductors are characterized by a relatively low mobility of p-type carriers. In addition, the typical concentration of holes is rather low in all of the p-type layers obtained [30]. At present, the low conductivity of p-type materials is one of the limiting factors in the technology of nitride devices. GaN is unstable to decomposition at high-temperatures, which led to high-pressure methods to be used in order to provide high-quality crystalline GaN substrates [31].

[1] A heterostructure is defined by the combination of multiple interfaces that occurs between two layers or regions of different crystalline semiconductors.
[2] The emissivity is a measure of a material's ability to absorb and radiate energy.

1.1.3 High-pressure materials

Pressure, as a thermodynamic factor, can modify the structure and properties of a substance in different ways. As a result new materials or materials with improved specific properties are obtained, such as mechanical (hard materials), electrical and electronic (superconductors, wide band gap semiconductors) properties.

The search for new materials with high hardness is of fundamental and technological interest, covering a large area in high-pressure research [32-37].
After synthetic diamond was commercialilized [38, 39], the research to produce new *hard materials* started and intensified in the following years. Diamond is a very important material being the hardest material known, having the highest refraction index known, with both, high thermal conductivity and very low electrical conductivity. All these outstanding properties make diamond an irreplaceable material for grinding tools, for drilling rocks for oil wells, cutting concrete, polishing stones and machining [40]. However, diamond has a major drawback in that it reacts with iron and cannot be used for machining steel. This has prompted the synthesis of a second superhard[3] material, cubic boron nitride (c-BN) [41], whose structure is derived from that of diamond with half the carbon atoms being replaced by boron and the other half by nitrogen atoms. Even though the hardness of c-BN is half of the value of diamond, it does not react with iron and hence it can be used for machining steel. However, its synthesis is more difficult than for diamond, and it has not been possible to prepare large crystals.

[3] Superhard materials are materials with a Vickers hardness exceeding 40 GPa [40].

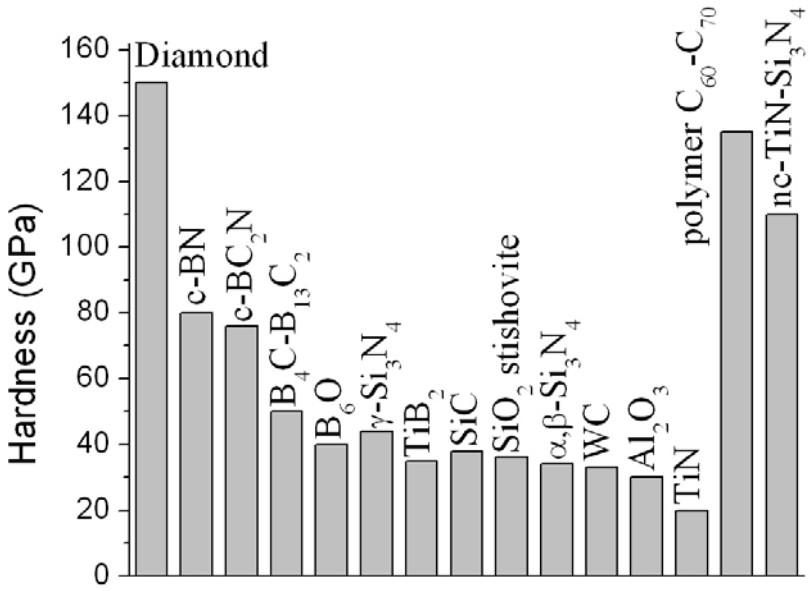

Figure 1.1 Various materials with the corresponding hardness values (graph made after [33].

Up to now the search for new hard materials has led to the discovery of novel compounds with hardness approaching the one of diamond. In Figure 1.1 some examples of known hard materials are given. BC_2N and the spinel-structured γ phase of Si_3N_4 are newly-discovered superhard and high-hardness materials [42, 43] which are under development for abrasive applications. The high hardness oxide family is represented by rutile-structured SiO_2 (stishovite) [44], B_6O [45], and cotunnite-type TiO_2[46] (hardness 38 GPa, value not shown in the Figure 1.1). A promising hard material is a highly dense form of carbon obtained by polymerization of C_{60}/C_{70} fullerites at high-pressure and high-temperature [35].

High-pressure synthesis strategies have long been exploited for growth of the special class of *semiconductor materials* for optical devices. Single-crystal growth of specifically p- and n-doped c-BN is now achieved in a large-volume-press environment and is being developed for high-temperature semiconductor applications [47]. Large, strain-free single crystals of diamonds for x-ray monochromators have been obtained in a similar way [48]. Single crystal AlN, a substrate material with high thermal conductivity, has also been obtained by high-pressure crystal growth [49].

High-pressure studies gave rise to a new family of wide band gap optoelectronic group-IV semiconductor nitrides. High-pressure syntheses gave a spinel-type Ge_3N_4 with a calculated direct band gap of 3.2 eV [43, 50]. Theoretical and experimental studies have indicated that $(SiGe)_3N_4$ solids form a new family of optoelectronic materials with applications over a wide range of visible and ultraviolet wavelengths [51, 52].

A potential drawback of materials prepared via high-pressure techniques is that they are usually obtained as powders or single crystals rather than as thin films. However, research has shown that thin films of useful high-density materials can also be obtained metastably, using chemical and physical deposition techniques such as Chemical Vapour Deposition (CVD), Molecular Beam Epitaxy (MBE) or laser ablation. Crystalline diamond films have been grown by CVD from hydrocarbon-containing precursors [53], while GaN and other II-VI semiconductors have been successfully deposited from molecular precursors [54].

In summary, even though the AlN-Al_2O_3 system has been the subject of an intense study due to its outstanding properties, and consequently wide industrial application range, one of its analogous systems, GaN-Ga_2O_3, has been scarcely investigated (see Section 1.3.3). This lack of study in the case of the Ga-O-N system has led to this intensive and systematic study on the gallium oxonitride system, which is the subject of this thesis. The high-pressure phase of gallium oxonitride has been predicted to have a considerable hardness and a direct band gap with a potential application in electronic or optoelectronic devices (see Section 1.3.3). As discussed above, by varying the relative concentration of nitrogen and oxygen in an oxonitride, the energy gap between the valance and conduction band can be controllably tuned in between the ones of the nitride and oxide. Hence, the mechanical and electronic properties have been experimentally investigated and reported in this thesis, thereby complementing the theoretical reports above. The reasons mentioned above and the fact that GaN, an end member of the gallium-oxide-nitride system, is extensively used in electronic and optoelectronic devices, have resulted in increased research on the gallium oxonitride phases in recent years.

1.2 Gallium-oxygen-nitrogen system – a literature review

This thesis is concerned mainly with the synthesis and characterisation of the recently obtained spinel-structured gallium oxonitride. In order to introduce the formation and properties of the oxonitride, the two end members in the Ga-O-N system, gallium nitride and gallium oxide, are now described.

Stable and metastable polymorphs of these compounds will be reviewed, with special attention to the crystal structure and the properties of these compounds. In Section 1.2.3, a literature review of the gallium oxonitride phases will be given. This section provides the starting point for the work performed and reported in this thesis. A good knowledge and understanding of the starting materials is extremely helpful for appreciating the relevance and importance of this study.

1.2.1 Gallium oxide, Ga_2O_3

The oxides of group-III elements (Al, Ga, In) are important compounds with different applications in fields such as structural ceramics, catalysts, and electronic materials [55]. Aluminium oxide, known also as alumina, exists in many metastable polymorphs, besides the thermodynamically stable α-Al_2O_3, corundum form. A detailed review of the crystal structure of transition sequences of alumina polymorphs can be found elsewhere [56]. Because of their fine particle size, high surface area, and catalytic activity of their surfaces, the transition aluminas (especially the γ form) find applications in industry as adsorbents, catalysts or catalyst carriers, coatings, and soft abrasives. Boron oxide (B_2O_3) is also an important industrial material, due to its excellent properties, such as hardness, isolation, low heat expansion, and high refractive index. Boron oxide has found applications as a fluxing agent for glass and enamels, as a starting material for synthesising boron carbide, as an additive used in glass bibres (optical fibres) and also in the production of borosilicate glass [57].

The stable polymorph of gallium oxide is the monoclinic-structured, β-Ga_2O_3 [58, 59]. The space group attributed to β-Ga_2O_3 is *C*2/*m* (No. 12) with two crystallographically non-equivalent positions of the gallium atoms, with tetrahedral and octahedral

arrangements of the oxygen atoms around the gallium atom, and three non-equivalent oxygen ions in the unit cell. The oxygen ions are arranged in a distorted cubic close-packed array (see Figure 1.2).

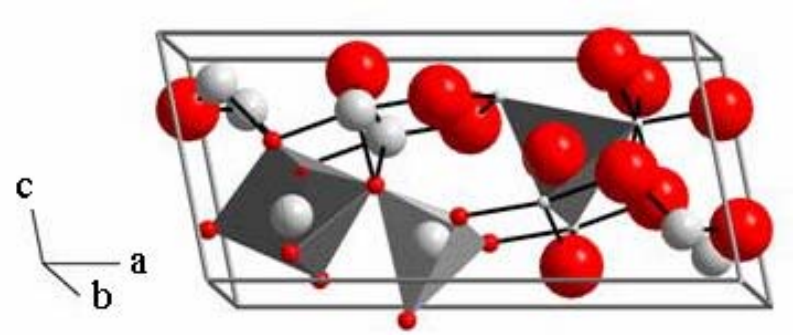

Figure 1.2 Crystal structure of β-Ga_2O_3. The dark grey balls represent the oxygen ions, and the light coloured balls represent the two types of gallium cations, which are octahedrally and tetrahedrally coordinated.

This compound is known to be a wide band gap semiconductor (E_g = 4.9 eV) and has a widely variable conductivity, depending upon the preparation conditions [60]. Hence, β-Ga_2O_3 has found applications as optical windows [61], as a magnetic memory material [62], high-temperature chemical sensors [63], and in dielectric thin films [64]. In recent years, intensive efforts have been made for the study of low-dimensional Ga_2O_3 materials, such as β-Ga_2O_3 nanowires [65].

The room pressure polymorphs of gallium oxide are the β, α, γ, δ, and ϵ phases (see Figure 1.3). The high-temperature phases α, γ, δ, and ϵ are metastable and known to transform at different temperatures and humidity conditions into the stable phase, β-Ga_2O_3 [66].

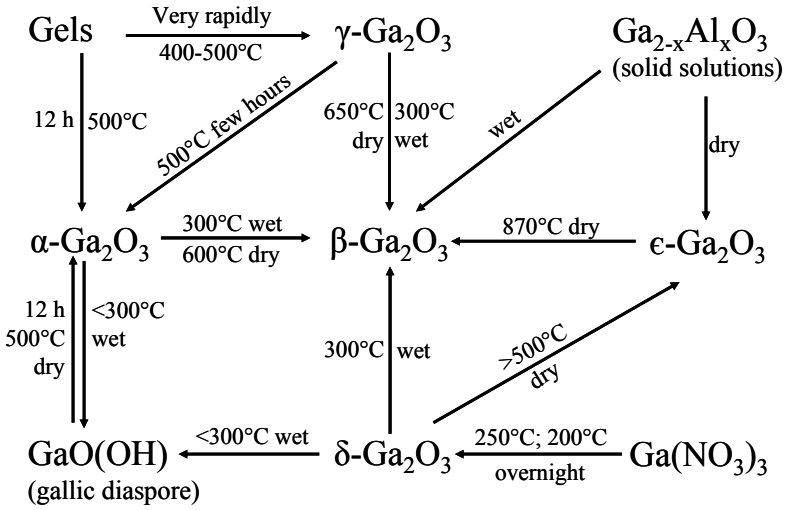

Figure 1.3 Schematic illustration showing the transformation relationships among the forms of gallia and its hydrates (after [66]).

γ-Ga_2O_3 is a mesoporous metastable compound which was synthesized by calcinations of a gallia gel [67-69], transforming into β-Ga_2O_3 at elevated temperatures. Two different structures have been reported for γ-Ga_2O_3, depending on the reaction paths. Roy *et al.* have reported a cubic structure (space group $Ia\bar{3}$, No. 206, a = 10 Å) of γ-Ga_2O_3, prepared by dissolving metallic gallium into HNO_3 and evaporating until dry [66]. The residue was heat treated to 550 K and then maintained at 500 K for 12 hours. A spinel-type γ-Ga_2O_3 (space group $Fd\bar{3}m$, No. 227, a_0 = 8.22 Å and a_0 = 8.30 Å, respectively) has been also reported having been synthesised either from fresh gels of gallium nitrate [68] or gallium hydroxide [69] and after a heat treatment at 773 K and 700 K, respectively.

The cubic polymorph is of great interest because of its catalyst efficiency, having a high surface area [68]. In fact, gallium-containing microporous materials showed good catalytic properties in processes such as cyclization of hydrocarbons, methanol conversion, and NO reduction [70-73]. The structure of γ-Ga_2O_3 is considered to be very similar to the one of γ-Al_2O_3, which is an important nanosized material that has been intensively studied from preparation, properties, and applications points of views [74]. Hence, the interest in γ-Ga_2O_3 has increased dramatically over the last years.

The high-temperature α-Ga_2O_3 is a metastable phase, but when synthesised under pressure it becomes stable. The β-α phase transition has been reported to occur at several different pressures, which has led to a big controversy in the field. Tu *et al.*

reported a β-α transition at 13.3 GPa [75]. Careful study of the diffraction patterns indicates that the diffraction lines of the starting material "α-Ga_2O_3" are really from the β phase rather than the α phase. Another study done by Lipinska-Kalita *et al.* reported that the phase transition occurs at 6 GPa [76]. In this case nanocrystalline β-Ga_2O_3 particles were embedded in a silica glass matrix and compressed in a DAC. What was not taken into account here is that the silica glass itself has large structural changes in this pressure range [77, 78], which casts doubt on the reported structural changes taking place at 6 GPa in the β-Ga_2O_3. An intensive x-ray diffraction and Raman study of the monoclinic phase under pressure has shown that the β-to-α phase transition to occur at pressures above 20-22 GPa [79].

Thin films of α-Ga_2O_3 grown by spray pyrolysis on borosilicate glasses were reported to have an optical band gap of 2.41 eV, much narrower than the one for β-Ga_2O_3 [80]. Both ambient and high-pressure polymorphs of gallium oxide are under continuous investigation due to their interesting and diverse properties and applications. It is also of great interest to study the pressure-induced phase transitions among the Ga_2O_3 polymorphs in order to determine stable and metastable phases and to evaluate their properties under different synthesis conditions.

1.2.2 Gallium nitride, GaN

The group-III nitrides (AlN, GaN, InN, and their alloys) have attracted much attention in recent years due to their potential in electronic and optoelectronic device technology [81-83]. Intensive studies have been done to characterise not only electronic and optoelectronic properties, but also their structural and mechanical properties [84]. Since the extensive use of GaN in electronic and optoelectronic devices has already been reviewed in Section 1.1.2, a more comprehensive physical description of this important compound is provided in this section.

At ambient pressure, GaN crystallises in a hexagonal (wurtzite) structure with the space group $P6_3mc$ (No. 186) and lattice constant a = 3.19 Å and c/a = 1.627 [85]. The structure contains two gallium cations and two nitrogen anions per unit cell, with all gallium cations tetrahedrically coordinated by nitrogen ions (see Figure 1.4).

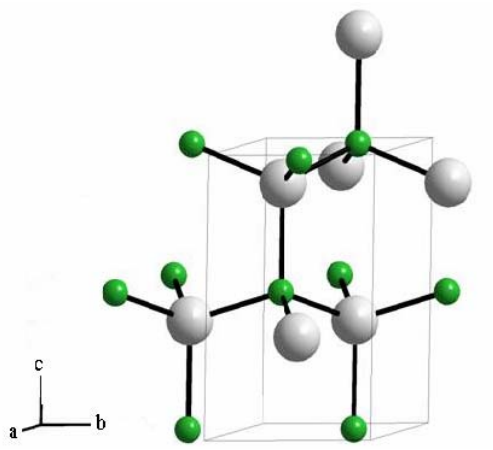

Figure 1.4 Crystal structure of w-GaN. Gallium cations (light grey) are tetrahedrically coordinated by the nitrogen (dark grey).

At non-ambient conditions, two other polymorphs of GaN are known with a zincblende and a rocksalt-type structure, respectively. A cubic zincblende phase of gallium nitride has been grown using organometallic vapour-phase epitaxy, molecular beam epitaxy, and radio-frequency magnetron sputtering processes [86-89]. A pseudomorphic stabilisation of the rocksalt phase of GaN within TiN/GaN multilayers has also been reported [90]. Nanoparticles of GaN with the rocksalt crystal structure have been synthesized using solvothermal techniques but other possible compounds of gallium were also observed to be present [91].

The stable high-pressure GaN polymorph exhibits a rocksalt-type structure. The pressure-induced phase transition from the wurtzite to the rocksalt structure has been reported at pressures of 37 GPa [92], 47-50 GPa [93] and 52.2 GPa [94]. This huge range of reported transition pressures has been attributed to the different probing techniques used in each case [94]. As well as x-ray diffraction techniques (*in-house* [94]or synchrotron facility [92]) x-ray absorption spectroscopy has also been used [93]. Large discrepancies in the measured transition pressure have also been reported for the pressure induced transition in AlN [95] and GaAs [96]. These discrepancies are also thought to arise from the difference in probing techniques used. In the case of GaN, theoretical studies predict that the pressure induced phase transition should occur between 42.9 and 51.8 GPa [97-99] which is in acceptable agreement with the experiments. At much higher pressures (above 87 GPa), a phase transition has predicted into the metallic β-Sn structure [100].

Various optoelectronic devices have been developed using GaN and have been fabricated by deposing GaN films on different substrates. Due to the residual strain introduced by different substrates, single crystals of GaN are ideal substrates for the homoepitaxial growth of high quality GaN films. Different techniques have been reported for the growth of GaN, such as melting using the Czochralski and Bridgman methods [101], at low pressures and temperatures [102], the hydrothermal method [103]. Polymer precursors [104] or molecular precursors such as $Ga_2(NMe_2)_6$ and $[H_2GaNH_2]_3$ [105-107] have also been used for GaN syntheses for ceramic applications or catalytic applications.

1.2.3 Gallium oxonitride phases

The gallium oxonitride system has been scarcely investigated in the last 40 years. Over that time, gallium oxonitride phases have been reported in thin films, ceramics, and as high-pressure and high-temperature phases. In this section a review of gallium oxonitride system is provided.

The first gallium oxonitride phase was reported by Verdier *et al*. in 1976 [108]. In their attempt to synthesise GaN by reacting ammonia with gallium oxide, an oxonitride side product was observed and identified as $Ga_{1-x/3}O_xN_{1-x}$ with a zincblende-type structure. The powder x-ray diffraction pattern was fitted with a zincblende-type structure with a cell parameter of 5.50 Å. The first attempt to deliberately obtain gallium oxonitride films was by Grekov and Demidov in 1979 [109]. The films were obtained by thermal decomposition of $GaCl_3{\cdot}NH_3$ at controlled humidity. The layers were found to be amorphous with variable N/O ratios.

In the following years, the interest in growing and characterising gallium oxonitride films intensified. GaO_xN_y films were deposited on GaAs surfaces by thermal decomposition of the ammonia (NH_3)-gallium trisbromide ($GaBr_3$) complex [110-112]. By varying the N/O ratio properties such as resistivity, adherence and surface state density were enhanced [111, 112]. The oxidation of GaN films grown on different substrates showed the formation of isolated islands of a gallium oxonitride [113, 114]. The Low-Energy Electron Diffraction (LEED) patterns before and after the oxidation indicated a hexagonal structure. Therefore, the oxonitride formed is in fact an oxygen

doped gallium nitride system, labelled as GaO_xN_y. Wolter *et al.* suggested a cubic structure for the oxonitride found, based on the similarity with the spinel γ-$Al_{(x+2)}N_{3x}O_{(3-3x)}$ seen in a diffraction pattern taken only from one orientation [114]. Also during the oxidation of GaN films, Puchinger *et al.* have found small oxidised areas on the surface and identified the phase as being a cubic gallium oxonitride with the composition $Ga_{2.8}O_{3.5}N_{0.5}$ and a cell parameter of 8.20 Å [115].

Gallium oxonitride has also been reported to form by nitridation of $NiGa_2O_4$ prepared via a citrate method [116]. The XRD pattern revealed a similar structure for the oxonitride with gallium nitride with three extra small reflections, which can be actually explained by oxygen incorporation. Gallium oxonitride film sensors have been prepared and investigated. A high response to ethanol was detected in comparison to GaN. Subsequently the same research group identified the crystal structure of gallium oxonitride synthesised from $NiGa_2O_4$ as a carborundum II (B6) type structure or 6H-SiC [117]. This is a hexagonal type structure with the cell parameter *c* three times larger than for a wurtzite structure. It can also be described as a coexistence of wurtzite and zincblende phases, a coexistence which was also shown to be present in the case of GaN [118, 119].

There is no systematic structural and/or compositional investigation of any of the gallium oxonitride phases discussed to this point. Nevertheless, the importance of gallium oxonitride films for industrial applications has been made clear.

Even the definition of what constitutes gallium oxonitride is not clear from the literature, since both gallium nitride doped with oxygen and gallium oxide doped with nitrogen have been described as gallium oxonitrides, despite the fact that the structure of the initial gallium compound does not change in either case. In the case of gallium nitride, independent reports have revealed a significant solubility of oxygen [120, 121]. Budde *et al*. showed that GaN films can incorporate around 15 % of oxygen at the nitrogen sites while still maintaining the wurtzite structure. Above 15 % oxygen content, the films were found to become amorphous. In addition, a nitrogen doped gallium oxide has been reported to form by adsorption of NO on CoGa(001) surfaces with a band gap of 4.1 ± 0.2 eV [122]. An independent report has shown that β-Ga_2O_3

can incorporate nitrogen at a concentration of 0.126 % without changing the crystallographic structure [123].

Despite the lack of a definitive structure for gallium oxonitride itself, investigations of gallium oxonitride films continued to extend into doping various elements into the structure, in the hope of enhancing different properties of the oxonitride. Manganese doping of gallium oxonitride with a hexagonal structure was investigated and produced a magnetic semiconductor [124]. The product nitrided at 1150 K showed an antiferromagnetic interaction with a Weiss temperature of -38 K. Substituting Ga^{3+} ions with 10 % of Li^{+} ions led to a decrease of the electrical conductivity of the gallium oxonitride [125]. Doping with 1 % of chromium Cr^{3+} ions in the wurtzite structure of gallium oxonitride gave rise to paramagnetic behaviour with a small amount of an antiferromagnetic impurity [126].

Gallium oxonitride phases have also been obtained from precursor-derived ceramics. Kinski *et al.* successfully transformed a molecular precursor into nanocrystalline gallium oxonitride ceramics [127]. Gallium (t-butoxide) dimethylamine adduct was used as molecular single source precursor and was transformed under an ammonia flow and at 650 K to gallium oxonitride ceramics with different N/O ratios. The precursor used presented all of the properties needed for the synthesis of gallium oxonitrides and for the use in CVD processes, thanks to its low melting point and high vapour pressure. During thin-film growth, it is possible to stabilise bulk metastable phases in thin-film form during epitaxial growth on substrates which have a crystal structure and lattice parameters that are similar to those of the metastable phase. This pseudomorphic stabilization has been observed in a wide range of materials systems, for example in γ-Fe [128], *bcc* Co on GaAs [129], and also in PbSe metastable films [86].

Different research groups have shown an increased interest in the gallium oxonitride system in recent years. Lowther *et al*. have reported detailed electronic structure calculations for GaN, β-Ga_2O_3 and for a cubic spinel in the form Ga_3O_3N [130]. The spinel gallium oxonitride with the ideal composition Ga_3O_3N was predicted to have a wide direct band gap and a calculated cell parameter of 8.228 Å.
A detailed theoretical investigation performed by Kroll *et al*. suggests that gallium oxonitride has a positive enthalpy of formation at ambient pressure, thereby

highlighting the importance of applying pressure and temperature in the syntheses of the spinel-type gallium oxonitride [131, 132]. A more recent theoretical study performed by Okeke and Lowther [133] described the electronic structure and mechanical properties of the spinel gallium oxonitride phase.

1.3 Spinel-structured gallium oxonitride: the subject of this work

In 2005 gallium oxonitride was synthesised for the first time as a high-pressure, high-temperature compound in a multi anvil press [134]. A nanocrystalline gallium oxonitride ceramic transformed successfully at 7 GPa and 1400 K into a spinel-structured gallium oxonitride. The structure, homogeneity, and composition were determined using Transmission Electron Microscopy (TEM) coupled with Electron Energy Loss Spectroscopy (EELS). The chemical composition was determined as $Ga_{2.81}O_{3.57}N_{0.43}$ with a cell parameter of 8.264(1) Å.
At the same time, a spinel-structured gallium oxonitride was independently synthesised at 5 GPa and 2000 K [135] having as starting material a fine mixture of GaN and Ga_2O_3 in 1/1 molar ratio. The experimental stoichiometry of the reaction product was $Ga_{2.8}O_{3.24}N_{0.64}$. Using first-principles calculations, the synthesis conditions and stability of the new phase were investigated. The calculated direct band gap energy for an ideal spinel gallium oxonitride was estimated to be around 4 eV, suggesting that the spinel phase could be a potential material for novel optoelectronic devices [135].

This thesis is primarily based on a detailed study related to synthesis and characterisation of the recently obtained spinel-type gallium oxonitride. The project was based on a collaboration between two research groups, one from the department of Chemistry and Biology at the Ludwig-Maximilians University in München (LMU) under the supervision of Prof. Hubert Huppertz and the other group from the Department of Materials and Earth Sciences at the Darmstadt University of technology (TUD) led by Prof. Ralf Riedel.

For the high-pressure and high-temperature (HP/HT) syntheses of the spinel-type gallium oxonitride, two different starting materials were used. A first approach for the synthesis of the spinel phase was by using different molar ratios of w-GaN/β-Ga_2O_3, and a second approach involved a precursor-derived gallium oxonitride ceramic as starting material. The high-pressure devices used for the syntheses were also varied. For the *in situ* syntheses and investigations a diamond anvil cell (DAC) was used in conjunction with x-ray diffraction and Raman spectroscopy. A multi-anvil press and a piston cylinder device were used in order to obtain larger amounts of the high-pressure phase for further investigations. All the high-pressure techniques and analytical methods used in this work are described in Chapter 2.

The high-pressure, high-temperature syntheses and characterisation of the spinel-structured gallium oxonitride are presented in Chapter 3. Section 3.1 is dedicated to the HP/HT synthesis of both the single source GaON-precursor (Section 3.1.1) and of the resulting high-pressure phase, the spinel-type gallium oxonitride (Section 3.1.2). A systematic investigation of the pressure-temperature relation in the GaN-Ga_2O_3 system is presented which has led to a preliminary binary phase diagram (Section 3.1.2.1). The phase transition under pressure and temperature of the gallium oxonitride ceramic is reported and discussed in Section 3.1.2.2.

In parallel, a high-pressure, high-temperature study of the gallium oxide polymorphs was performed (Section 3.2). The cubic metastable phase γ-Ga_2O_3 and the thermodynamically stable β-Ga_2O_3 are studied under high-pressure and high-temperature, using a diamond anvil cell loaded with nitrogen.

Section 3.3 is dedicated to the characterisation of the spinel-structured gallium oxonitride. A single crystal structure determination of the phase of interest is reported in Section 3.3.1. For the first time, the crystal structure of gallium oxonitride was determined on the basis of single crystal x-ray diffraction data. The combination of energy-dispersive x-ray spectroscopy with electron energy-loss spectroscopy allowed the quantification of nitrogen and oxygen for structural refinement. The elasto-mechanical properties of the gallium oxonitride are reported in Section 3.3.2. Compressibility studies of the spinel phase were performed using a diamond anvil cell coupled with x-ray diffraction, thereby determining the bulk modulus (see Section

3.3.2.1). In parallel, preliminary investigations of the material hardness were performed and are reported in Section 3.3.2.2. The thermal properties of the high-pressure phase were studied and are presented in Section 3.3.3. The thermal expansion coefficient and the thermal behaviour are also reported and discussed. The last section of this chapter is dedicated to the experimental and theoretical band structure determination for the spinel-type gallium oxonitride (Section 3.3.4).

Finally, Chapter 4 summarises the research results and discusses perspective future work in the field of GaON phases.

2 Experimental techniques

In the present chapter, the techniques and devices that have been used in this work are described. In the first Section (2.1), the syntheses and characterisation of the gallium oxonitride ceramics are presented. The ceramics were farther on used in the HP/HT syntheses of the spinel-type gallium oxonitride. In the following section, the HP/HT devices, such as diamond anvil cell, multi anvil press and piston cylinder press are over viewed. Besides a technical description, valuable experimental aspects are presented and discussed, which will be reffered to in the results chapters. Analitical methods used for the *in situ* and *ex situ* investigations of the spinel-structured gallium oxonitride phases, namely x-ray diffraction, x-ray spectroscopy, transmission electron microscopy, and Raman spectroscopy are presented in Section 2.3. The last part of this chapter deals with techniques for investigation of the elasto-mechanical properties (compressibility measurements, indentation methods) of the investigated gallium oxonitride phase.

For all the experimental techniques described in this chapter, besides a technical description of the used devices, valuable experimental aspects are presented and discussed, which will be reffered to in the results chapters.

2.1 Syntheses and characterisation of gallium oxonitride ceramics

One of the starting materials for obtaining the high-pressure phase of gallium oxonitride was a (GaON) ceramic. In order to obtain the ceramic, a molecular precursor, gallium tris(t-butoxide) dimethylamine adduct, $Ga(O^tBu)_3.HNMe_2$ was synthesized and then ammonolyzed leading to gallium oxonitride ceramics with different oxygen to nitrogen ratios.

2.1.1 Syntheses of the molecular precursor of gallium alkoxide complex, $Ga(O^tBu)_3{\cdot}HNMe_2$

The compound was synthesized using the published synthesis path, first reported by Valet *et al.* in 2001 [136]. The organic synthesis path is described by the chemical reactions:

(1) $HNMe_2 + LiBu = LiNMe_2 + HBu$

(2) $6\ LiNMe_2 + 2\ GaCl_3 = [Ga(NMe_2)_3]_2 + 6\ LiCl$

(3) $[Ga(NMe_2)_3]_2 + 6\ ^tBuOH = 2\ Ga(O^tBu)_3{\cdot}HNMe_2 + 4\ HNMe_2$

Methyl groups ($-CH_3$) are represented here by 'Me' and buthyl groups ($-CH_2(CH_2)_2CH_3$) are represented by 'Bu'. Dimethyllithiumamine, $LiNMe_2$, and bis(trisdimethylamino)gallane, $[Ga(NMe_2)_3]_2$, were synthesized by following the protocols described in references [137, 138]. Dimethylamine, $HNMe_2$, buthyllithium, LiBu, gallium trichloride, $GaCl_3$, and tert-butanol, ^tBuOH, were purchased from Aldrich and used without any further purification.

All the organic compounds involved in the syntheses are air and moisture sensitive. Therefore, all the reactions were performed under an argon atmosphere using the Schlenck-technique. The products were handled and kept in an oxygen-free argon glove box. Solvents (n-hexane, tetrahydrofuran and toluene) were dried over potassium/sodium alloys.

2.1.2 Ammonolysis of the molecular precursor

In order to obtain gallium oxonitride ceramics, the molecular precursor gallium tris(t-butoxide)dimethylamine adduct, $Ga(O^tBu)_3{\cdot}HNMe_2$, was heat treated in an ammonia flow. Since the product is air and moisture sensitive, it was first handled in an argon filled glove box. A quartz boat was first filled with the yellowish precursor powder and then placed in a Schlenck tube under argon. The tube was then placed in a furnace for the heat treatment. Following the work of Kinski *et al.* [127] the ammonolysis of the molecular precursor was done using an ammonia flow (99.999%) from a gas bottle. The choice of ammonia gas was made based on few factors, such as the low amount of residual carbon and ratio N/O closer to 1/3. In order to avoid

hydrolysis of ammonia, the gas was passed through an inner hose directly into the tube. Through the outer hose a constant dried flow of argon was kept. The heating was done at a rate of 400 K/h till 650 K, at which the temperature was kept for 3 hours and 30 minutes. The cooling was done with the same program, at a rate of 400 K/h until room temperature, keeping the gas flows continually running. After switching off the furnace, the tube with the sample inside was opened in an argon filled glove box and the ceramic was recovered.

2.1.3 Hot-gas-extraction elemental analysis

The elemental quantification of each produced ceramic was done using a hot-gas-extraction analyser LECO (LECO Corporation). The nitrogen and oxygen content in the (GaON) ceramics was determined using a LECO TC-436 analyser. The ceramics were finely ground, put into graphite crucibles and then placed into a furnace under helium atmosphere. The temperature reached was around 3000 K. The oxygen content was determined after the ceramics reacted with carbon, forming carbon monoxide which was further oxidized to carbon dioxide using a copper monoxide catalyst. The CO_2 was then quantitatively analysed using infrared absorption. At high-temperature, molecular nitrogen was released from the powders and measured by the thermal conductivity method (ASTM E1019; LECO TC-436 instrument manual). The residual carbon content was also closely analysed for all the (GaON) ceramics using a LECO C-200 carbon analyser. The fine powder was weighed in alumina crucibles mixed with tungsten and iron. Subsequently, the crucible with the mixture was placed in a high frequency electric field and burned up in an oxygen field. Once again, the carbon was oxidised to carbon monoxide and further transformed into carbon dioxide before passing to the infrared cell. The amount of carbon is determined using the Lambert Beer's absorption law from the direct proportionality between the amount of carbon dioxide and the initial amount of carbon in the sample.

Using these techniques, the different elemental content in the samples was determined with an accuracy of 5 ppm and 1% of the measured amount, respectively. Titanium nitride (TiN), O-containing titanium metal, N/O-containing steels (LECO Corporation) and silicon carbide were used as standards for the analyser calibration. In order to obtain good statistics at least five measurements were made for each sample.

2.2 High-pressure synthesis techniques

As mentioned in the introduction part of this thesis, the spinel-type gallium oxonitride has been synthesised under HP/HT conditions. In this order, the main technique employed for the syntheses and *in situ* investigations of the high-pressure phase was a diamond anvil cell. Nevertheless, large volume presses, like a piston cylinder and multi anvil press have been as well used to produce larger amounts of sample. Since the diamond anvil cell was mainly used, a more detailed description of the technique is given in Section 2.2.2, emphasising the main steps in the construction of the cell. In Section 2.2.3 a general description for the piston cylinder and multi anvil presses employed in this work is given.

2.2.1 Introduction

High-pressure is a synthesis and characterization method widely applied in many branches of physics, chemistry and biology. Pressure is a powerful tool for controllably tuning the volume and as a result the properties of the sample. An applied pressure can produce structural, electronic and other phase transitions, polymerization of organic substances, and many other phenomena.

A wide range of high-pressure devices is continuously being developed. Depending on the goals of the scientists, suitable devices for specific applications are used. A main parameter to consider for the choice of the high-pressure device is the pressure required. Static pressures of 0.1-1 GPa can be created in gas containers, autoclave presses, and high-pressure apparatus of a piston-cylinder type.

For pressures between 1-3 GPa, piston-cylinder devices can be used. Beyond 3 GPa, Bridgman-anvils devices are required. In the Bridgman-anvils type, different anvil materials can provide various pressures: for hard alloy anvils 15-20 GPa; for SiC anvils – 20-70 GPa; and for diamond anvils – 100-300 GPa. However, the maximum achievable pressure is strongly dependent on the volume of the high-pressure zone which ranges between ~ 0.01-1 m^3 for both autoclaves and piston cylinder type devices and 10^{-1}- 10^{-6} mm^3 in Bridgman-anvils type devices.

2.2.2 Diamond anvil cell - construction

The diamond anvil cell (DAC) is a miniaturized version on the "opposed anvil" device that was developed in the early days of high-pressure research [139]. The principles upon which the diamond anvil cell operates are relatively simple. The sample is placed in a pressure chamber created between the flat parallel faces (culets) of two opposed diamond anvils and the hole penetrating a hardened metal foil (gasket) (see Figure 2.1). Pressure is applied by bringing together the two anvils which causes the gasket to extrude around the diamond culets, sealing the pressure chamber.

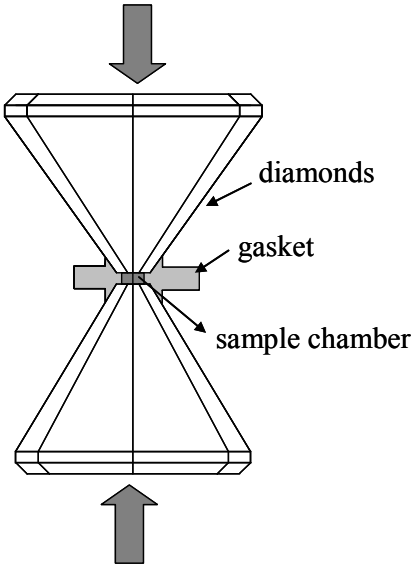

Figure 2.1 Schematic representation of a diamond anvil cell.

Even for the highest pressures attainable, the required force is not large and can be achieved through simple mechanical mechanisms. A crucial factor in reaching the desired pressures though is the alignment maintenance of the diamond culets.

Besides enabling very high-pressures, the diamond anvil cells present a set of other advantages, such as the possibility of performing *in situ* investigations, due to the small size of the cells and also because of the particular properties of the anvil material. Diamond is the hardest substance known up to now and relatively transparent to electromagnetic radiation over a wide spectral range, from the infrared to hard x-rays (5 eV to 10 keV). Therefore, diamond provides a mean for probing

samples *in situ* at non-ambient pressure and at ambient or high temperature conditions using different techniques.

In the work reported here the synthesis experiments were performed using a modified Merrill-Basset-type (four-pin opposite-plate type) laser-heated diamond anvil cell. In the following paragraphs the construction of the cells is described, detailing the main steps in preparing the experiments.

2.2.2.1 Choice of the type of diamond

Diamond anvils are produced from gem-quality and inclusion-free single crystals (at high-pressures, inclusions can cause cracks). Natural diamonds can contain significant concentrations of defects which strongly affect their properties.
The diamonds are classified function their characteristics, absorption and mechanical properties in two classes, type-I and type-II respectively [140, 141].
The selection of diamonds and their size depend upon the type of DAC and the nature of the investigation. In the present work, for the DAC syntheses of the spinel-type gallium oxonitride, type-IIa diamonds have been used enabling diffraction, and spectroscopy experiments to be performed. This type of diamonds contains lattice defects, and they are electrical insulators [141]. For instance, for light scattering studies, diamonds with very low luminescence have to be used and type-II diamonds usually satisfy this criterion [140]. Considering the size, in general, larger diamonds are preferred for high-pressures and for a larger pressurized volume. The culet sizes varied between 300 and 450 μm.

2.2.2.2 Diamond mounting and alignment

One of the simplest methods to mount the anvils to the backing plates (seats) is to glue them down [142]. A main disadvantage of this method is the short lifetime of the glue material. It reacts at least partially with cleaning reagents such as acetone and alcohol. In the work presented here the diamonds were glued to cubic BN seats.

Different seat materials can be used, depending on the intended investigations using diamond anvil cells. For example, tungsten carbide seats can be used in laser heating

experiments, spectroscopy, or diffraction (usually with a small opening angle). Beryllium is usually used in single-crystal diffraction investigations, boron nitride in a DAC which is to be heated, and diamond seats are also used in single-crystal diffraction with a CCD camera.

Maintaining the alignment of the diamond anvils is a crucial factor in reaching the highest possible stable pressure and for avoiding any damage of the diamonds during the experiment. The alignment is checked by bringing the two anvils slowly together till they are very close, while observing transversely through a microscope. Proper cleaning of the anvil surfaces is very important for perfect alignment. At first an axial alignment is performed by matching laterally the two anvils through an X-Y translation. A second step of the alignment is done through a radial / rotational alignment by observing and minimizing the Newton interference fringes. These fringes are formed by interference between the wavefronts reflected between the two nonparallel anvil faces. As they become more parallel, the number of fringes is reduced until a homogenous “grey” appears which indicates a perfect parallelism.

2.2.2.3 Gasket preparation

The use of a metal gasket in a diamond anvil cell was first demonstrated by Van Valkenburg (1965) [140] which paved the way to make the DAC a quantitative tool for high-pressure research.

The gaskets serve two purposes: they are drilled with a hole which provides the high-pressure chamber for the sample and also gives lateral support to the anvils. Under pressure gaskets flow and are generally assumed to provide some support for the flack region of the anvils by forming a supporting ring. There is a pressure rise from the edge of the culet towards the centre, while the gradient is proportional to the shear strength and inversely proportional to the thickness of the gaskets [143].

Different types of material are known to be used as gasket materials. Stainless steel or different alloys (Steel T301, Thyrodur 2701, Inconel Ni, Cr, Fe alloy) have the advantages of being inexpensive and easy to drill. For pressures in Mbar ranges, tungsten and rhenium are used, and they show strong x-ray absorption. Rhenium is suitable also for high-temperatures experiments. Beryllium is x-ray transparent but its main disadvantage is the danger to health that it presents.

For all the DAC experiments performed and reported in this work, rhenium gaskets have been used with a thickness between 250-300 μm. By closing up the cell, a pre-indentation into the gasket with a thickness of around 30-50 μm was done. The thickness of the gasket indentation has been measured mechanically by using a micrometer. A hole was then drilled with a spark erosion machine. The quality of the centring is important to ensure the stability of the experimental volume under pressure.

2.2.2.4 Pressure transmitting media

For diffraction experiments, it is very crucial to ensure that the pressure applied to the sample is homogeneous and free of any differential stress or shear strain. To achieve this, the sample within the pressure chamber is immersed in a medium that displays hydrostatic behaviour, like a liquid or a gas, at any of the attained pressure conditions. Such a hydrostatic medium cannot, by definition, support shear stresses because it has no shear strength. The motivations for avoiding non-hydrostatic conditions in an experiment are many-fold. From an experimental point of view, non-hydrostatic stresses create inhomogeneous strains in the sample. In a diffraction pattern, for example, this is reflected in broadening of the peaks from the sample which results in a reduction of the signal-to-noise ratio of the measured diffraction signal. The use of non-hydrostatic pressure media can modify the relative evolution of cell parameters of crystalline samples with pressure [144] and can lead to difficulties in reading the pressure by the commonly used ruby fluorescence technique [145, 146] or by an internal diffraction standard (see Section 2.2.2.5). Furthermore, through coupling to the spontaneous strain, non-hydrostatic stresses can also promote or suppress phase transitions [147, 148] and they can promote the amorphisation of crystalline samples [149].

In the work reported here nitrogen has been used as the pressure medium in most cases. Neon and a solid medium such as lithium fluoride have also been used as well for reasons which will be discussed in the Results and Discussions section (see Chapter 3). For gas loading, a gas-loading system was used which was designed and made at the Bayerisches Geoinstitut, by the group of Prof. Dubrovinsky. Detailed descriptions of the system can be found elsewhere [150].

2.2.2.5 Pressure measurements

The measurement of pressure is one of the major contributions to uncertainties in high-pressure experiments. Therefore, different methods have been developed and used with the aim of increasing the accuracy of pressure reading. Pressure and pressure changes can be determined accurately and rapidly by spectroscopic measurement of a pressure-induced wavelength shift in the fluorescence of certain materials, such as ruby [151, 152], samarium YAG crystals [153], or Sm^{2+}-doped SrB_4O_7 [154].

For high precision equation of state measurements and accurate pressure determination, an internal diffraction standard can be used. The determination of pressure by diffraction is based on the high precision measurement of unit cell volumes of the standard material. The pressure is then derived from the equation of state of the material. Some common internal pressure standards are NaCl (P < 29.3 GPa) [155], LiF [156], or N_2 [157].

In the present work, the pressure was mainly determined using the ruby fluorescence scale. LiF and N_2 were as well used as internal pressure standards for a more accurate pressure determination.

The fluorescence associated with the R_1 and R_2 transitions of a Cr^{3+} ion at around 14400 cm^{-1} at ambient pressure shifts by 7.57 $cm^{-1}GPa^{-1}$ under pressure, and pressure variations of ~ 100 GPa can be measured with a modest spectrometer. Excitation-argon-laser powers of ~ 10 mW are sufficient to obtain measurable signals. Calibrations of the ruby scale have been performed up to 110 GPa [151, 152, 158, 159], which can be described by Equation 2-1:

$$P = \frac{1904}{B}\left[\left(1+\frac{\Delta\lambda}{694.24}\right)^{B}-1\right] \qquad (2.1)$$

where P is in GPa and $\Delta\lambda$ is the ruby R_1 line wavelength shift in nm. Parameter B is equal to 7.665 for quasi-hydrostatic conditions, and B equals 5 for non-hydrostatic conditions.

2.2.2.6 Methods for heating diamond anvil cells

The heating of samples inside diamond anvil cells has been an important objective for decades. The most common methods are electrical resistive heating (external and internal) and laser heating.

In the case of an *external resistive heating*, wire windings are placed externally around the diamond and sample region. Many early experiments used external resistive heating methods, and particular advantages and disadvantages of these heating methods are discussed in detail elsewhere [140, 160, 161]. An external heating assemblage allowing DAC experiments at Mbar pressures and temperatures above 1200 K was constructed by Dubrovinskaia and Dubrovinsky in 2003 [162].

For an *internal resistive heating* system, the gasket is made of a thin layer of alumina placed in between two layers of conducting AlSi alloy/stainless steel. A hole is drilled through all three layers and a Fe heating wire bridges the conducting sheets within the hole. Current is applied by a pair of electrodes attached to the opposing conducting layers. A modification of this assembly was done by separating two metallic gaskets, each of them 200 μm thick, with two 20 to 50 μm layers of mica [163]. Pressures up to 10 GPa and temperatures to 3000 K have been reached using an internal hating system coupled with a DAC [164].

The highest temperatures attainable in a diamond anvil cell can be achieved with the use of *laser heating*. For the HP/HT syntheses of gallium oxonitride a laser heating system was employed. A Nd:YLF laser with a maximum power of 50 W (Quantronix Inc., 1064 nm wavelength) was used for the high-temperature DAC experiments. The system was developed in the group of Dubrovinsky L., Bavarian Geoinstitute, Germany. More technical details can be found in the reference [165].

In this technique Nd:YAG, Nd:YLF or CO_2 laser beams are highly focused onto the sample, creating a 20-50 μm hot-spot which, in certain cases, can exceed 5000 K [166]. The sample is heated after absorbing the infrared laser light which can pass through diamond anvil(s) with very little intensity loss. An aspect which has to be considered in laser-heated DAC experiments is the thermal insulation of the sample from the diamonds. Inert gases like argon, neon or nitrogen are generally used due to their low thermal conductivity, being transparent, chemically inert and give simple diffraction patterns. Other materials used as insulators include Al_2O_3, BN, NaCl and CsCl.

Possible disadvantages for these materials are the complications of diffraction patterns and the possible chemical reactions between the sample and the pressure/insulating medium.

Temperature measurements in laser heated DACs is not a trivial matter [140, 167]. In the case of laser heating, the temperature is measured from the thermal emission of the sample and by fitting the emission profile with the Planck equation for black-body emission:

$$I(\lambda) = \frac{\varepsilon c_1 \lambda^{-5}}{e^{c_2/\lambda T} - 1} \qquad (2.2)$$

Where $I(\lambda)$ is the measured intensity, ε is the emissivity, and c_1 and c_2 are constants. This calculation includes several approximations. Equation 2.2 is valid for an ideal black body (emissivity ε equal to 1), whereas real systems are grey bodies (emissivity values less then 1).

2.2.3 Large-volume presses

During the last few decades, large-volume presses have been developed which have enabled higher pressures and larger sample volumes to be attained, increasing the possible pressure range up to 25 GPa and temperatures up to 3000 K [168-171]. For generating pressures exceeding 1 GPa and for a relatively high amount of material, a few different setups can be used: piston-cylinder systems, belt-type apparatuses, toroid-type cells, and multi-anvil setups. For all these devices the design is based on the two main principles of static pressure generation: piston-cylinders and opposite anvils.

In addition to the DAC syntheses (see Section 3.2.1.2), a multianvil device (based on a Walker-type module used in conjunction with a 1000 t press) and a piston cylinder setup were used for the HP/HT syntheses reported in this thesis (see Sections 3.2.1.3, 3.2.1.4, and 3.2.2.2). These devices are described in the following paragraphs.

Markedly higher volumes under high-pressure are attainable with end-loaded and non-end-loaded piston cylinder setups [140, 172]. They consist of a simple piston which

is forced into a cylinder, resulting in the compression of the solid materials in the furnace assembly. The end-loaded piston cylinder apparatus used in the HP/HT syntheses of the spinel-type gallium oxonitride consists of a WC pressure vessel supported by a steel ring (the bomb). The load is applied to the WC piston, which in turn is pushed into the bomb thereby applying pressure to the sample (see Figure 2.2). The pressure in the sample cell is automatically controlled by a hydraulic pump. These devices are relatively easy to operate up to 5 GPa, when heated by a resistance furnace assembly up to 2000 K. The resistance furnace assembly is located within the pressure chamber. The volume of a high-pressure chamber can vary from 1 to 100 cm^3.

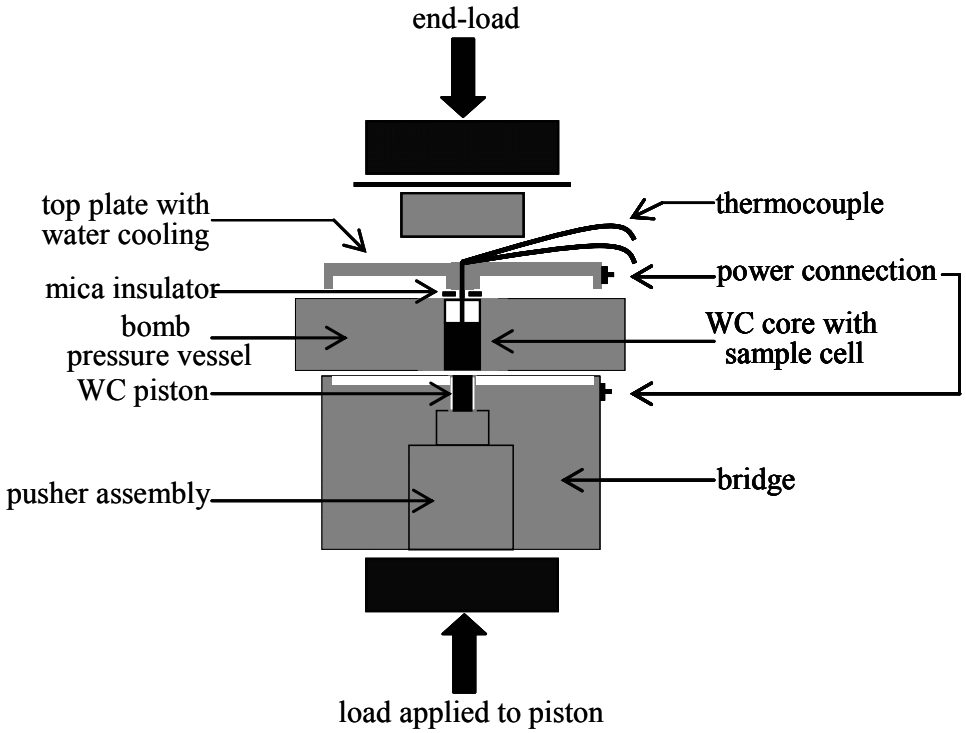

Figure 2.2 Schematic drawing of an and-loaded piston cylinder.

In the following, a brief description of the multi-anvil assemblage is given, which has been used for the HP/HT syntheses of the gallium oxonitride phase presented in this work.

Depending on the chemical system to be studied, the sample is placed in a capsule made of different materials, such as h-BN, copper, molybdenum, platinum, or gold.

Then, the capsule with the sample is located directly in the centre of an octahedron made of porous MgO ceramic doped with Cr_2O_3. For heating, cylindrical resistance heaters surrounding the capsule material were used. Up to pressures of 10 GPa and temperatures of 1800 K, graphite (RW403, SGL Carbon, Bonn, Germany) was used successfully as the heater material. Above these limits, the graphite starts to convert to diamond and its performance dramatically degrades. As an alternative, $LaCrO_3$ (Cherry-O, Amagasaki-City, Japan) was used as heater material to generate temperatures up to 3000 K. The temperature was measured using a thermocouple, which can be inserted along the vertical axis. After setting the inner part into the drilled octahedron, eight tungsten carbide cubes were arranged around it.

Detailed descriptions of the preparation of the assembly can be found elsewhere [169, 170, 173, 174].

For the syntheses of the spinel-type gallium oxonitride, presented in this work, an assembly 18/11 was used, which consists of an octahedron with an edge length of 18 mm, together with eight tungsten carbide cubes which have truncated triangular faces with an edge length of 11 mm. The pressures have been previously calibrated as a function of hydraulic oil pressure.

2.3 Physico-chemical characterisation

As revealed in the HP / HT techniques chapter (see Section 2.2), one of the main inconveniences of these synthesis techniques is the small size of the resulting samples. For specimens obtained in DACs, with lateral dimensions of several μm, the most common techniques used for structural and physical/chemical investigations are *in situ* x-ray diffraction and optical methods such as Brillouin scattering, Raman scattering, and Infrared spectroscopy. The high-pressure large volume techniques (see Section 2.2.3) can provide samples with sizes of the order of several mm, which can mean that the sample size is no longer an impediment for using different types of techniques, depending of course on the characteristics of the sample and the properties of interest.

For the characterisation of the spinel-structured gallium oxonitride, techniques like x-ray diffraction using in-house facilities (see Section 2.3.1.1) or synchrotron radiation (see Section 2.3.1.2), soft x-ray specroscopy (see Section 2.3.1.3), electron

microscopies (see Section 2.3.2) and Raman spectroscopy (see Section 2.3.3) are described in the following sections.

2.3.1 X-ray diffraction and spectroscopy

2.3.1.1 In-house x-ray diffraction

X-ray powder diffraction is a powerful non-destructive testing method for determining a range of physical and chemical characteristics of materials. It is widely used in all fields of science and technology. The applications include phase analysis, i.e. the type and quantities of phases present in the sample, the crystallographic unit cell and crystal structure, crystallographic texture, crystalline sizes, macro-stress and micro-strain, and also electron radial distribution functions.

X-ray diffraction results from the interaction between x-rays and the electrons of atoms. Depending on the atomic arrangement, constructive interferences of the scattered rays occur when the path difference between two diffracted rays differs by an integral number of wavelengths. This selective condition is described by the Bragg equation, also called "Bragg's law":

$$2d_H \sin\Theta_H = n\lambda \qquad (2.3)$$

where λ is the wavelength, d_H the d-spacing and Θ_H the Bragg angle, which is half the angle between incident and reflected beam. *H* describes the Miller indices triplet *hkl* which define each lattice plane.

Diffraction data may be viewed as a Fourier transformation from direct or crystal space into reciprocal space, yielding intensity data in reciprocal space. Detectors register intensities *I(hkl)*, which are directly proportional to the squares of the crystallographic structure factors *F(hkl)*: the intensity *I* is proportional to $|F|^2$. *F* is defined as:

$$F(hkl) = \sum f_j \exp(hx_j + ky_j + lz_j) \qquad (2.4)$$

where f_j is the form factor or atomic scattering factor of atom j, hkl are the Miller indices and x, y, z the relative atomic positions in the unit cell. The summation j runs over all atoms in one unit cell. For crystalline materials, $F(hkl)$ is the Fourier transform of a single unit cell (superimposed on the Fourier transform of the crystal lattice, the reciprocal lattice). As the intensity is the square of the structure factor, the measurement is sensitive only to the absolute value of the structure factor ($|F|$), while the phase of F is lost. The phase of the structure factor however is needed for further investigation of the crystal structure. Determination of the phase is the main obstacle in crystallography. In order to determine a structure, one has to make a try for the positions of the atoms in the unit cell, and then use the obtained structure to calculate *F(hkl)* and thus *I(hkl)*.

The formation of spinel-type gallium oxonitride was observed and investigated *in situ* diamond anvil cell using x-ray diffraction. The experiments were performed at Bayerisches Geoinstitut (BGI), Bayreuth, Germany. The x-ray system consists of three major components: a RIGAKU FR-D high-brilliance source, an Osmic Confocal Max-Flux optics, and a SMART APEX 4K CCD area detector [175]. The FR-D high-brilliance x-ray Mo rotating anode generator operates at loads up to 3.3 kW.

To investigate the gallium oxonitride samples obtained via HP/HT syntheses using a large-volume press, an *in-house* powder x-ray diffractometer was used. The experiments were performed at the FG Structurforschung, FB Material- und Geowissenschaften, TU Darmstadt. The powder XRD pattern of spinel-type gallium oxonitride was measured in the Debye-Scherrer geometry using a STOE STADI P diffractometer (Stoe & Cie GmbH) with Cu-$K_{\alpha 1}$ radiation (λ = 1.540598 Å). The diffractometer is equipped with a position sensitive detector with a 6° aperture. For preliminary calibration of the sample-to-detector distance a NIST-NBS640b Si standard was used. The sample for XRD was obtained by grinding parts of the bulk gallium oxonitride until the sample was very finely ground, and then fixing it between two foils.

For the single crystal structure determination, the intensity data were collected at room temperature on a STOE IPDS-I diffractometer equipped with an area detector (Stoe &Cie GmbH, Darmstadt, Germany) or on a Kappa CCD diffractometer (Bruker

AXS / Nobius, Karlsruhe, Germany) equipped with a rotating anode, designed for small crystals. In both diffractometers graphite monochromatised Mo-$K_{\alpha 1}$ radiation ($\lambda = 0.7107$ Å) was applied.

2.3.1.2 Synchrotron radiation techniques

Powder diffraction patterns in general suffer from overlapping diffraction peaks, a background which is often difficult to define leading to errors in intensity values, or preferred orientation of the grains. The widely available synchrotron radiation can overcome all these inconveniences, due to its high primary intensity, low divergence, tunable wavelength and linear polarization. The problem with the preferred orientation of the grains is removed by rotating the sample during the measurement time.

Two types of experiments presented in this work were performed using synchrotron radiation. Due to the advantage of tuning the wavelength, synchrotron radiation is ideal in performing x-ray spectroscopy, probing the electronic structure of the high-pressure phase of gallium oxonitride. The accurate determination of lattice parameters was successfully achieved using synchrotron radiation, thus allowing a thermal expansion study for the investigated gallium oxonitride phase.

X-ray Absorption Near Edge Spectroscopy (XANES) and X-ray Emission Spectroscopy (XES) were used to probe the unoccupied and occupied Local Partial Density of States (LPDOS), respectively of the spinel-type gallium oxonitride. The spectra were collected under ultra-high-vacuum conditions (5×10^{-9} Torr) and room temperature at beamline 8.0.1 of the Advanced Light Source (ALS) at the Lawrence Berkeley National Laboratory, California, USA. The samples were ground into a fine powder and pressed onto carbon tape. The spectra were calibrated using the reference BGO ($Bi_4Ge_3O_{12}$) with the peak locations near the band gap at 526.4 eV and 532.7 eV for XES and XANES, respectively. The XANES spectra were recorded in both Total Electron Yield (TEY) and Total Fluorescence Yield (TFY). These detection methods differ primarily by their probe depth. TEY probes typical 5 nm into the surface, while at 500 eV the TFY probes approximately 250 nm. This allows the examination of both surface and bulk properties.

The thermal expansion studies of spinel gallium oxonitride were performed at ID31 – The High-resolution Powder Diffraction Beamline at the European Synchrotron Radiation Facility (ESRF), Grenoble, France. The XRD data was collected by a bank of nine detectors, each of them preceded by a Si 111 analyzer crystal using a monochromatic synchrotron radiation (wavelength λ = 0.4 Å). The powder sample was filled in a quartz capillary of 0.3 mm diameter, which was rotated during the accumulation time. For the high-temperature studies a hot-air blower (commercialized by Cyberstar, France) was used which provided a maximum temperature of 1200 K.

2.3.1.3 Soft x-ray spectroscopy

Soft X-ray Spectroscopy (SXS), which utilises synchrotron radiation from modern third generation sources is a powerful tool for probing the electronic structure of materials. The two techniques employed in this work for the band structure investigation of the spinel-type gallium oxonitride were X-ray Absorption Near Edge Spectroscopy (XANES) and X-ray Emission Spectroscopy (XES).

XANES and XES directly probe the electronic structure or more specifically the Electronic Density of States (DOS). During a XANES measurement, the conduction band is probed by exciting a core electron into a previously empty conduction band state. The transition rate at which electrons are promoted is proportional to the density of unoccupied states in the conduction band. XES measurements are sensitive to the relaxation process when a valence band electron refills the core hole and the energy is released in the form of a fluorescence photon. The rate at which photons are emitted is proportional to the density of occupied states. The physical principles of x-ray absorption and x-ray emission processes are schematically shown in Figure 2.3.

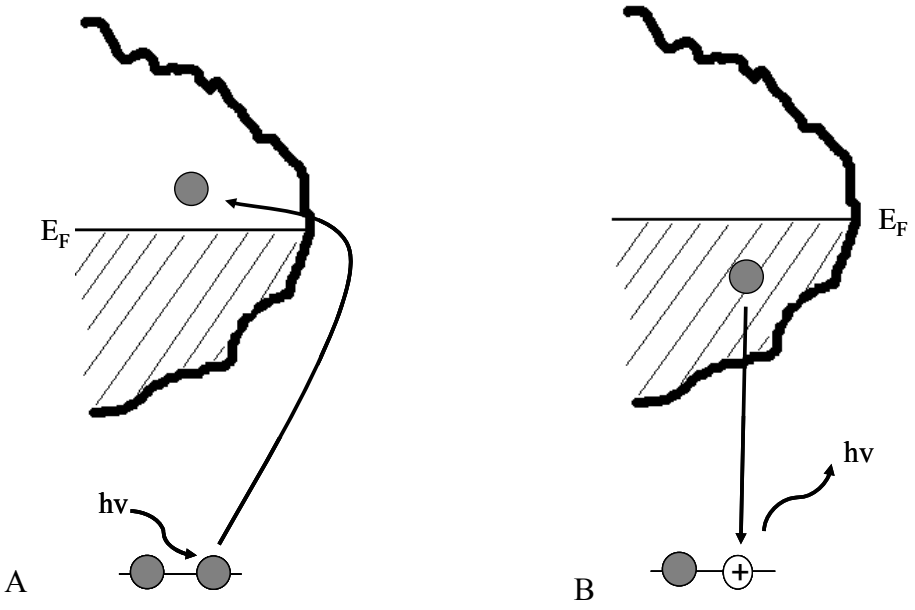

Figure 2.3 Schematic representation of the absorption, XAS (A) and emission, XES (B) processes which take place after a x-ray interacts with a specimen.

The DOS are dependent on energy, therefore the energy scale for a XANES measurement is the excitation energy required to excite an electron into the conduction band and for an XES measurement it is the emitted photon energy. While in general XANES and XES measurements probe the conduction and valence band states respectively, there are limitations which turn out to be advantageous to the measurements. Since a photon has an angular momentum $L = 1$ and momentum must be conserved, only transitions that are dipole allowed ($\Delta l = \pm 1$) are likely to be observed. In a strict one-electron picture, the final state of a XANES measurement a core hole is present and an extra electronic charge resides in the conduction band [176]. The final state of an XES measurement involves no missing core hole but a missing charge in the valence band.

The experimental spectra are always subject to inherent experimental broadening which can result from the: presence of the core hole [177], the short lifetime of the final state of the material [178] and the finite spectral resolution on the instrument [179, 180].

The band gap of a material is the difference in energy between the highest occupied DOS (the top of the valence band – probed by XES) and the lowest unoccupied DOS (the bottom of the conduction band – probed by XANES). The band gap can therefore be determined by combining XES and XANES measurements at a common energy

scale. These measurements are indirect and the resolution is usually less than when probing transitions across the band gap directly by an optical or UV excitation. The x-ray spectroscopic technique can determine the band gap of wide band gap semi-conductors or insulators, which can be difficult to access with UV excitations.

Since most of the properties of a material, such as conductivity, optical absorption, chemical bonding, energy gap, or catalytic performance are governed by its electronic structure, the measurements and calculations of the electronic structure give valuable insights into the functionality of a material and its possible device performance.

The electronic structure of the spinel-structured gallium oxonitride was probed using the SXS techniques (combined with theoretical calculations) at beamline 8.0.1 of the Advanced Light Source (ALS) at the Lawrence Berkeley National Laboratory, California, USA. More experimental details of the measurements are given in the previous section (2.3.1.2. Synchrotron radiation techniques). The electronic structure investigation was performed combining the x-ray technique with *ab initio* calculations. Hence, in the next paragraphs the calculation methods used in this study will be described (see also Section 5.4).

The XES and XANES spectra were simulated using electronic structure calculations which only require as input the crystal structure parameters. The full core hole potential was used in the XANES simulations in a supercell configuration. The spectra are then broadened using a combination of Lorentzian and Gaussian functions to simulate the core hole lifetime, final state lifetime and instrumental broadening effects [181, 182].

The *ab initio* density functional theory (DFT) calculations were carried out using the commercially available WIEN2k DFT software [183]. This code uses the Kohn-Sham methodology with spherical wave functions to model core orbitals and Linear Augmented Plane Waves (LAPW) to model semi-core and valence states [184, 185]. The exchange interaction used was the Generalized Gradient Approximations theory (GGA) [186]. This approximation tends to underestimate the band gap, but gives a very good agreement with the shape of the valence and conduction bands. The input crystal structure parameters were determined by x-ray diffraction. The size of the supercell

used in the case of XANES simulated spectra was 2 x 1 x 1 of the unit cell (112 atoms) with a 100 k-point mesh.

2.3.2 Transmission Electron Microscopy (TEM)

In a transmission electron microscope the electrons are accelerated to high energies (a few hundreds of keV) and focused on a material. They can scatter or backscatter elastically or inelastically, produce many interactions, source of different signals such as x-rays, Auger electrons or light. A transmission electron microscope can perform in imaging mode or diffraction mode. It is constituted of: (1) two or three condenser lenses to focus the electron beam on the sample, (2) an objective lens to form the diffraction in the back focal plane and the image of the sample in the image plane, (3) some intermediate lenses to magnify the image or the diffraction pattern on the screen [187].

If the sample is thin (< 200 nm) and contain light chemical elements, the image presents a very low contrast when it is focused. To obtain an amplitude contrasted image, an objective diaphragm is inserted in the back focal plane to select the transmitted beam. The crystalline parts in the Bragg condition appear dark and the crystalline parts not in Bragg condition and the amorphous areas appear bright. This imaging mode is called bright field (BF) mode. If the diffraction is constituted by many diffracting phases, each of them can be differentiated by selecting one of its diffracted beams with the objective diaphragm. To do that, the incident beam must be tilted so that the diffracted beam is put on the objective lens axis to avoid off-axis aberrations. This mode is called dark field (DF) mode. The BF and DF modes are used for imaging materials on the nanometer scale.

The selected area diaphragm is used to select only one part of the imaged sample, for example a small particle. This mode is called selected area diffraction (SAED). SAED of a crystal permits to obtain the symmetry of its lattice and calculate its interplanar distances (using Bragg's law). This is useful to confirm the identification of a phase, after assumptions generally based on the literature of the studied system and on chemical analyses.

2.3.2.1 Electron Energy Loss Spectroscopy (EELS)

When a high energy electron beam passes through a material, coulombic interactions take place between the electrons in the beam and the electrons in the material, resulting in inelastic scatterings of the high energy electrons. The energy spectrum of the high energy electrons can be measured after they pass through the material. Of course, total energy is conserved, so the energy lost from the high energy electrons is gained by the electrons in the material. The excitation spectrum of the material therefore can be deduced from a so-called Electron Energy Loss Spectroscopy (EELS) spectrum [187].

In an EELS spectrum there are two distinct regions offering specific information on the material. The low-loss region ($\Delta E < 50$ eV) contains information about the specimen thickness, valence and conduction electron density. The low energy plasmon excitations are due to core loss events which involve the excitations of inner electrons out of the atom. The high-loss region ($\Delta E > 50$ eV) provide information on the elemental composition, chemical bonding and electronic structure, coordination numbers or interatomic distances.

The quantification procedure using the EELS technique contains the following steps:

- Choosing the right absorption edges to measure;
- Setting the experimental conditions (i.e. beam energy, collection angle, convergence angle);
- Extracting the edge intensities via background fitting and subtraction, fitting the reference edge profile plus background model;
- Correcting the plural scattering[4] by using deconvolution procedures;
- Obtaining the ionisation cross-section.

The general equations used in determining the ratio of two elements present in a specimen studied using EELS are functions of:

- I_k, which is number of electrons having excited the k^{th} inner shell;
- P_k , the probability of exciting the k^{th} shell;
- I_0, the incident electron current.

[4] For a thick specimen, there is a high probability that the fast electron loses energy by excitation of valence electrons. Hence, the measured spectrum contains a mixed inner-shell and valence excitations.

These parameters are defined by the equations:

$I_k = P_k \times I_0$ (2.5) with $P_k = N \times \sigma_k$, (2.6) N being the number of atoms of the particular element analysed and σ_k the ionisation cross-section for the k^{th} shell. From equations (2.5) and (2.6), N becomes:

$$N = \frac{I_k}{\sigma_k \times I_0} \qquad (2.7)$$

Now considering the edges of two elements, A and B which are present in the same spectrum, the ratio of those two can be written:

$$\frac{I_A}{I_B} = \frac{\sigma_A}{\sigma_B}\frac{N_A}{N_B} \qquad (2.8)$$

Now, since the measurement is done over a finite energy window (δE) and a finite angular window (β), the equation 2.8 can be rearranged as:

$$\frac{N_A}{N_B} = \frac{\sigma_B(\delta E, \beta)}{\sigma_A(\delta E, \beta)}\frac{I_A(\delta E, \beta)}{I_B(\delta E, \beta)} \qquad (2.9)$$

The structure and composition of the spinel gallium oxonitride were also examined by transmission electron microscopy. The homogeneity and the nitrogen to oxygen ratio of the synthesized spinel-type gallium oxonitride phase were determined using a transmission electron microscope (FEI CM12 operated at 120 kV, equipped with a LaB6 cathode), coupled with an EEL spectrometer (Gatan DigiPeels 766 parallel electron spectrometer, attached to the FEI CM12). The high-pressure bulk gallium oxonitrides were finely ground, dispersed in isopropanol and deposited on a Cu grid.

2.3.3 Raman spectroscopy

Raman scattering is a fundamental form of spectroscopy discovered by Krishna and Raman in 1928 and has been well documented since [188]. Raman scattering is sensitive to the change in the polarizability of the molecule or crystal with respect to

its vibrational motion. The interaction of the polarizability with the incoming radiation creates an induced dipole moment in the molecule, and the radiation emitted by this induced dipole moment contains the observed Raman scattering. The light scattered by the induced dipole consists of both Rayleigh scattering and Raman scattering. Rayleigh scattering corresponds to the light scattered at the frequency of the incident radiation, whereas the Raman radiation is shifted in frequency, and hence energy, from the frequency of the incident radiation by the vibrational energy that is gained or lost in the molecule.

A Raman spectrum consists of scattered intensity plotted vs. energy. Each peak corresponds to a given Raman shift from the incident light energy $h\nu_0$.
According to quantum mechanics [189], a vibration is Raman-active if the component(s) of the polarizability belong(s) to the same symmetry species as that of the vibration. Thus, only those transitions involving $\Delta l = \pm 1$ are allowed (with l – atomic energy level). The Raman-active modes corresponding to different symmetries can be calculated using the factor group analysis [190]. The Raman shift is independent of the wavelength of the incident radiation, thus the spectrum is a characteristic fingerprint of a material and can be used for identification of known phases, by-products or impurities.
From symmetry analysis, the spinel-type gallium oxonitride which has a cubic symmetry is expected to present five Raman-active modes:

$$\Gamma_{optic(R)} = 3T_{2g} + 1E_g + 1A_{1g} \qquad (2.10)$$

In the case of two other nitride spinels, γ-Si_3N_4 and γ-Ge_3N_4, the two modes with A_{1g} and T_{2g} symmetry were shown to occur in the high-frequency region, and the other three modes, $2T_{2g}$ and $1E_g$ in the low-frequency region, respectively [191].

Raman scattering spectra on the high-pressure, high-temperature gallium oxonitride phases were measured in reflection geometry using a micro-Raman spectrometer (Labram HR 800 open microscope). *In situ* LH-DAC syntheses were also monitored via Raman spectroscopy.

2.4 Determination of elasto-mechanical properties

Elasto-mechanical properties of a material include the hardness and elatic moduli, such as bulk modulus (K), shear modulus (G), Young's modulus (E), and Poisson's ratio (ν). The spinel-phase of gallium oxonitride had its hardness and elastic moduli investigated and are reported in this work. Therefore, definitions and concepts of these properties are discussed in the following paragraphs.

2.4.1 Compressibility

In order to investigate the behaviour of the volume of a solid under strong compression, the dependence of the volume as a function of pressure is measured, and by fitting the experimental data with one of the chosen equation of state (EOS), the bulk modulus (K) and its pressure derivatives (K') can be determined. In the last seventy years, different isothermal equations of state have been suggested [192-196]. In all these equations the parameters are the isothermal bulk modulus (K_0) and its pressure derivative (K'_0), and the starting volume (V_0) at room pressure.

The isothermal bulk modulus for a material is defined by the following equation:

$$K = -V\frac{dP}{dV} = \rho\frac{dP}{d\rho} = \frac{dP}{d\ln\rho}, \qquad (2.11)$$

where ρ is the material density.
One of the most used EOS is the third order Birch-Murnaghan equation [193, 197]:

$$P = \frac{3}{2}K_0 f(1+2f)^{5/2} \times \left[1+\frac{3}{2}(K_0' - 4)f\right], \qquad (2.12)$$

where $f = ((V/V_0)^{-2/3}-1)/2$ represents the Eulian finite-strain, so

$$P = \frac{3}{2}\mathrm{K}_0\left[\left(\frac{\mathrm{V}}{\mathrm{V}_0}\right)^{-7/3} - \left(\frac{V}{V_0}\right)^{-5/3}\right] \times \left\{1-\frac{3}{4}(4-K_0')\left[\left(\frac{V}{V_0}\right)^{-2/3}-1\right]\right\}. \qquad (2.13)$$

This equation can be reduced to a second order equation in the case of very small strains. Hence, equation (2.13) becomes:

$$P = 3K_0 f(1+2f)^{5/2} = \frac{3}{2}K_0\left(\left(\frac{V}{V_0}\right)^{-7/3} - \left(\frac{V}{V_0}\right)^{-5/3}\right). \qquad (2.14)$$

The compressibility studies of the spinel-type gallium oxonitride were performed using the DAC technique (see Section 2.2.2) coupled with *in situ* x-ray diffraction (see Section 2.3.1.1).

2.4.2 Hardness

As discussed also in the introduction part of this thesis, the two well known superhard materials, diamond and c-BN are of great importance for grinding and cutting tool industry [40] (see also Section 1.1.3). The search for new hard materials with fundamental and technological interest has continued with the syntheses of cubic Si_3N_4 [43], cotunnite-type TiO_2 [46], C_{60} [198] and cubic BC_2N [42], etc.

Hardness is the common property characterising these materials and is defined as the resistance of a material to an external mechanical load ending with a permanent deformation on the material's surface. From the mode of action on the sample, the hardness test methods are classified into static methods (scratch and indentation) and dynamic methods (contact abrasion, impact abrasion and indenter impact) [199].

The hardness of an investigated material depends, on one side, on the measurement technique and load range, and on the other side on the sample morthology (defects, porosity, grain size, impurities, etc.) [199, 200]. For example, the hardness of a specimen decreases exponentially with the increase of porosity: $H = H_0 \exp(-bp)$, where b is a constant, p is the volume fraction porosity, H and H_0 are the hardness of the corresponding porous and dense specimen, respectively [201].

In the present work, indentation hardness tests were performed on HP/HT spinel-type gallium oxonitride. In the following two Sections (2.4.2.1 and 2.4.2.2), the two

indentation methods used are presented: the Vickers indentation method and depth-sensing (nano) indentation using the Oliver-Pharr method [202].

2.4.2.1 The Vickers indentation hardness method

The indentation hardness of ceramics is usually determined using indenters such as Vickers, Knoop or Berkovich indenters [203]. In the present work micro-indentation hardness tests were performed using a Vickers indenter. The Vickers diamond indenter has a square-based pyramid form with an angle between the opposite faces of 136° and between opposite edges of 148°. The Vickers hardness, H_V is calculated from the indenter load and the surface area of the impression, using the following expression:

$$H_V = \frac{2P}{d^2}\sin\frac{136°}{2} = 1.854\frac{P}{d^2} \qquad (2.15)$$

where P is the applied load in kilogram-force (kgf) and d is the length of the measured diagonal of the impression in millimetres (mm). Hence, the corresponding units of H_V are kilograms-force per square millimetre (kgf/mm^2). In the present work, the Vickers hardness values are given in SI units, GPa (1 GPa = 10^9 N/m^2).

The Vickers hardness tests reported in this work were performed using a LECO Microhardness tester, Type M-400 G2.

2.4.2.2 Depth-sensing (nano) indentation using the Oliver-Pharr method

In the depth-sensing indentation testing, the applied load and the depth of penetration on an indenter into the sample are recorded and used to indirectly determine the area of contact and hence the hardness of the specimen. The nano-indentation technique is very popular in testing thin films or specimens which have mechanical properties that need to be measured over small size scales.

The indenter for nano-indentation testing usually is a three-sided Berkovich indenter with the face half-angle of 62.3° giving the same projected area to depth ratio as a four-sided Vickers indenter [203]. The reason for using a Berkovich indenter is that it

can be made very sharp, avoiding in this way the line of conjunction usually found in a Vickers indenter (a line usually appears at the vortex of the four-sided pyramid).

The main outcome of a depth-sensing (also known as instrumented indentation) test is the load-displacement curve. A schematic representation of the load as a function of indenter displacement is shown in Figure 2.4. The curve consists of a loading part, containing both elastic and plastic deformations, followed by an unloading part, usually thought to be wholly elastic.

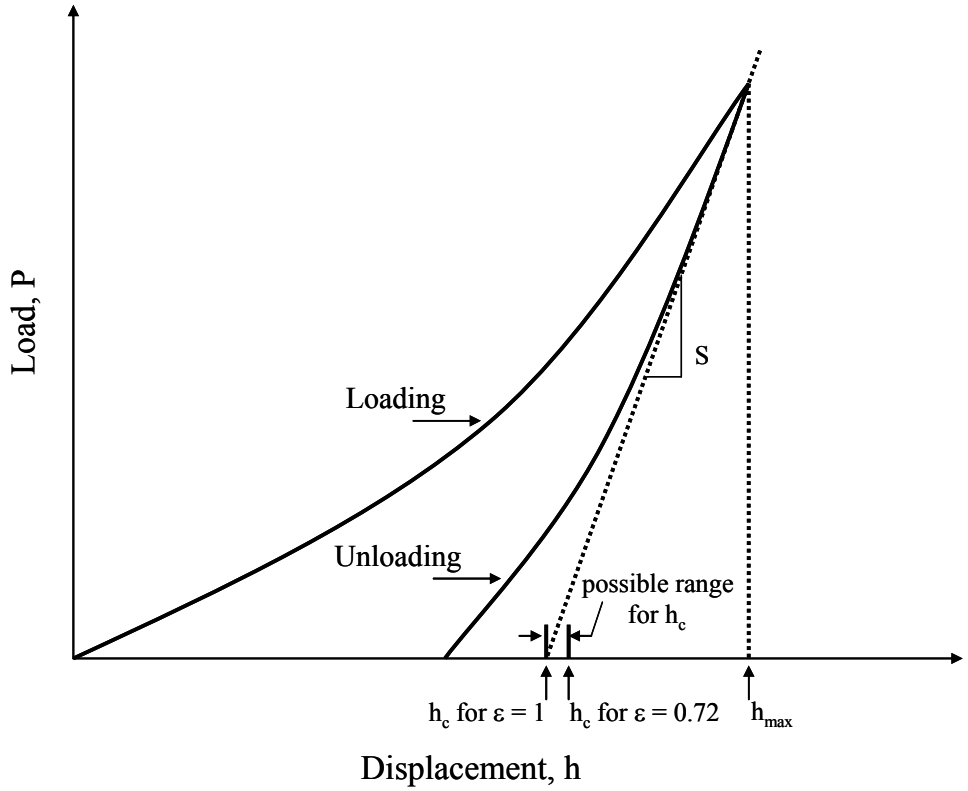

Figure 2.4 Load versus indenter displacement.

The notations in Figure 2.4 represent the following quantities: S is the measured stiffness (the slope of the unloading curve at any point), h_c is the contact depth (the vertical distance along which contact is made), h_{max} is the displacement at maximum load and ε is a geometrical constant of the indenter.

The analyses of the loading-unloading curves have been performed using the Oliver-Pharr method [202]. The hardness is defined as the mean pressure that the specimen will support under load, $H = P_{max}/A$, with A being the projected area of contact at maximum load. Using the same technique, the Young's reduced modulus (E_r) can be

determined. The reduced elastic modulus is defined as a function of the Poisson's ratio (ν) as follows:

$$\frac{1}{E_r} = \frac{(1-\nu^2)}{E} + \frac{(1-\nu_i^2)}{E_i} \qquad (2.16)$$

where E_i and ν_i are the Young's modulus and Poisson's ratio for the indenter.
From the unloading curve, the contact stiffness, S is determined, which can be written as:

$$S = \frac{dP}{dh} = \frac{2}{\sqrt{\pi}} E_r \sqrt{A} \qquad (2.17)$$

The projected area A at peak load is computed from the relation $A = F(h_c)$, where the functional form of F is experimentally determined. The total displacement, h, is determined as the sum of the contact depth, h_c and the displacement of the surface at the perimeter of the contact, h_s. The latter is defined as $h_s = \varepsilon (P_{max}/S)$ with ε equal to 0.75 [202].

3 Results and Discussion

In this chapter, the high-pressure, high-temperature syntheses and characterisation of the spinel-structured gallium oxnitride is discussed. Section 3.1 is dedicated to the HP/HT syntheses of spinel gallium oxonitride from different mixtures of GaN-Ga_2O_3 and from (GaON) ceramics derived from a single source precursor. A parallel study of gallium oxide polymorphs under high-pressure is presented in Section 3.2. A detailed characterisation of the high-pressure phase of gallium oxonitride will be discussed in Section 3.3, in particular a single crystal structure determination (Section 3.3.1), its elasto-mechanical properties (Section 3.3.2), its thermal properties (Section 3.3.3), and an investigation of its band structure (Section 3.3.4).

3.1 High-pressure, high-temperature synthesis of spinel-type gallium oxonitride

In this section, the high-pressure, high-temperature syntheses of the spinel-type gallium oxonitride will be presented. In Section 3.1.1 the gallium oxonitride ceramics syntheses will be reported as well as some characterisations of the ceramics. For the HP/HT synthesis of the spinel-structured gallium oxonitride, two different synthesis paths were chosen. In Section 3.1.2.1 the syntheses of the target phase through a solid state reaction will be reported. Different molar ratios of GaN and Ga_2O_3 from 1/9 to 9/1 were used in HP/HT syntheses, bringing new insights on the pressure-temperature-composition field stability of gallium oxonitride. In parallel, a different starting material was used for the HP/HT syntheses, results which will be presented and discussed in Section 3.1.2.2. Gallium oxonitride ceramics with different elemental compositions led to the HP/HT phase of gallium oxonitride. Under pressure and temperature a phase transition takes place from an x-ray amorphous powder to a well crystallised spinel-type gallium oxonitride. Different HP devices were used for different syntheses, such as diamond anvil cells, piston cylinder presses and multi anvil presses.

3.1.1 Gallium oxonitride ceramic synthesis and characterisation

As described in Chapter 2 (see Section 2.1), a single source molecular precursor was used in order to obtain gallium oxonitride ceramics, which were then used as starting materials for high-pressure syntheses of the spinel-structured gallium oxonitride. Gallium tris(t-butoxide) dimethylamine adduct, $Ga(O^tBu)_3.HNMe_2$, was heat treated in a continuous ammonia flow, at 650 K for 3 hours and 30 minutes. Kinski *et al.* [127] showed that the choice of ammonia as the gas atmosphere and this temperature program were the best parameters for decreasing the amount of residual carbon and also for obtaining a more suitable N/O ratio in the obtained ceramics. Since the ideal composition of the target phase - the high-pressure phase of gallium oxonitride - is Ga_3O_3N, the goal was to prepare starting compounds with an N/O ratio as close as possible to 0.33.

Different runs of syntheses were performed, obtaining gallium oxonitride ceramics with different elemental compositions. For determining the chemical composition of the ceramics a hot-gas extraction elemental analysis was used (see Section 2.1.3). Here a set of 4 ceramics is presented which will be considered and discussedin the following. In Table 3.1 the corresponding elemental compositions are given with the calculated N/O ratio.

Table 3.1 Gallium oxonitride ceramics with the corresponding chemical formula and N/O ratios.

Sample	Weight %				Chemical formula	N/O
	O	N	C	Ga		
(GaON)1	23.46	7.24	1.43	67.87	$Ga_{1.00}O_{1.55}N_{0.55}C_{0.13}$	0.35
(GaON)2	11.92	12.13	2.75	73.20	$Ga_{1.00}O_{0.72}N_{0.83}C_{0.22}$	1.15
(GaON)3	14.18	11.82	2.85	71.15	$Ga_{1.00}O_{0.88}N_{0.82}C_{0.24}$	0.93
(GaON)4	14.65	10.29	3.08	71.98	$Ga_{1.00}O_{0.89}N_{0.71}C_{0.26}$	0.80

The calculations were performed by normalising the oxygen, nitrogen and carbon to one atom of gallium, and keeping in mind the ideal N/O ratio of 0.33. The weight percent of gallium was determined by difference from 100 %.

The gallium oxonitride ceramics presented in Table 3.1 were used as starting materials in different HP/HT experiments to synthesise spinel-structured gallium oxonitride phases, which are described in detail in Section 3.1.2.2.

3.1.1.1 Thermal stability of the gallium oxonitride ceramics

The crystallinity of gallium oxonitride ceramics synthesised from a molecular precursor, $Ga(O^tBu)_3{\cdot}HNMe_2$, was investigated previously by Kinski *et al.* [127] using x-ray powder diffraction technique. Powdered (GaON)-ceramic with an N/O ratio of 0.86 and a carbon content of 1.2 ± 0.1 wt % was placed in a glass capillary under an inert atmosphere. Up to 900 K the XRD pattern showed only a broad background due to nanocrystalline particles. At temperatures above 1000 K the stable hexagonal phase w-GaN was detected.

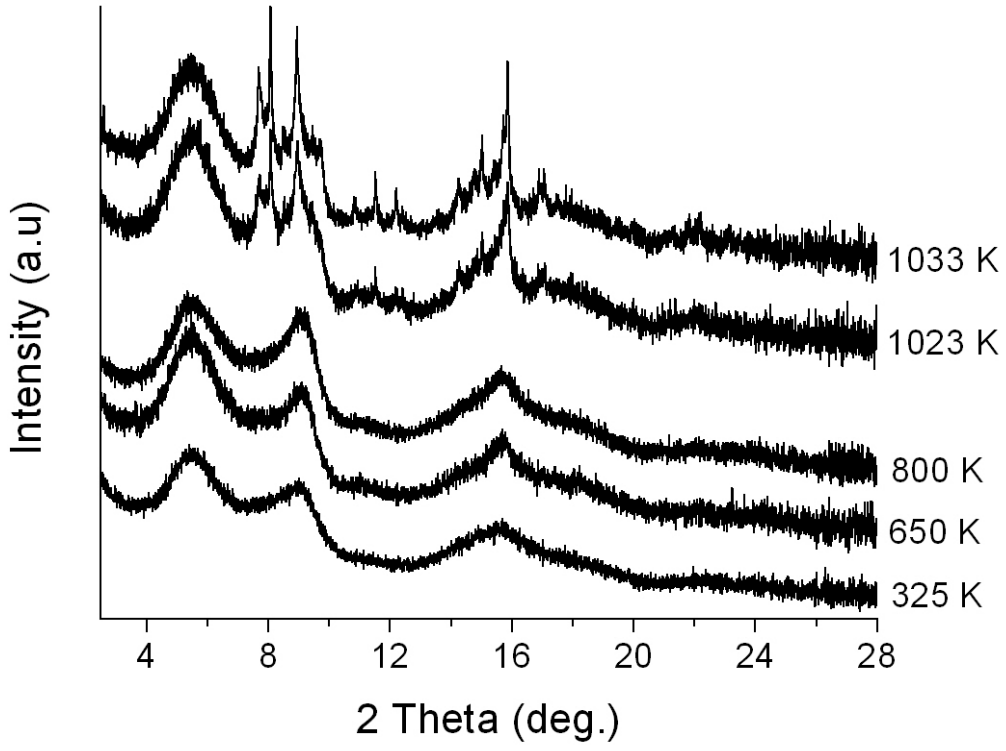

Figure 3.1 XRD patterns (synchrotron radiation, λ = 0.4 Å) for (GaON)1 ($Ga_{1.00}O_{1.55}N_{0.55}C_{0.13}$) collected at different temperatures. A crystallization of β-Ga_2O_3 and w-GaN is observed at and above 1023 K.

This XRD study has been continued here by a further study of the thermal stability of (GaON)1 (see Table 3.1). This investigation took place at the European Synchrotron

Radiation Facility (ESRF), Grenoble, France. The measurements were performed at ID31, The High-Resolution Powder Diffraction beamline (see Section 2.3.1.2). The ceramic was finely ground and put into quartz capillaries in a helium atmosphere. The sample was heated up to around 1100 K with a ramp of 300 K/min.
In Figure 3.1 XRD patterns collected at different temperatures are given. Up to around 1000 K, no characteristic lines were observed in the diffraction patterns. Above this temperature, the presence of monoclinic β-Ga_2O_3 and in a lesser amount w-GaN, started to appear. Considering the initial N/O ratio in the (GaON)1 ceramic of 0.35, and that the XRD shows the presence of a small amount of GaN with increasing temperature, the loss of nitrogen could be explained by a strong oxygen contamination of the ceramic before and/or during heating leading to predominantly Ga_2O_3-phase.

3.1.2 HP/HT synthesis of spinel-type gallium oxonitride

In this section HP/HT syntheses of the spinel-structured gallium oxonitride are presented. Using different high-pressure devices (DAC, multi-anvil press, and piston cylinder press), the spinel phase was synthesised via two different routes. The first route involved a solid state reaction between the hexagonal w-GaN and the monoclinic β-Ga_2O_3 under pressure and temperature, enabling a systematic investigation of the formation and stability field of the high-pressure oxonitride phase to be made. The second synthesis route involved a phase transition from nanocrystalline gallium oxonitride ceramics under pressure and temperature, which required less extreme conditions.

3.1.2.1 HP/HT synthesis from mixtures of gallium nitride and gallium oxide

Three different types of high-pressure device were used for the syntheses described in this section. A diamond anvil cell, multi anvil press and a piston cylinder device were employed for the syntheses of the high-pressure phase of gallium oxonitride from the two end members, w-GaN and β-Ga_2O_3.

3.1.2.1.1 Performing solid state chemical reactions in a DAC

Diamond anvil cell syntheses were performed using different mixtures of gallium oxide and gallium nitride. Ratios from 9/1 to 1/9 were loaded in different pressure media in order to obtain and investigate the spinel-structured gallium oxonitride. In this work three sets of DAC syntheses will be presented, with different aspects for the formation of HP/HT gallium oxonitride phase discussed in each case.

X-ray powder diffraction is one of the most commonly used methods in the study of solid state chemical reactions. Performing chemical reactions in DACs coupled with laser heating is not a trivial matter. There are several difficult aspects needed to be considered: on one side, the experimental technique itself and on the other side, the sample preparation, which limits the success of a solid state chemical reaction. For the cell preparation special care should be taken in choosing the gasket material, since at high-pressures and high-temperatures, the metal gasket might react with the sample. *In situ* laser-heating experiments coupled with x-ray diffraction are demanding, especially due to large temperature gradients within the laser heated spot. As discussed in Section 2.2.2, the diamonds have a high thermal conductivity; therefore the sample should not touch either of the diamond faces during the experiments. Poor insulation of the sample would lead to only partial heating or even no heating of the specimens.

Performing chemical reactions between two or more reagents which also should be loaded in DAC bring other impediments for a successful experiment. Since the sample chamber volume is so small, of the order of 10^{-5}-10^{-6} mm^3, the uncertainty of exact ratios of the mixed powders is high. *In situ* Raman spectroscopy has been proven to be a very useful technique to verify at least the presence of both powders (GaN and Ga_2O_3) in the sample chamber (see Section 2.3.3). The characteristic Raman active modes for the wurtzite GaN and the monoclinic Ga_2O_3 were observed prior to starting the HP/HT experiments. But the amount of each powder in the mixture loaded in a DAC was not possible to determine. Therefore, using LH-DAC does not give reliable information over the pressure (temperature) – composition stability range for the spinel gallium oxonitride phase. Nevertheless, valuable observations and results were obtained using this high-pressure technique, which will be described in the following section (3.1.2.1.2).

3.1.2.1.2 DAC synthesis

For one set of HP/HT experiments in a DAC, a thin pellet of a mixture of w-GaN and β-Ga_2O_3 in a molar ratio of 3/2 was loaded into a diamond anvil cell, with compressed nitrogen used as a pressure-transmitting medium [204]. After applying a pressure of 3 GPa and a temperature of about 1600 K, the *in situ* x-ray diffraction pattern exhibited the formation of a spinel-type gallium oxonitride phase (space group $Fd\bar{3}m$, No. 227), as well as residual w-GaN. The experiment performed at 1.3 GPa using the same starting mixture showed no formation of gallium oxonitride. This result implies that for the synthesis of spinel-structured gallium oxonitrides using nitride and oxide mixtures with a molar ratio of 3/2 the low-pressure limit ranges between 1.3 and 3 GPa. The dependence of the enthalpy of formation as a function of pressure of the spinel-type gallium oxonitride has been theoretically studied by Kroll [132]. At the phase transition of gallium oxide from the monoclinic crystal system (β-Ga_2O_3) to the rhombohedral corundum structure (α- Ga_2O_3) at 2.6 GPa, the enthalpy of formation of the oxonitride is predicted to be minimal. Therefore, the syntheses of spinel-type gallium oxonitride by the solid state reaction of gallium nitride with gallium oxide have a maximum driving force at the β to α transition in gallia. Accordingly, the experimental results presented in this work which display the formation of the spinel-type gallium oxonitride at 3 GPa are in good agreement with the theoretical predictions [132]. The pressure of 3 GPa is the lowest measured pressure to date at which the spinel gallium oxonitride has been synthesized from different w-GaN/β-Ga_2O_3 mixtures under high-pressure and high-temperature synthesis conditions in a DAC.

The same molar ratio, 3/2, GaN/Ga_2O_3 was used in a different set of DAC syntheses, also loaded in nitrogen as the pressure medium. *In situ* x-ray diffraction was used to monitor the formation of the spinel-structured gallium oxonitride and the behaviour of the starting materials during compression and decompression of the cell (see Figure 3.2 A and B). The cell was initially compressed to 1.3 GPa and then laser heated to ~ 1600 K from both sides of the cell for 15 minutes. The diffraction patterns (Figure 3.2 A) show no sign of reaction between the two adducts. This measurement confirms the assertion that below 3 GPa the gallium oxonitride phase does not form.

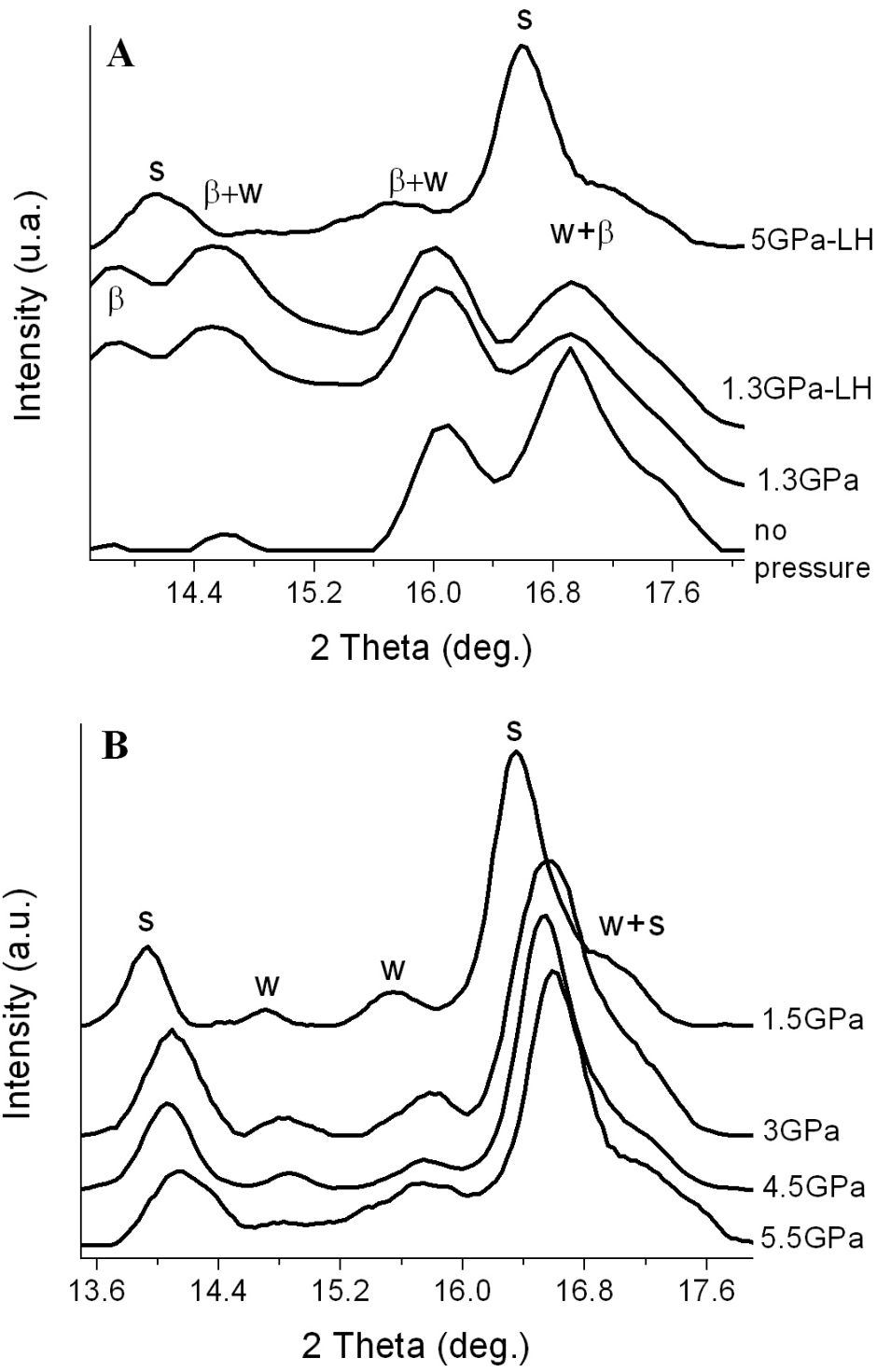

Figure 3.2 X-ray diffraction patterns (Mo-K_α=0.7108 Å) from an in situ LH-DAC being compressed up to 5 GPa and laser heated twice, at 1.3 GPa and 5 GPa **(A)**; the patterns show the presence of the initial materials, w-GaN (w) and β-Ga_2O_3 (β) up to 1.3 GPa-LH, and the formation of the spinel-type gallium oxonitride (s) at 5 GPa-LH .

In **(B)**, the XRD patterns from the LH-DAC are shown during decompression from 5.5 GPa to 1.5 GPa. During decompression the spinel phase stays stable up to the lowest measured pressure, 1.5 GPa.

Increasing the pressure up to 5 GPa and maintaining the same temperature via laser heating, the Bragg reflections of spinel gallium oxonitride appeared as well as the ones from the w-GaN, formed as a side-product. Another interesting observation is that as soon as the spinel gallium oxonitride forms at high-pressure and high-temperature, β-Ga_2O_3 reacts with w-GaN or transforms into the high-pressure phase α-Ga_2O_3, corundum type. During the decompression (Figure 3.2 B) the spinel phase of gallium oxonitride stayed stable until room pressure, showing no distortions or decomposition whatsoever.

A third set of HP/HT syntheses was performed using a mixture of 9/1 molar ratio of GaN/Ga_2O_3 and loaded in a DAC. The pressure was increased up to 20 GPa and then laser-heated up to ~ 1600 K. The *in situ* x-ray diffraction pattern (see Figure 3.3) revealed the presence of the spinel gallium oxonitride phase, GaN and the high-pressure phase of gallium oxide, α-Ga_2O_3, corundum-type structure. Also, a strong Bragg reflection from the diamond appears in the pattern, which is most probably due to a crack in one of the anvils. The small amount of the synthesised gallium oxonitride can be explained also by the fact that no pressure medium was used in this experiment. Hence, the heat was easily conducted through the diamonds. Still, a sign of a chemical reaction was observed also during the heating: the sample became black while the laser beam was scanning the sample chamber.

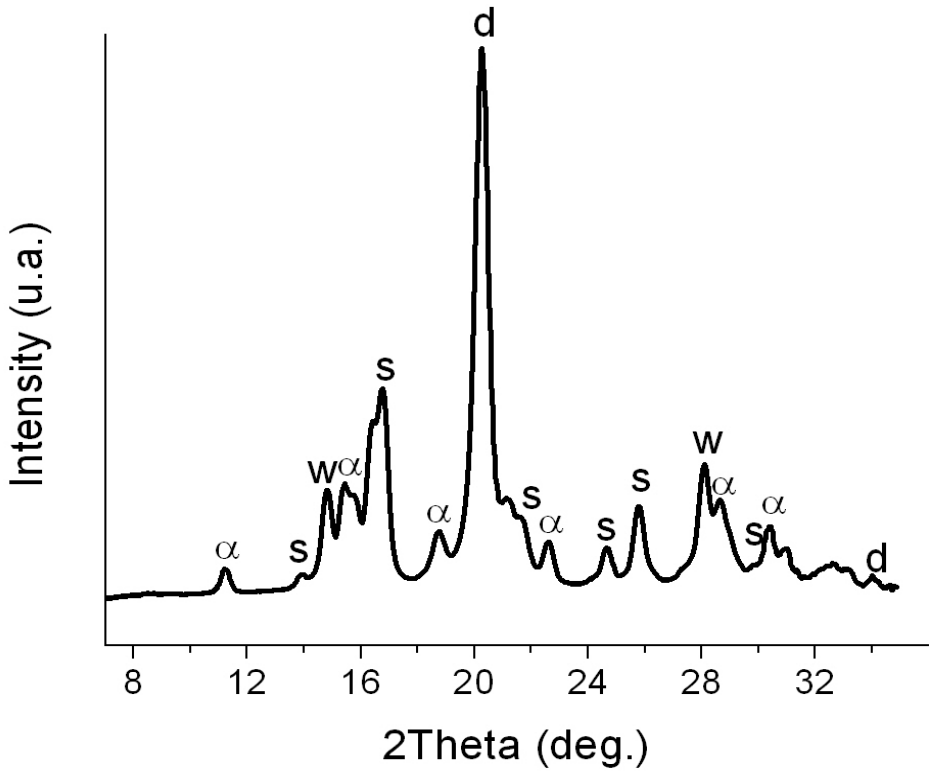

Figure 3.3 X-ray diffraction pattern (Mo-K_α=0.7108 Å) from an in situ LH-DAC at 20 GPa and ~ 1600 K, showing the spinel-type gallium oxonitride (s), the starting materials, w-GaN (w) and the high-pressure phase, α-Ga_2O_3 (α). (d) states for diamond reflections.

This experiment reveals that not even at 20 GPa and 1600 K, the full transformation or recovery of the spinel-structured gallium oxonitride could be completed. Soignard *et al.* performed a similar experiment and have also observed that even when the temperature is increased above 2300 K, the starting materials can still be identified in addition to the products [135]. Their starting material was a mixture of GaN (99.99 %) and Ga_2O_3 (99.99 %, containing a mixture of α + β phases) in a 1/1 molar ratio and was loaded with nitrogen as pressure medium in a DAC. They compressed their cell up to 10 GPa and laser-heated to peak temperatures in excess of 2300 K.

Both the work described here and the work by Soignard *et al.* emphasise the importance of temperature for the HP/HT syntheses of the spinel-type gallium oxonitride. Kroll suggested a temperature around 2000 K for the spinel gallium oxonitride to form [132], but by applying a considerable pressure, the needed temperature for the synthesis can be shifted to much lower values.

3.1.2.1.3 Piston cylinder synthesis

Since the diamond anvil cell syntheses revealed the formation of gallium oxonitride at pressures as low as 3 GPa, a piston cylinder press was employed in order to obtain a larger sample volume for further investigations of the material. Pressures were varied from 2 to 3 GPa and temperatures between 1400 – 1800 K. The compression and heating schedules for the piston cylinder experiments are shown in Figure 3.4. In addition to pressure and temperature, there were three main parameters which were varied during the experiments, in order to obtain the spinel-phase of gallium oxonitride from the two end members. In Table 3.2 a summary is given of the syntheses performed with the corresponding experimental conditions.

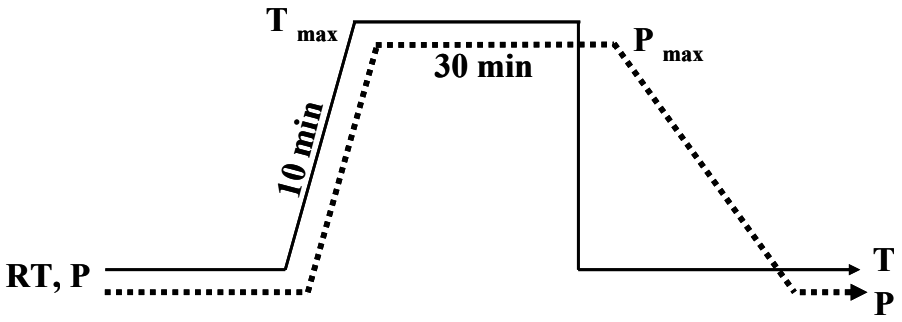

Figure 3.4 General compression and heating schedules for the piston cylinder experiments.

Previous multi-anvil press experiments showed that molar ratios 7/3 and 3/2 of the starting powders were most favourable for the synthesis of the spinel-type gallium oxonitride (see Section 3.1.2.1.4). Therefore these two mixtures of GaN/Ga_2O_3 were chosen for the piston cylinder syntheses, which were loaded in different capsule materials (BN, Au, Pt). The recovered samples were analysed using *in-house* x-ray diffraction (see Section 2.3.1.1). Millimetre size sample fragments were isolated and glued on the top of quartz capillaries. The experiments which were performed in BN capsules at 3 GPa and temperatures between 1500 and 1800 K led to no reaction between the starting materials. Although phase separations or only the presence of β-Ga_2O_3 was observed, no gallium oxonitride phase appeared.

Table 3.2 Summary of piston cylinder syntheses starting from different mixtures of GaN and Ga_2O_3 loaded under different experimental conditions.

GaN/Ga_2O_3 Molar ratios	Capsule material	Pressure (GPa)	Temperature (K)	Pressure medium	Products
7 / 3	BN	3	1500	-	β-Ga_2O_3, w-GaN
	BN	3	1600	-	w-GaN, β-Ga_2O_3
3 / 2	BN	3	1600	-	w-GaN, β-Ga_2O_3
	BN	3	1800	-	w-GaN, β-Ga_2O_3
	Pt	2	1800	N_2	w-GaN, β-Ga_2O_3
	Au	2	1400	N_2	β-Ga_2O_3

These results led us to the conclusion that an external nitrogen source would be needed which would also play a role of the pressure medium. Therefore, mixtures of 3/2 molar ratios of GaN/Ga_2O_3 were loaded in Pt or Au capsules, filled with nitrogen and sealed. None of these experiments showed any reaction between the loaded nitride and oxide. This may have been due to a problem with the sealing of the capsules, insufficient nitrogen loaded and/or the uni-axial pressure distribution in the sample assembly. Further iterations of this synthesis method may still lead to gallium oxonitride formation.

3.1.2.1.4 Multi anvil press synthesis

In parallel with the diamond anvil cell and piston cylinder experiments, a systematic investigation of the formation of spinel-structured gallium oxonitride was performed in collaboration with our project partners, Prof. Hubert Huppertz's group from Ludwig-Maximilians-University, Munich. Molar ratios of wurtzite-structured GaN and monoclinic Ga_2O_3 from 1/9 till 9/1 were used as starting materials for multi anvil press syntheses of spinel-type gallium oxonitride [205].

The pressure conditions ranged from 1.0 GPa up to 11.5 GPa in small steps of 0.5, 1.0 or 2.5 GPa. In addition to the systematic pressure investigations, the influence of temperature on the formation of the gallium oxonitride spinel phases and their decomposition was examined. Also the heating protocols were varied to see if there were differences in the sample formation, yield, or the degree of crystallinity of the spinel phase, depending on a long or short heating protocol, a slow or fast cooling, or an annealing phase. A distinction was also drawn between long-term heating periods, with heating segments of about 1 h and long annealing phases of 3 – 5 h. Shorter heating protocols were also applied, with heating up in about 10 min, maintaining the maximum temperature for 15 – 25 min, followed by an annealing phase of about half an hour. Another special program contained two annealing phases at lower temperatures, a first one at 500 K, holding the temperature there for 5 – 10 min, and then increasing it afterwards to a maximum temperature of 900 – 1000 K. The standard heating program comprised three relatively equal heating sequences, *viz.* heating up in 5 – 10 min, holding the temperature for at least 10 – 20 min, and cooling down to a lower temperature (approximately 1100 – 1400 K) in about 5 – 15 min.

The formation of the gallium oxonitride phase was observed from 2.5 up to 8 GPa and 1500 up to 1650 K. The increase of pressure up to 11.5 GPa at 1500 K led to samples containing cubic spinel-type material with a low degree of crystallinity. The temperature protocols had a remarkable influence on the fraction of the spinel phase. The degree of crystallinity could be improved by high heating rates and short holding times, for example upon heating up the mixture in 10 min to 1550 K, holding the temperature for 15 min, and cooling down to 1100 K in 25 min. In the experiments with temperatures exceeding 1600 K, but pressures as low as 2 and 3.5 GPa, metallic gallium formed as a decomposition product, and no spinel-structured gallium oxonitride appeared. A decrease of the initial temperature below 1300 K at all pressures led to samples consisting of the educts w-GaN, β-Ga_2O_3, or the high-pressure modification α-Ga_2O_3.

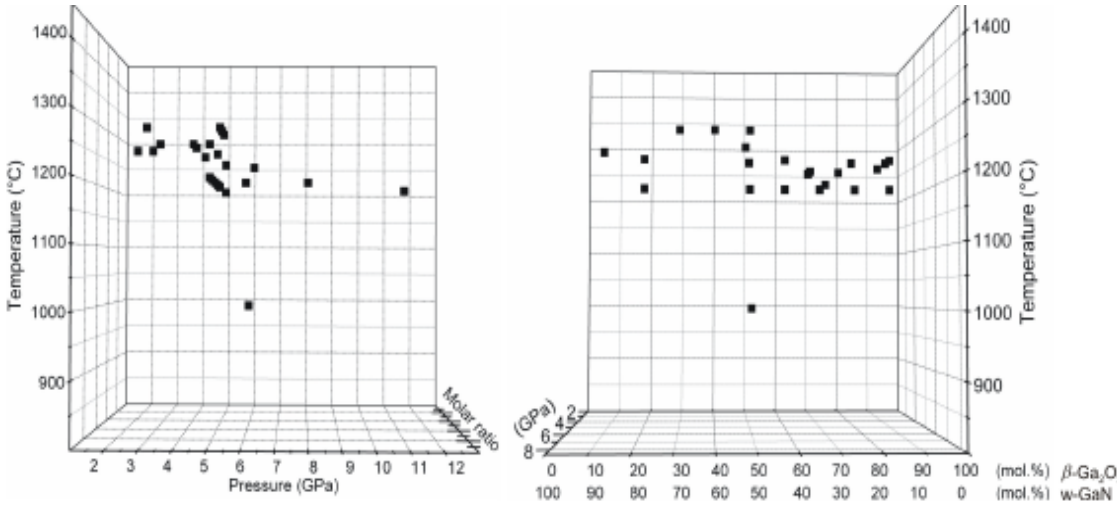

Figure 3.5 Survey of the products leading to the spinel-type gallium oxonitrides in dependence of pressure, temperature, and molar ratio of the starting materials, w-GaN and β-Ga_2O_3 [205].

Figure 3.5 gives a survey of the experiments to produce spinel-type gallium oxonitrides. The figure illustrates the effects of pressure, temperature, and molar ratio of the starting mixture on the syntheses of the spinel gallium oxonitride. The left side of the figure provides an overview of the pressure and temperature conditions; the right side shows the same results, rotated by 90°, to expose the corresponding molar ratios of the starting mixtures. In the figure information is not included about heating protocols, remaining educts (w-GaN and β -Ga_2O_3), or the high-pressure phase of gallium oxide, α-Ga_2O_3.

From Figure 3.5 it can be concluded that the spinel-type gallium oxonitride can by synthesized in a wide range of pressures, from 2.5 GPa up to 11.5 GPa and temperatures between 1300 K and 1650 K. The ratio of the starting mixture in the investigated system was not decisive for the formation of the spinel-type structure. All the experiments, having as starting materials molar ratios of w-GaN/β-Ga_2O_3 from 9/1 to 1/9, resulted in the formation of the spinel structured phases, obtained by experiments which were performed under identical conditions.

3.1.2.2 HP/HT synthesis from gallium oxonitride ceramics

Gallium oxonitride ceramics have also been used as precursors for the HP/HT synthesis of crystalline gallium oxonitride phases, as they have the advantage of the

gallium being directly bonded to predefined amounts of nitrogen and oxygen atoms on atomic level. Diamond anvil cells and piston cylinder devices were employed for the syntheses.

3.1.2.2.1 DAC synthesis and in situ characterisation

One of the synthesised gallium oxonitride ceramics, (GaON)2, used in the high-pressure experiments, exhibited an N/O ratio equal to 1.15 determined by elemental analysis. The ratio is calculated from the chemical formula $Ga_{1.00}O_{0.72}N_{0.83}C_{0.22}$ (see Table 3.1).

The diffraction pattern showed that the material is x-ray amorphous, similar to that observed in the low temperature data in Figure 3.2. The sample loaded in a LiF pressure-transmitting medium was compressed to 1 GPa and afterwards laser-heated to around 1600 K [204]. After heating, the pressure dropped to 0.7 GPa. The *in situ* x-ray diffraction pattern of the heated sample displayed crystalline spinel-type gallium oxonitride (see Figure 3.6), in addition to Bragg reflections from the pressure medium LiF. No by-products were found in the recovered samples, as was the case in the HP/HT syntheses of spinel-type gallium oxonitride starting from mixtures of w-GaN and β-Ga_2O_3 (discussed earlier in Section 3.1.2.1.2).

The end member mixtures gave under HP/HT the spinel phase of gallium oxonitride at minimum 3 GPa in a DAC (see Section 3.1.2.1.2) and minimum 2.5 GPa in a multi-anvil press (see Section 3.1.2.1.4). The single source gallium oxonitride ceramics allowed the formation of the spinel gallium oxonitride at even much lower pressures, below 1GPa.

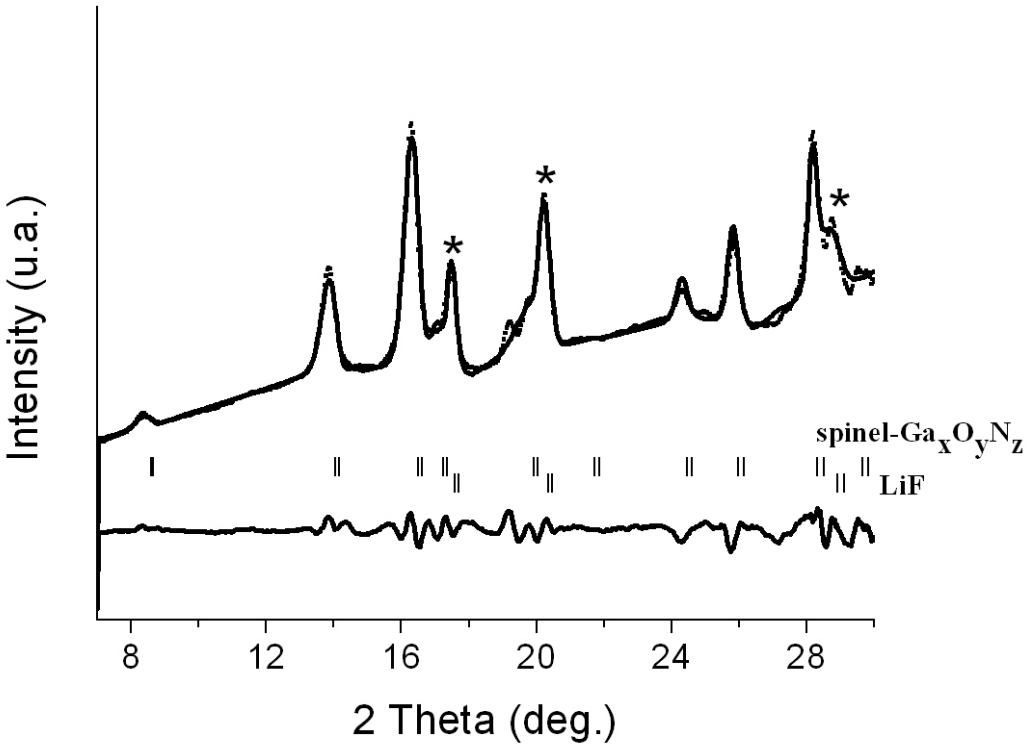

Figure 3.6 X-ray diffraction pattern (Mo-K_α=0.7108 Å) collected *in situ* of the spinel-structured gallium oxonitride and LiF (labeled with *) during LH-DAC synthesis (0.7 GPa, 1600 K). The experimental data points are shown as a dotted line and the fit to the data as a solid line. The reflection at 2θ 19.3 ° is attributed to the gasket material Re.

The cell parameter of the spinel phase derived from a Rietveld refinement of the *in situ* obtained diffraction pattern was a_0 = 8.2042(1) Å. After decompression, the value of the cell parameter of the recovered spinel-structured phase was 8.2095(8) Å. The experimental values of lattice parameters of the spinel-structured gallium oxonitride reported so far range between 8.200(7) and 8.280(1) Å [115, 206], and the calculated values for the ideal spinel-structured gallium oxonitride are between 8.228 and 8.267 Å (LDA) and 8.425 Å (GGA) [130, 133]. The lattice parameter of spinel-type γ -Ga_2O_3 has been found to be 8.238(6) Å [67], which is lower than the experimental values for the gallium oxonitride but close to the value analyzed for the material synthesized in the DAC. However, the formation of γ -Ga_2O_3 can be excluded because:

- γ -Ga_2O_3 is a metastable compound which was synthesized by calcination (at 800 K) of a gallia gel [67, 68], transforming into β-Ga_2O_3 at elevated temperatures

- nitrogen serves as stabilizer in the spinel structure proven for γ -aluminum oxynitride phases [21], which are analogous to gallium oxonitride
- (c) the diffraction patterns of the products displayed no presence of unreacted gallium nitride next to gallium oxide.

In situ Raman study

In Figure 3.8 a Raman spectrum from an *in situ* DAC synthesis is shown. The sample was compressed to 3.75 GPa and laser heated up to around 1600 K. The five corresponding modes for the spinel structure can be identified at around 285, 440, 530, 675 and 780 cm^{-1}. In the same figure there are also given the calculated Raman-active modes for ideal Ga_3O_3N from the work of Soignard *et al.* [135]. These calculated values were obtained considering a small rhombohedral distortion from the ideal cubic structure which was found with the lowest equilibrium energy. Thus, it was considered to provide the ground state configuration of Ga_3O_3N in their theoretical study. This pseudocubic *R*3*m* structure is predicted to have nine Raman-active modes from which the five modes for the spinel symmetry were derived.

In Table 3.3 a comparison is showed with other reported spinels, providing independent support to the work discussed here.

Table 3.3 Raman-active modes for the spinel-structured gallium oxonitride synthesised at 3.5 GPa and 1600 K. A comparison with other different spinel compounds is given.

Symmetry	**$Ga_xO_yN_z$** exp. this work	**Ga_3O_3N** Cal. [135]	**γ-Si_3N_4** expt. [191]	**γ-Si_3N_4** cal. [207]	**γ-Ge_3N_4** expt: [208]	**γ-Ge_3N_4** cal: [208]
T_{2g}	285	216	-	413	325	245
E_g	440	373	519	518	472	467
T_{2g}	530	506	729	500	593	576
T_{2g}	675	640	840	838	730	710
A_{1g}	780	782	975	946	858	830

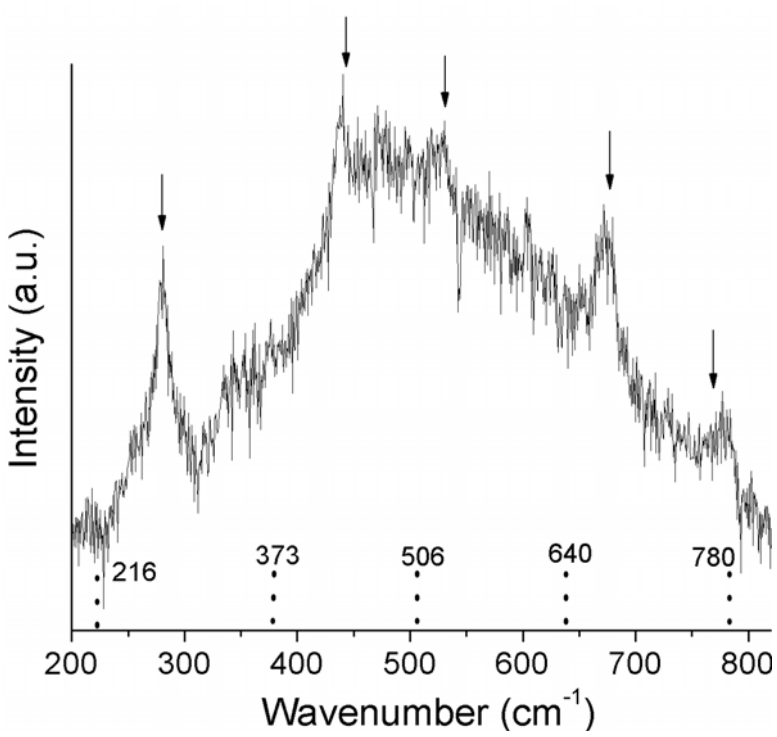

Figure 3.7 Raman spectrum collected from an in situ DAC at 3.75 GPa and laser heated at around 1600 K. The dotted lines indicate the active Raman modes calculated for an ideal Ga_3O_3N by Soignard et al. [135].

As it can be observed in the Figure 3.7, the experimental values are in reasonable agreement with the calculated ones [135] for the high-pressure phase of gallium oxonitride. All the Raman modes are shifted towards higher frequencies, the octahedral corresponding modes being shifted more then the tetrahedral ones. These shifts might be due to the presence of a smaller amount of nitrogen in the structure.
In addition, the Raman spectrum contains broad background features which affect also the intensity of the observed modes. The broad background is due to the intense fluorescence from the diamonds and from the sample itself. The broadness of the Raman modes is probably due to the N/O disorder within the spinel structure, and to the vacancies on the cationic and probably anionic sites [135]. Even so, with a longer accumulation time, the signal to noise ratio could have been improved.

In summary, Soignard *et al.* reported the only experimental Raman spectrum from the high-pressure phase of gallium oxonitride [135]. Comparing with the spectrum reported in this work, the Raman shifts are less well defined, being broad and suppressed by a considerable background.

3.1.2.2.2 Piston cylinder synthesis

As discussed in Section 3.1.2.2.1, DAC loaded with single-source precursor-derived (GaON) ceramics gave the spinel phase of gallium oxonitride at pressures as low as 1 GPa. Therefore, different ceramics were used as starting materials for high-pressure, high-temperature syntheses using a piston cylinder press. Different types of experiments were conducted in order to get the phase of interest as pure as possible. In this paragraph we will discuss two experiments performed at different pressures, temperatures, and in different sample environments.

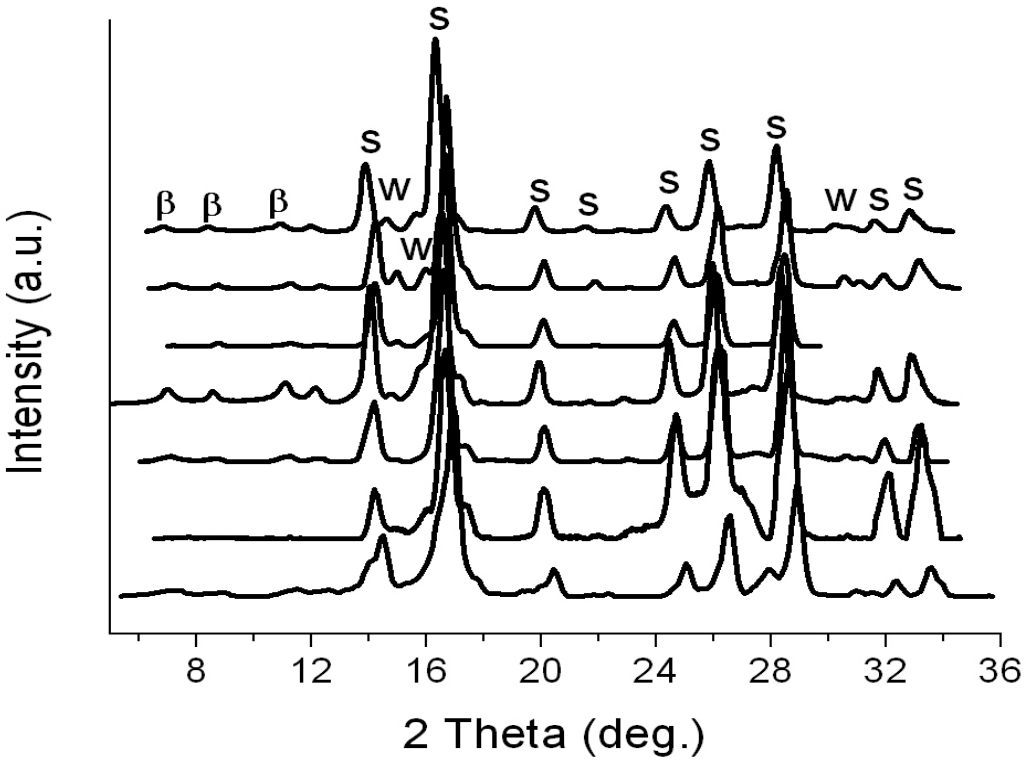

Figure 3.8 X-ray diffraction patterns (Mo-K_α=0.7108 Å) from spinel $Ga_xO_yN_z$ synthesised in a piston cylinder press at 1.9 GPa and 1600 K. Different patterns correspond to different pieces of the reaction mixture separated from the same synthesised bulk. As well as the spinel phase (s), Bragg peaks which originate from w-GaN (w) and β-Ga_2O_3 (β) can be observed.

A gallium oxonitride ceramic with a chemical formula $Ga_{1.00}O_{0.89}N_{0.71}C_{0.26}$, labeled in this work as (GaON)4, was loaded in a Pt capsule (5 mm length and 2 mm diagonal). Before sealing the capsule, nitrogen was also loaded next to the sample. The capsule was compressed to 1.9 GPa and heated up to 1600 K using a S-type thermocouple (Pt-

10% Rh, temperature range 0 – 1750 K). The compression-heating program is the same as shown in Figure 3.4: the high-pressure assembly was compressed to 1.9 GPa, keeping the pressure stable during heating; the maximum temperature was reached in 10 minutes, hold at 1600 K for 30 minutes and then quenched to room temperature.

After the recovery of the sample, different parts were isolated and glued on top of quartz capillaries for x-ray investigation. In Figure 3.8, x-ray diffraction patterns collected from the investigated sample pieces are shown. As can be observed, in addition to the spinel-type gallium oxonitride, w-GaN and in a much smaller amount, β-Ga_2O_3 were also present as side products. It was possible to isolate almost pure gallium oxonitride from the bulk, as it had a darker-grey colour compared with the other investigated pieces.

In a different experiment, one of the synthesised gallium oxonitride ceramic was used for the HP/HT synthesis of the spinel-structured $Ga_xO_yN_z$. From the elemental analyses, the ceramic was found to have the chemical formula $Ga_{1.00}O_{0.72}N_{0.83}C_{0.22}$ with a N/O ratio of 1.15, being labelled in this work as (GaON)2. The powder was loaded this time in a BN capsule, with no external nitrogen loading. The high-pressure assembly was compressed to 2 GPa and heated to 1600 K using the same temperature-pressure schedule as discussed above.

After sample recovery, several pieces were isolated for x-ray diffraction. The XRD pattern of one of the isolated samples displayed crystalline spinel-type gallium oxonitride with the lattice parameter a_0 = 8.1336(30) Å (see Figure 3.9), as well as Bragg reflections of w-GaN produced as a side product. All the investigated samples from the bulk showed similar results. As discussed in Section 3.1.2.2.1, gallium oxonitride was recovered from a LH-DAC synthesis with a cell parameter of 8.2095(8) Å. The spinel phase synthesised in a piston cylinder press assembly at 2 GPa showed an even lower cell parameter. For the both syntheses the same ceramic was used, (GaON)2, with the composition $Ga_{1.00}O_{0.72}N_{0.83}C_{0.22}$.

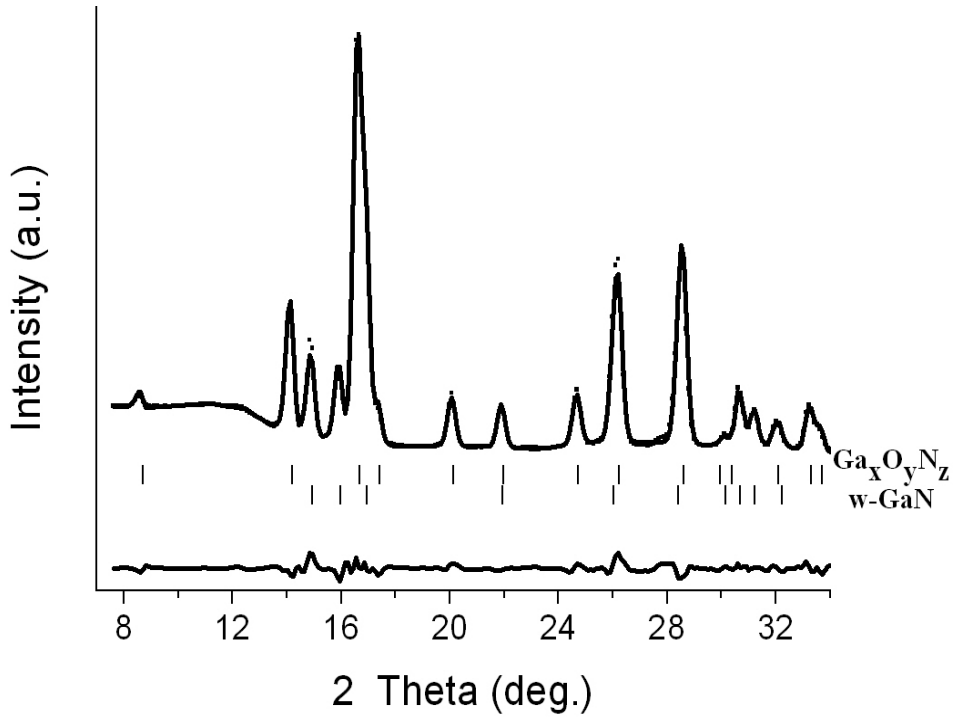

Figure 3.9 Powder XRD pattern (Mo-K_α = 0.7108 Å) from a piston cylinder synthesis of spinel-type $Ga_xO_yN_z$ and w-GaN as side product: measured (circles) and calculated (solid line) intensities. The difference curve is given at the bottom of the graph. The calculated peak positions of the two phases are denoted by tick marks. Starting material was $Ga_{1.00}O_{0.72}N_{0.83}C_{0.22}$ ceramic, compressed at 2 GPa and heated at 1600 K.

Huppertz *et al.* established that a linear dependency of the cell parameters for the spinel-type gallium oxonitride with an increasing ratio N/O is questionable [206]. The presence of vacancies on cationic and anionic sites within a spinel-type structure has a noticeable impact on the size of the unit cell, reducing it to a smaller size then expected. Even so, all the reports on spinel-gallium oxonitride show that increasing the nitrogen amount in the structure leads to an increase of the cell parameters. McCauley *et al.* discussed the same tendency of the cell parameters of the spinel phase of aluminium oxynitride with the nitrogen content [209]. It can be concluded, therefore, that one of the reasons for obtaining the high-pressure phase of gallium oxonitride with a smaller cell parameter is due to the reduced amount of nitrogen within the structure.

Another important element to consider is the presence of carbon in the gallium oxonitride ceramics used as starting materials for the high-pressure syntheses. Raman spectroscopy was unable to observe any presence of free carbon in the high-pressure products. This finding may be due to that there was genuinely no free carbon after the

high-pressure, high-temperature syntheses, or alternatively the Raman-active modes for free carbon (D and G modes) were suppressed by a considerable fluorescence background.

Table 3.4 Comparison of the cell parameters of γ-Ga_2O_3 and gallium oxonitride phases with a spinel-type structure.

Phase	N/O	Lattice parameter, a_0 (Å)	Ref.
γ-Ga_2O_3	-	8.22; 8.238(6); 8.2243 (GGA); 8.0748 (LDA)	[67, 69, 131, 210]
$Ga_{22}O_{30}N_2$	0.06	8.2714 (GGA); 8.1201(LDA)	[131, 210]
$Ga_{2.81}O_{3.57}N_{0.43}$	0.12	8.264(1)	[134]
$Ga_{2.8}O_{3.5}N_{0.5}$	0.14	8.200(7)	[115]
$Ga_{23}O_{27}N_5$	0.185	8.2981 (GGA); 8.1488 (LDA)	[131, 210]
$Ga_{2.8}O_{3.24}N_{0.64}$	0.20	8.281(2)	[135]
$Ga_{2.79}O_{3.05}N_{0.76}$	0.25	8.280(1)	[206]
Ga_3O_3N	0.33	8.200(7); 8.3261 (GGA); 8.1763 (LDA)	[130, 131, 210]

In the hypothesis that there was no free carbon in the final HP/HT products, it is expected that the initial carbon was incorporated into the spinel structure of gallium oxonitride by substituting oxygen or nitrogen, and causing in this way the decreasing of the cell parameters.

In summary, the two piston cylinder syntheses presented in this work have proven that by using a gallium oxonitride ceramic as the starting material for high-pressure syntheses of spinel-type gallium oxonitride, there is no need for an external nitrogen source.

To conclude, in Section 3.1 were presented the high-pressure, high-temperature syntheses of the spinel-type gallium oxonitride. Two different starting materials were used leading to important insights about the pressure/temperature conditions for the syntheses of the gallium oxonitride phases. Using different molar ratios of GaN /

Ga_2O_3, the spinel-structured gallium oxonitride formed in a diamond anvil cell at pressures as low as 3 GPa and temperatures around 1600 K (see Section 3.1.2.1.2). Increasing the pressure up to 20 GPa, the full transformation/recovery of the spinel phase could not be achieved. The multi anvil press device gave the target phase at pressures starting with 2.5 GPa till 11.5 GPa and temperatures above 1300 K (see Section 3.1.2.1.3). Molar ratios from 1/9 till 9/1 of the two end members gave oxonitride phases in a wide pressure-temperature range.

Gallium oxonitride ceramics show a phase transition to a crystalline, spinel-structured gallium oxonitride at pressures of 0.7 GPa in a diamond anvil cell (see Section 3.1.2.2.1). No by-products were observed in all the diamond anvil syntheses having as starting material the (GaON) ceramic. In order to obtain bigger amounts of the spinel phase, a piston cylinder press was used (see Section 3.1.2.2.2). In this case, GaN was also observed in the final product, but the spinel gallium oxonitride was possible to isolate having a darker colour and having a higher density than that of the nitride.

3.2 Gallium oxide polymorphs under high-pressure

The spinel-type gallium oxonitride was predicted by Kroll to have a favourable energy of formation from GaN and β-Ga_2O_3 at the β-to-α phase transition of gallia [132] (discussed also in Section 3.1.2.1.2). On the other hand, the multi anvil press syntheses of gallium oxonitride from different mixtures of w-GaN, β-Ga_2O_3 have shown that β-Ga_2O_3 transforms into the corundum phase at a pressure of 2 GPa and a temperature of 1600-1800 K, in the presence of w-GaN [205]. A reaction mechanism which takes place under extreme conditions is not a trivial problem to solve. The study of different gallium oxides under pressure would therefore provide new and important insights for a better understanding of the spinel-type gallium oxonitride formation. Hence, a separate HP/HT study of gallium oxide phases was required and is now reported in the following section.

In the present section a high-pressure, high-temperature investigation of different polymorphs of gallium oxide is presented. In the first section the synthesis of the spinel-type gallium oxonitride from the cubic γ-Ga_2O_3 is discussed. The oxide was loaded in a DAC next to nitrogen, as a reagent and also as pressure medium. In the second section the phase transition of β-Ga_2O_3 into α-Ga_2O_3 under high-pressure and temperature is described. The experiments were performed also in DACs using N_2 as the pressure medium.

3.2.1 HP/HT syntheses of spinel gallium oxonitride from the cubic γ-Ga_2O_3

γ-Ga_2O_3 powder was synthesised by calcinations of a gallia gel at 600 K [211]. In Figure 3.10 the x-ray diffraction pattern of the calcinated sample is given. The reflections were fitted with a spinel-type structure, with a low degree of crystallinity.

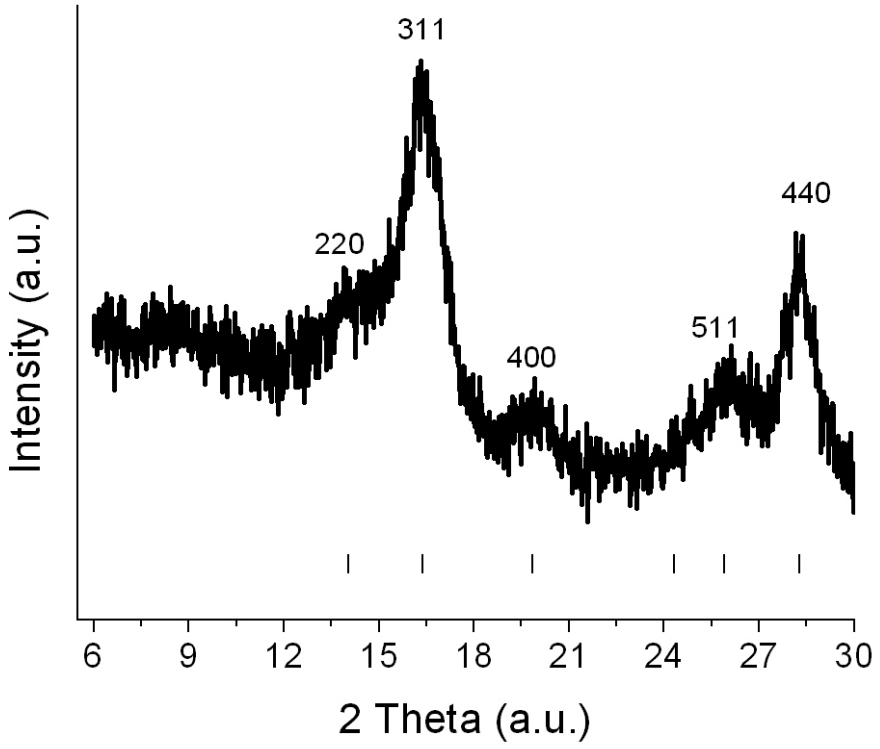

Figure 3.10 *Ex situ* powder x-ray diffraction pattern (Mo-K_α=0.7108 Å) of γ-Ga_2O_3. The reflections were fitted to the reference spinel γ-Ga_2O_3 from ICDD data base (020-0426).

A thin pellet of nanocrystalline γ-Ga_2O_3 powder was pressed and loaded in a diamond anvil cell using nitrogen as the pressure medium. *In situ* x-ray diffraction and Raman spectroscopy were used to monitor the HP experiments. The cell was slowly compressed up to 4.2 GPa without any change being observed. The diffraction pattern from the sample at room pressure and temperature showed reflections coming from nitrogen (β phase [212]) and rhenium, the gasket material (see Figure 3.11). As mentioned above, the starting material is a nanocrystalline γ-Ga_2O_3 powder; hence the diffraction pattern shows a mostly amorphous phase. Even so, a cubic γ-Ga_2O_3 phase with a $Ia\bar{3}$ (No. 206) symmetry could be better fitted than a $Fd\bar{3}m$ (No. 227) one.

After laser heating the cell (1300 – 1800 K) a clear phase transition from γ-Ga_2O_3, (the cubic phase) to the high-pressure stable phase of gallium oxide, α-Ga_2O_3 was observed. More interestingly, in addition to the α-Ga_2O_3 phase, a spinel-structured phase also appeared. The cell was further compressed up to a pressure of 10.7 GPa, at which point it was laser heated again. No structural changes have been observed up to

the maximum pressure reached in this work as well as during cell decompression. In Figure 3.11 the phase transition at 4.2 GPa-LH is shown with the appearance of a cubic phase (labelled as γ) and the corundum-type α-Ga_2O_3 (labelled as α). The diffraction pattern from the recovered sample is also given, showing the stability of the two phases at room conditions. Here, and through all the high-pressure experiments reported in this work, a recovered sample denotes that the cell was completely decompressed, and then opened. The sample remains in the initial pressure chamber, only an anvil is removed for the x-ray diffraction experiment.

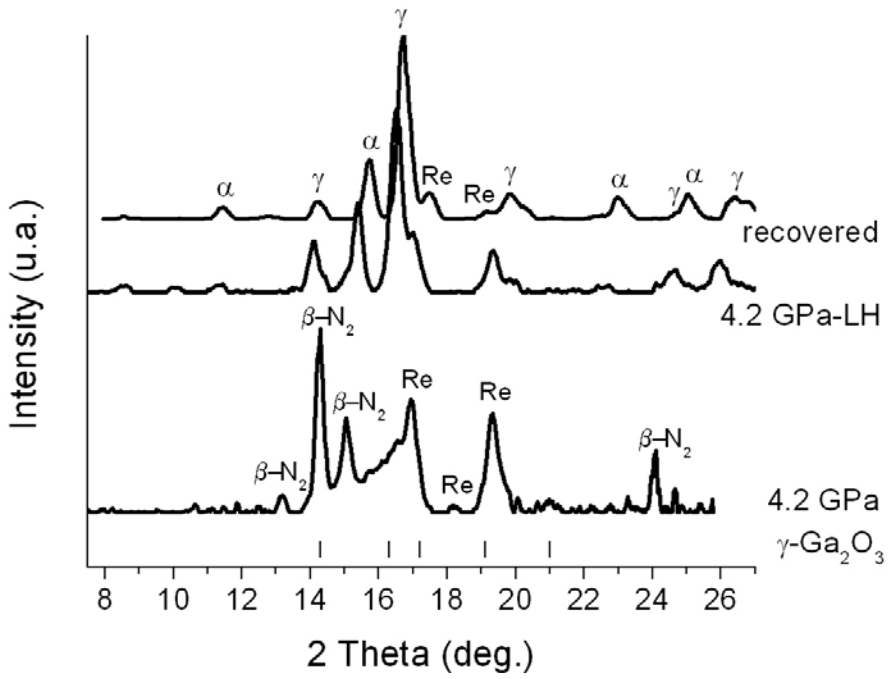

Figure 3.11 XRD patterns (Mo-K_α=0.7108 Å) from *in situ* DAC experiments. The starting material is a nanocrystalline γ-Ga_2O_3 pellet loaded with N_2. The Bragg positions from γ-Ga_2O_3 ($Ia\bar{3}$ space group) are shown. At 4.2 GPa a crystalline N_2 phase is present, with a hexagonal-type structure (β-N_2). After laser heating (4.2 GPa-LH) the corundum-type α-Ga_2O_3 (labelled as α) and a spinel-type (labelled as γ) phase appeared.

Concerning the spinel-phase which appeared after laser heating, and knowing that one of gallium oxides polymorphs has a spinel-type structure, it was assumed initially that the synthesised phase is indeed γ-Ga_2O_3. But, as mentioned also in the beginning of this section, γ-Ga_2O_3 has been shown to be a metastable phase that is highly porous which is obtained at temperatures around 800 K and transforms into the β phase at lower temperatures. Another helpful piece of information came from the *in situ*

Raman investigations, which also casts doubt on the hypothesis of a stable cubic gallium oxide formation at high-pressures.

Nitrogen Raman active modes appeared in all the spectra collected up to 4.2 GPa, (see Figure 3.12) shifting with increasing pressure towards smaller frequencies. After laser heating at 4.2 GPa, once the appearance of the spinel phase occurred, no Raman shift was detected for nitrogen. The disappearance of nitrogen in the same time with the formation of the spinel phase was also observed in the x-ray diffraction patterns (see Figure 3.11). Since the diamond anvil cell is a closed system, the nitrogen could only react inside the cell. This observation strongly supports the conclusion that the spinel phase formed was gallium oxonitride with a cell parameter a = 8.262(4) Å and not γ-Ga_2O_3. The result also complements the findings discussed in Section 2.2.2.1 concerning the DAC syntheses of the spinel-type gallium oxonitride from (GaON) ceramics. Once incorporated into the structure, nitrogen is a stabiliser for the spinel phase.

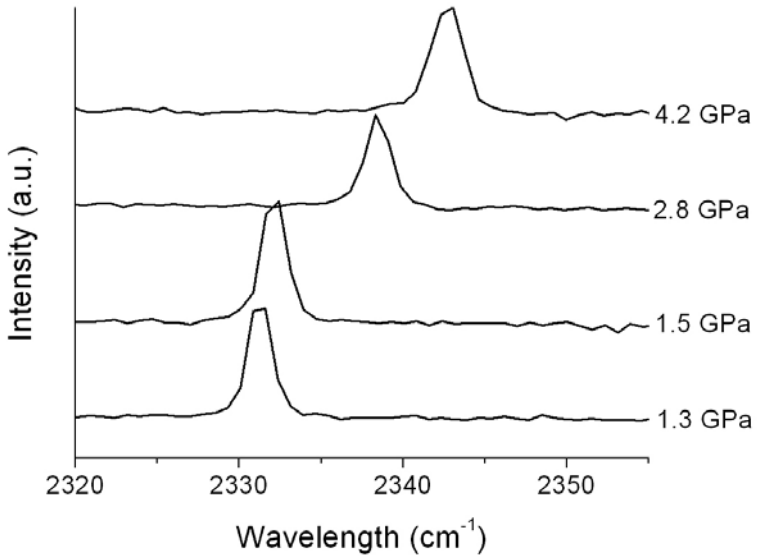

Figure 3.12 Raman spectra collected in situ DAC at pressures between 1.3 and 4.2 GPa.

During decompression of the diamond anvil cell, the β-N_2 appeared again in the diffraction pattern at 7.5 GPa, in addition to extra reflections which could not be fitted. After further decompression, another *in situ* x-ray pattern was made at 4.7 GPa, when nitrogen reflections disappeared again together with the unexplained reflections from the 7.5 GPa pattern. Hence, it is assumed a partial decomposition product to

have appeared at 7.5 GPa. In the Figure 3.13 the *in situ* x-ray diffraction pattern collected at 7.5 GPa is shown. This figure shows Bragg peaks due to α-Ga_2O_3, the spinel-type gallium oxonitride (labelled as γ) and also the β phase of nitrogen.

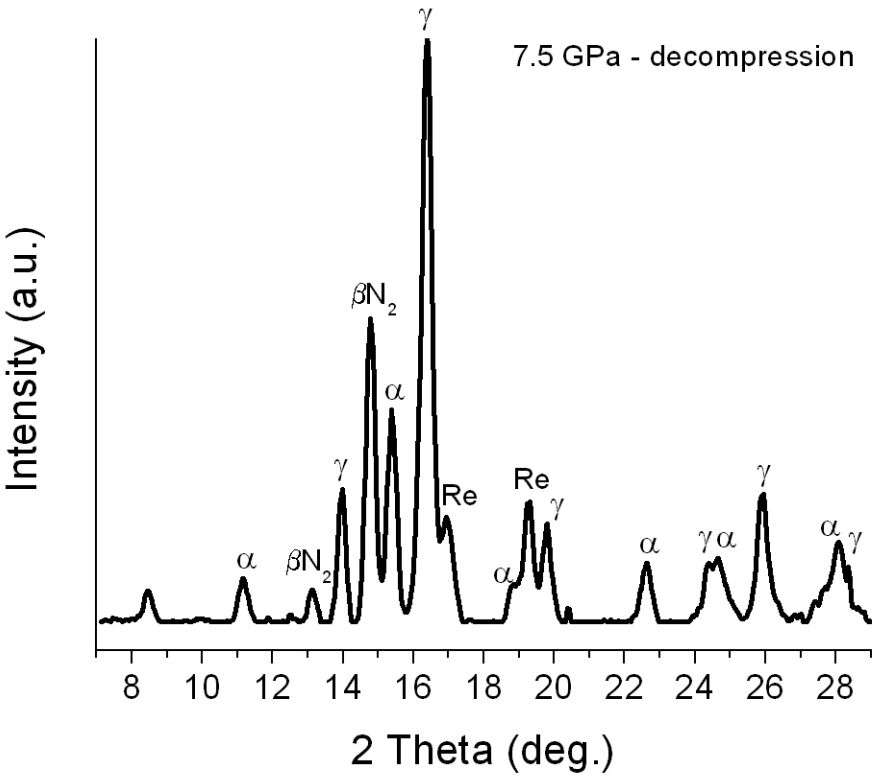

Figure 3.13 *In situ* DAC x-ray diffraction pattern (Mo-K_α=0.7108 Å) collected during decompression at 7.5 GPa, showing the appearance of nitrogen (β-N_2) in addition to α-Ga_2O_3 (labelled as α), spinel gallium oxonitride (labelled as γ) and rhenium (Re-gasket material).

The ultimate proof for the formation of the spinel-type gallium oxonitride from the cubic gallium oxide under nitrogen came from another independent DAC experiment.

The same material, γ-Ga_2O_3, was loaded in a diamond anvil cell but neon was used as the pressure medium, instead of nitrogen. The cell was compressed up to 16 GPa and laser-heated twice, at 5 GPa and 11.5 GPa. The *in situ* XRD showed next to the high-pressure phase of gallium oxide, α-Ga_2O_3, Bragg reflections from gallium (at 15.2 GPa) and several unfitted reflections. Since the diffraction patterns were not yet solved entirely, they are not shown here. Up to this point, what is important is that no spinel phase was formed from γ-Ga_2O_3 being loaded with neon, a fact which again

proves that the cubic gallium oxide is a high-temperature phase and not a high-pressure one. Even more, it is proven once again that the spinel-structured gallium oxonitride was the one synthesised in the DAC from γ-Ga_2O_3 and nitrogen. This investigation requires further experimental work to be done in order to understand the unexplained Bragg reflections.

3.2.2 β-to-α phase transition of Ga_2O_3

As already discussed in the beginning of this Chapter, the β-to-α phase transition of Ga_2O_3 was reported at different pressures. A pressure induced phase transition occurred at pressures between 20-22 GPa [79]. The presence of an external system combined with heating can decreases the transition pressure of gallia to 6 GPa [76]. In this work, as we are interested in the behaviour of β-Ga_2O_3 under high-pressures and temperatures and the presence of nitrogen (as the real system in the gallium oxonitride syntheses from GaN and β-Ga_2O_3), the oxide was loaded in a DAC in nitrogen and compressed slowly with several heating steps between compressions.

A thin pellet of β-Ga_2O_3 was loaded in a DAC with nitrogen under pressure. No changes were observed during cell compression up to 10.9 GPa, which included laser heating at 5.1 and 7 GPa. After laser heating at around 2100 K of both sides of the cell, the x-ray diffraction pattern showed the full transition β-to-α phase of gallium oxide.

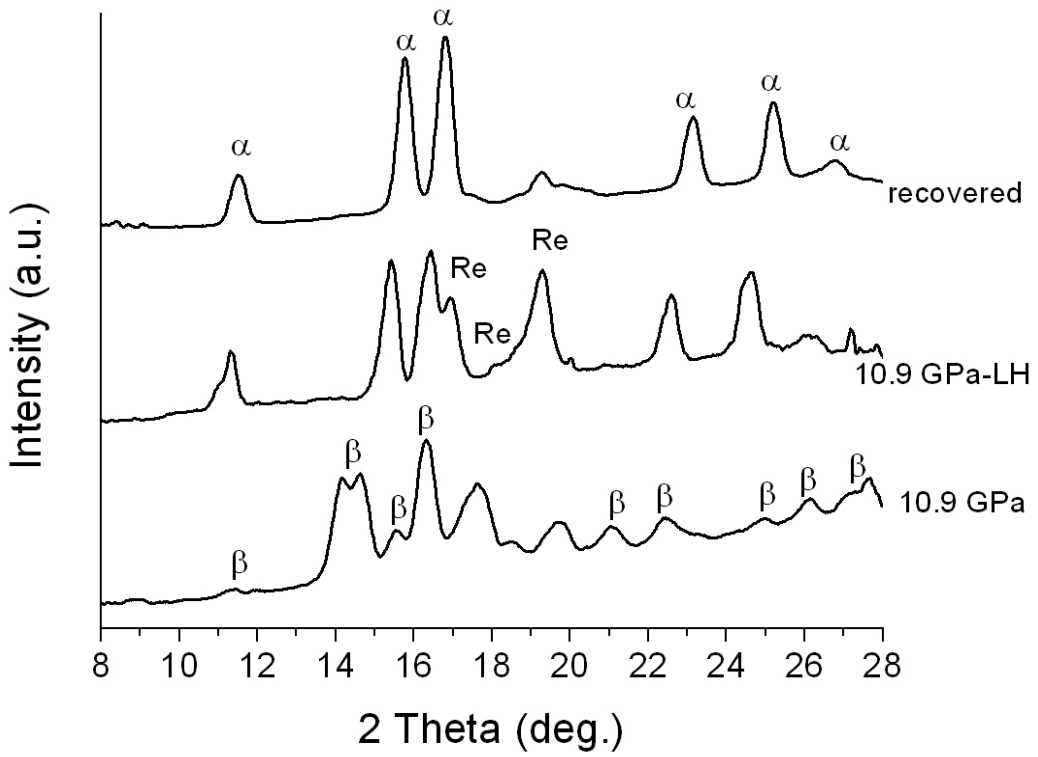

Figure 3.14 XRD patterns (Mo-K_α=0.7108 Å) collected *in situ* DAC at 10.9 GPa before and after laser heating, and *ex situ* from the recovered sample. The diffraction patterns show the presence of the starting material β-Ga_2O_3 (labelled as β) at 10.9 GPa and after laser heating (10.9 GPa-LH) the full transition of β-to-α of gallia is found.

In Figure 3.14 the x-ray diffraction patterns collected *in situ* at 10.9 GPa and after laser heating (10.9 GPa-LH) are given, showing the phase transition between the two polymorphs. During compression up to 10.9 GPa as well as after laser heating at 5.1 and 7 GPa, nitrogen Raman active modes were observed. Once the transition from β-to-α occurred, no nitrogen was observed in the Raman spectra. Cho *et al.* showed and discussed the nitrogen incorporation in both β and α phases, studies based on luminescence measurements [123].

The cell was further compressed up to 13.5 GPa showing no changes in the diffraction pattern. The decompression of the cell was done step-wise collecting XRD patterns for each reached pressure. The recovered sample (the cell being completely opened with one anvil removed) showed also only the high-pressure phase of gallium oxide, α-Ga_2O_3 (see Figure 3.14).

To conclude, in Section 3.2 a comprehensive study was performed on gallium oxides polymorphs under pressure. γ-Ga_2O_3 reacted with nitrogen and transformed into spinel-structured gallium oxonitride at 4.2 GPa and temperatures between 1500-1800 K, in a diamond anvil cell. This observation was supported by *in situ* Raman spectroscopy showing no nitrogen Raman active modes once the spinel phase appeared. The cubic γ-Ga_2O_3 loaded with neon instead of nitrogen in a DAC, gave no spinel under pressure and after laser heating, providing yet more evidence that the syntheses of the spinel-type gallium oxonitride were successful after γ-Ga_2O_3 reacted with nitrogen.

In Section 3.2.2, the phase transition β-to-α was reported to occur at 10.9 GPa and laser heated at around 2100 K. the experiment was done in a DAC with nitrogen as the pressure medium. During the experiments the incorporation of nitrogen into the gallium oxide structure was also observed.

3.3 Characterisation of the spinel-type gallium oxonitride

The second main part of this thesis is dedicated to the characterisation of the spinel-structured gallium oxonitride phases. A single crystal structure determination of the spinel phase is discussed in Section 3.3.1. Single crystals have been isolated from a HP/HT bulk sample and their crystal structure was investigated by single crystal x-ray diffraction technique. In Section 3.3.2, the elasto-mechanical properties of the spinel phase are reported. Compressibility measurements performed in a diamond anvil cell (Section 3.3.2.1) and nano indentation hardness using the Oliver-Phar method (Section 3.3.2.2) yieleded the determination of the bulk modulus, hardness and Young's modulus. The thermal properties of the spinel phase have been as well investigated and reported in Section 3.3.3. The high-temperature stability and the determination of the thermal expansion coefficient for the HP/HT gallium oxonitride phase are discussed. At last but not least, the electronic band structure of the spinel phase has been investigated and discussed in Section 3.3.4. Soft X-ray Spectroscopy has been used for these investigations and the band gap value for the phase of interest was determined.

3.3.1 Single crystal structure determination of a spinel-type gallium oxonitride

The crystal structure of gallium oxonitride has been determined on the basis of single crystal x-ray diffraction data. Energy-dispersive x-ray spectroscopy (EDS) and energy-loss spectroscopy were used for determining the N/O ratio, the value from which was used in for the structure refinement. The composition of the characterised crystal is found to be $Ga_{2.79}\square_{0.21}(O_{3.05}N_{0.76}\square_{0.19})$, revealing anionic vacancies in a single crystal structure determination of a spinel-type structure for the first time. The results and discussions presented in this chapter are the result of a collaboration with Prof. Huppertz, who was at that time based at Ludwig-Maximilians-Universität München, and co-workers [206].

3.3.1.1 HP/HT syntheses of spinel-structured gallium oxonitride single crystals

To synthesize the gallium oxonitride spinel, hexagonal GaN and monoclinic β-Ga_2O_3 were mixed thoroughly in a molar ratio of 9 / 1, and put into a hexagonal boron nitride crucible. The boron nitride crucible was positioned into the center of an 18/11-assembly, which was compressed by eight tungsten carbide cubes. The assembly was compressed to 5 GPa in 2 h, using a multianvil device, based on a Walker-type module, and a 1000 t press. A detailed description of the preparation of the assembly can be found in Section 2.2.3. The sample was heated up to 1550 K (cylindrical graphite furnace) in 10 min, kept there for 15 min, and cooled down to 1150 K in 25 min at constant pressure. Afterwards, the sample was quenched to room temperature by switching off the resistive heating, followed by a decompression period of 6 h. A crystalline product could be separated from the surrounding boron nitride of the crucible. Small colourless, air-resistant crystals of the reaction product were isolated from the bulk sample and tested on a Buerger camera.

3.3.1.2 Spectroscopic (EDS, EELS) and Transmission Electron Microscopic (TEM) investigations

The crystal structure of the examined crystals was verified using Selected Area Diffraction (SAD) before any other analysis. Simultaneous use of EDS and EEL spectroscopy allows nitrogen and oxygen to be quantified in the matrix and their distribution in the microstructure to be characterised.

The homogeneity and the nitrogen to oxygen ratio of the synthesized spinel-type gallium oxonitride phase were determined through a Transmission Electron Microscopy (TEM), together with Electron Energy Loss Spectroscopy (EELS) and an Energy Dispersive X-ray (EDX) spectrometer (see Section 2.3.2). Several series of spectra were taken from small crystals of the reaction product. For one crystal, different areas were examined using EELS, all of which showed the spinel structure. To avoid the loss of nitrogen during the investigation, which would be caused by a heating process through the interaction of highly accelerated electrons with the sample (ionization), we used a double tilt liquid nitrogen cooling stage (Gatan, Model 613) for the sample holder.

Table 3.5 EELS measurements of $\overline{N/O}$ ratios from different points on a gallium oxonitride single crystal.

meas. no.	**1**	**2**	**3**	**4**	**5**
$\overline{N/O}$	0.30 ± 0.067	0.29 ± 0.061	0.31 ± 0.070	0.30 ± 0.072	0.18 ± 0.051
meas. no.	**6**	**7**	**8**	**9**	**10**
$\overline{N/O}$	0.32 ± 0.069	0.20 ± 0.046	0.21 ± 0.052	0.27 ± 0.062	0.17 ± 0.046
meas. no.	**11**	**12**			
$\overline{N/O}$	0.16 ± 0.043	0.24 ± 0.053			

Table 3.5 gives a survey over the results of 12 measurements on one single crystal of the spinel gallium oxonitride phase. Each value represents a different position at the crystal. These measurements yield a mean value of $\overline{N/O}$ of 0.25 ± 0.06, representative for this single crystal. Figure 3.15 shows a representative EELS spectrum, recorded on a single crystal. All further measurements on different crystals led to similar results, definitively confirming a considerable amount of nitrogen in the examined spinel-type gallium oxonitride crystals of the high-pressure sample.

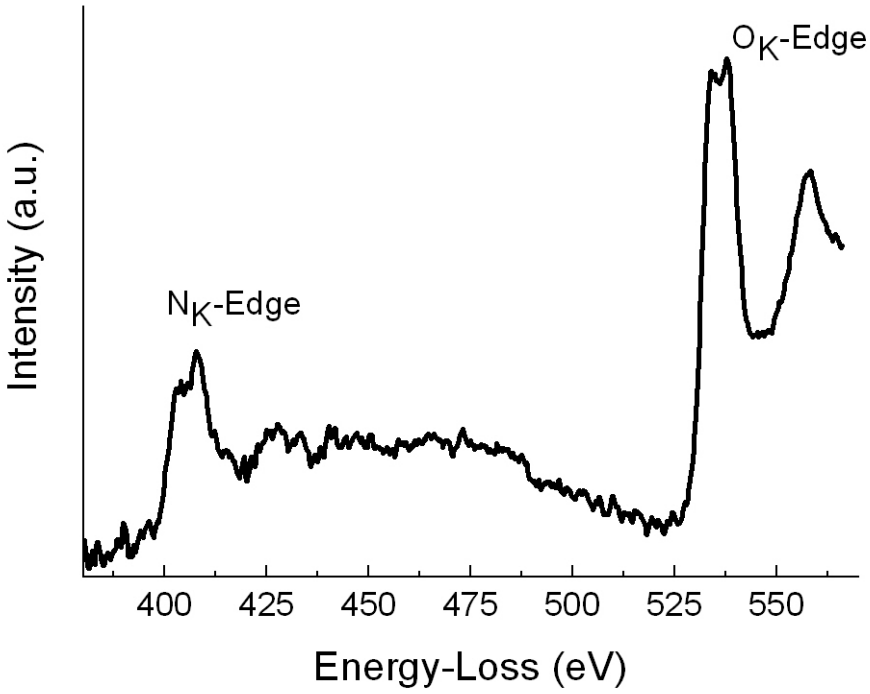

Figure 3.15 Typical EEL spectrum from a selected area of a single crystal of spinel-type gallium oxonitride.

The ideal composition of a defect free spinel gallium oxonitride is Ga_3O_3N, which corresponds to the highest possible amount of nitrogen in the structure. Taking into account the determined value of $\overline{N/O}$ = 0.25 ± 0.06, the molar ratio of oxygen / nitrogen is 3.2 / 0.8. As a result of the fact that charge neutrality in the colourless spinel must be guaranteed, the total composition of the spinel gallium oxonitride crystal averages to $Ga_{2.93}(O_{3.20}N_{0.80})$, based on the preliminary acceptance of a filled anion model (see Section 3.3.1.3.1).

3.3.1.3 Crystal structure analysis

The high-pressure phase of gallium oxonitride crystallises into a spinel-type structure (space group $Fd\bar{3}m$, No. 227). This structure has a cubic close packing (*fcc*) arrangement of anions which holds two types of voids or interstices, namely tetrahedral and octahedral interstices. The unit cell of an ideal spinel structure contains 56 atoms (24 cations and 32 anions) with 64 tetrahedral and 32 octahedral interstices between the anions. However, only 8 and 16 of the tetrahedral and octahedral sites are occupied by the cations. The spinel crystal structure of the gallium oxonitride is given in Figure 3.16.

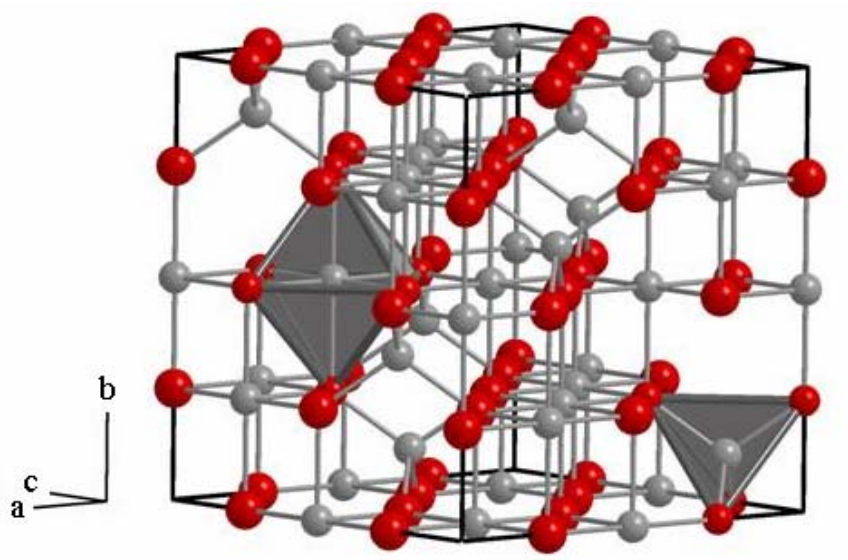

Figure 3.16 Crystal structure of the spinel-type gallium oxonitride. The grey coloured balls are the gallium cations (octahedrally and tetrahedrally coordinated) and the black coloured are the oxygen and nitrogen anions.

The powder diffraction pattern of the reaction product was collected with a Stoe Stadi P diffractometer, using monochromated $Cu_{K\alpha}$ = 1.54051 Å radiation (see Section 2.3.1.1). Figure 3.17 illustrates the result of a Rietveld refinement, showing reflections of the starting material hexagonal gallium nitride (w-GaN) and reflections of the cubic spinel phase. The reflections of the latter were indexed on the basis of a cubic unit cell, leading to a refined lattice parameter of a_0 = 8.280(1) Å [213, 214].

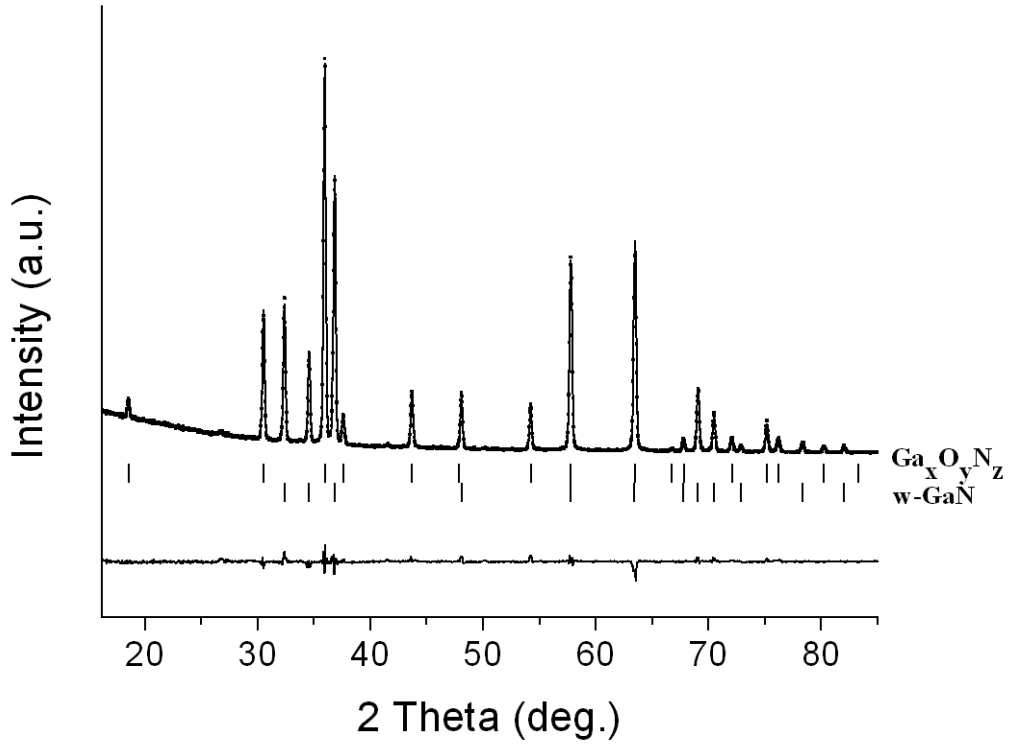

Figure 3.17 Rietveld refinement of the powder diffraction pattern (Cu-K_α = 1.54501 Å) of the reaction product, including the spinel phase $Ga_xO_yN_z$ next to w-GaN as side product. The experimental data points are shown as a dotted line and the fit to the data as a solid line.

Single crystal intensity data were collected at room temperature from a colorless crystal (dimensions: 0.025 × 0.025 × 0.020 mm^3), using an Enraf-Nonius Kappa CCD with graded multilayer x-ray optics ($Mo_{K\alpha}$ = 0.71073 Å). According to the Laue symmetry $m\bar{3}m$ and systematic extinctions $h + k = 2n$, $h + l$, $k + l = 2n$, $0kl$ with $k + l = 4n$ and $k, l = 2n$, and $h00$ with $h = 4n$, the cubic space group $Fd\bar{3}m$ (No. 227) was derived, which was suitable for the solid state structure solution (direct methods) and refinement.

Table 3.6 Crystal data and structure refinement for $Ga_{2.79}\square_{0.21}(O_{3.05}N_{0.76}\square_{0.19})$.

Empirical formula	$Ga_{2.79}(O_{3.05}N_{0.76})$
Molar mass, g/mol	254
Crystal system	cubic
Space group	$Fd\bar{3}m$ (No. 227)
a, Å	8.278(1)
Volume, nm^3	0.5673(2)
Formula units per cell	$Z = 4$
Temperature, K	293(2)
Calculated density, g/cm^3	5.95
Crystal size, mm^3	$0.025 \times 0.025 \times 0.020$
Absorption coefficient, mm^{-1}	26.13
Total no. reflections	171
Goodness-of-fit (F^2)	1.153
Final R indices (all data)	$R_1 = 0.0191$
	$wR_2 = 0.0528$

However, the starting positional parameters were taken from the structural refinement of $Ga_{2.81}O_{3.57}N_{0.43}$ [134] to adjust these results to the previously published data. Ga1 occupies the Wyckoff site 8*a* (1/8,1/8,1/8), Ga2 the position 16*d* (1/2,1/2,1/2), and the oxygen and nitrogen anions are at 32*e* (origin choice 2). As the differentiation between oxygen and nitrogen on the mixed Wyckoff site 32*e* is impossible from x-ray data, the results of the above-reported EELS measurements were used to restrain the ratio of $\overline{N/O}$ = 0.25 / 0.06 in the structural refinement. The refinement of the occupancy parameter of the tetrahedrally coordinated gallium site (Ga1, 8*a*) showed full occupation within two standard deviations so that full occupancy was assumed in the final cycles. In contrast, the octahedral gallium site (Ga2, 16*d*) exhibited a site occupation deficiency of about 10% in all steps of the refinement. To maintain charge neutrality, the negative charge resulting from the occupancy of the anionic site was set equal to the sum of positive charges from Ga1 and Ga2. The final least-squares cycles resulted in a total occupation of 95.4(4) % for the anionic site. From these data, the nominal composition $Ga_{2.79}(O_{3.05}N_{0.76})$ is derived, which implies vacancies on the

cationic and on the anionic part of the structure. All relevant details of the data collections and evaluations are summarised in Table 3.6. Structure solution and parameter refinement with anisotropic displacement parameters for all atoms (full-matrix leastsquares against *F*2) were performed by the SHELX-97 software suite [215, 216].

Table 3.7 Atomic coordinates, isotropic equivalent displacement parameters U_{eq} (in $Å^2$), and site occupation factors (S.O.F) for $Ga_{2.79}\square_{0.21}(O_{3.05}N_{0.76}\square_{0.19})$.

atom	Wyckoff position	x	y	z	U_{eq}	S.O.F
Ga1	8a	⅛	⅛	⅛	0.0075(3)	1
Ga2	16d	½	½	½	0.0114(3)	0.895(4)
O	32e	0.2569(2)	*x*	*x*	0.0083(7)	0.763(3)
N	32e	0.2569(2)	*x*	*x*	0.0083(7)	0.191(1)

The final difference Fourier synthesis did not reveal any significant residual peaks. Additionally, the positional parameters, occupancy factors (Table 3.7), anisotropic displacement parameters (Table 3.8), interatomic distances, and angles (Table 3.9) are listed. On the basis of the structure refinement of the single crystal data, the bond length between the tetrahedral gallium site (Ga1) and the mixed occupied anionic position comes to 1.891(3) Å, and the corresponding value for Ga2 is 2.014(2) Å.

Table 3.8 Anisotropic displacement parameters U_{ij} (in $Å^2$) for $Ga_{2.79}\square_{0.21}(O_{3.05}N_{0.76}\square_{0.19})$.

atom	U_{11}	U_{22}	U_{33}	U_{23}	U_{13}	U_{12}
Ga1	0.0075(3)	U_{11}	U_{11}	0	0	0
Ga2	0.0114(3)	U_{11}	U_{11}	-0.0017(2)	U_{23}	U_{23}
O/N	0.0083(7)	U_{11}	U_{11}	-0.0005(6)	U_{23}	U_{23}

As discussed above, the structure refinement showed a not fully occupied octahedral site 16*d* (Ga2). Soignard *et al.* obtained similar results during their Rietveld refinement of the phase $Ga_{2.8}O_{3.24}N_{0.64}$ [135]. In the beginning of their refinement of the powder pattern, the occupancies of the tetrahedral and octahedral gallium sites were

refined freely. Similar to the results reported in this work, they observed that the occupancy of the tetrahedral site remained close to unity. In contrast, the octahedrally coordinated gallium site was determined to be 0.90(4), resulting in the composition $Ga_{2.8}O_{3.24}N_{0.64}$ by keeping charge neutrality. This behaviour is nearly identical to our results from single crystal data, where the tetrahedral site is fully occupied and the occupancy of the octahedral site comes to 0.895(4).

Table 3.9 Interatomic distances (in Å) and angles (in deg.) calculated with the single lattice parameters of $Ga_{2.79}\square_{0.21}(O_{3.05}N_{0.76}\square_{0.19})$.

Ga1 – O/N Ga2 – O/N	1.891(3) 2.014(2)	4X 6X
O/N – Ga1 – O/N O/N – Ga2 – O/N O/N – Ga2 – O/N O/N – Ga2 – O/N	109.5 180 86.71(9) 93.29(9)	

The complete description of the spinel-type structure requires an additional parameter, designated as the "anion parameter *u*" [217]. If the value *u* is equal to 0.25, the anions form a perfect cubic close packed structure, defining regular tetrahedral and octahedral coordinations around the sites 8*a* (point symmetry $\bar{4}3m$) and 16*d* ($m\bar{3}m$), respectively. In the present structure refinement, the parameter *u* has a value of 0.2569(2), slightly higher than that of the ideal value of 0.25. This causes an enlargement of the tetrahedral site at the expense of the octahedral one and a degeneration of the octahedral site symmetry to $.\bar{3}m$ (displacement of the oxygen atoms along the [111] direction).

3.3.1.3.1 Constant anion model vs. constant cation model

Since gallium oxonitride reported here contains more nitrogen (EELS results) than that of the above-mentioned compound of Soignard *et al.*, the total composition is necessarily calculated to $Ga_{2.79}O_{3.05}N_{0.76}$ [135]. This result leads to vacancies on the cation site (octahedrally coordinated site 16*d*) and on the anion site 32*e*, relative to the ideal spinel structure, leading to the notation $Ga_{2.79}\square_{0.21}(O_{3.05}N_{0.76}\square_{0.19})$. This finding differs from former models, used in the structural characterization of spinel-type

oxonitrides. For example, the ideal structure of γ-alon Al_3O_3N would have a cubic spinel type structure (space group $Fd\bar{3}m$, No. 227) with oxygen and nitrogen atoms, randomly distributed at the Wyckoff site 32*e,* and the aluminum atoms at the tetrahedral (8*a*) and octahedral (16*d*) sites. The assumption of crystal defects, based on deviations from the ideal composition, led to the introduction of new structure models by Adams *et al*., Lejus *et al*., and McCauley [218-220]. The first model, designated as *the constant anion model*, is based on aluminum vacancies and can be formulated as $Al_{(2+x/3)}\square^{Al}_{(3-4x)/12}O_{3-x}N_x$ [219], $Al_{(8+x)/3}\square^{Al}_{(1-x)/3}O_{4-x}N_x$ [220]; all values multiplied by 4/3 to correspond with the ideal spinel composition AB_2O_4), or $Al_{(64+x)/3}\square^{Al}_{(8-x)/3}O_{(32-x)}N_x$ [218] (standardized to 32 anions inside the unit cell of the spinel-type structure). The second model of McCauley is *the constant cation model*, represented by the formula $Al_{24}O_{(72-3x)/2}N_x\square_{[(72-x)/2-32]}$, in which the cationic part of the structure is always fully occupied. Up to now, ab initio calculations between the constant anion and the constant cation model in the alon systems revealed that the constant anion model with vacancies on the Al sites is preferred, whereas a model with oxygen interstitial anions is unlikely [221]. This model was also confirmed by structure refinements, based on XRD and neutron diffraction data [222]. Thus, the alon spinel unit cell has eight aluminum cations in tetrahedral sites and 15 Al and one vacancy in the 16 octahedral sites $(Al_8^{[4]}Al_{15}^{[6]}\square^{[6]}O_{27}N_5)$[209].

The calculations on γ-alons and on the gallium oxonitrides are always based on the constant anion model with a completely filled anionic part of the structure. This model may not be the only one possible, as already noted by McCauley [218]. The experimental data presented in this work led to the composition $Ga_{2.79}\square_{0.21}(O_{3.05}N_{0.76}\square_{0.19})$. Therefore, the validity of the approximation of a constant anionic part of the structure is in question. From the existing models, the formation enthalpy of the oxonitride spinels is unfavourable relative to the low-energy structures of the oxides. Up to now, the deficiency in enthalpy can only be balanced with contributions that arise from a mixing of oxygen and nitrogen in the anionic part of the structure. It is believed that this contribution can be additionally enhanced by the assumption of defects on site 32*e*. A problem for a reliable calculation of the enthalpy is the fact that a true distribution of oxygen and nitrogen gives a substantial

contribution to the configurational entropy. Now, additional vacancies in the anionic part of the structure as well as the already included cationic defects on the octahedral site ought to be considered.

To conclude, the data from the single crystal structure refinement of the presented spinel-type gallium oxonitride confirm a fully occupied tetrahedral gallium site and vacancies at the octahedrally coordinated gallium position, coupled with vacancies on the anionic site (Wyckoff position 32*e*). The composition of the characterized single crystal is analysed to $Ga_{2.79}\square_{0.21}(O_{3.05}N_{0.76}\square_{0.19})$, revealing anionic vacancies in a single crystal structure determination of a spinel-type structure for the first time.

3.3.2 Elasto-mechanical properties of the spinel-structured gallium oxonitride

Hardness and elastic moduli are important and widely used parameters for the characterisation of technological materials. In particular, the search for hard materials with potential practical application is one of the most lively areas of the high-pressure research [32-35, 223, 224].

In our attempt to characterise the high-pressure, high-temperature spinel-type gallium oxonitride, the elasto-mechanical properties such as the bulk modulus K (GPa), nanoindentation hardness H (GPa), and the Young's modulus E (GPa) were also investigated.

3.3.2.1 Compressibility studies

Compression-decompression studies were carried out using a DAC (see Section 2.2.2) coupled with an *in situ* x-ray diffractometer (see Section 2.3.1.1) in order to determine the bulk modulus of the spinel-type gallium oxonitride. The results reported in this section were published in High-Pressure Research journal [204].

As starting material for the synthesis of the spinel phase, a gallium oxonitride ceramic labbled in this work as (GaON)1 (see Table 3.1) was loaded in a DAC. LiF was used as pressure transmitting medium as well as pressure standard [156]. After applying a pressure of 0.7 GPa and a temperature of around 1600 K, complete crystallization of the amorphous ceramic was detected by *in situ* powder x-ray diffraction (XRD). The

crystalline phase was identified as the spinel-type gallium oxonitride within the space group $Fd\bar{3}m$ (No. 227) and a cell parameter of a = 8.2042 Å (see Figure 3.6).

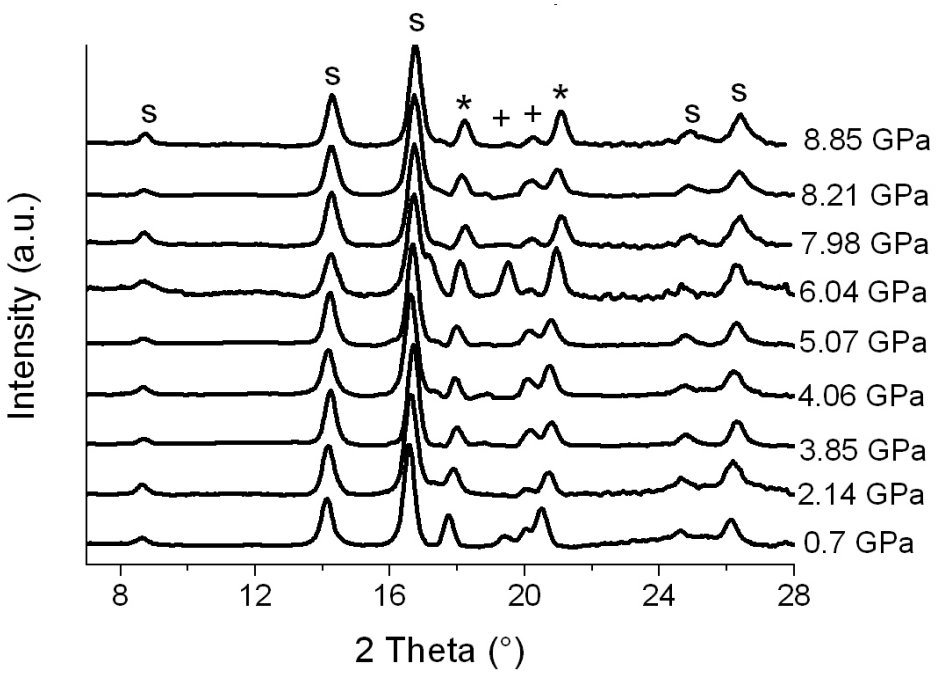

Figure 3.18 XRD patterns of the spinel-structured gallium oxonitride (s) upon compression in a DAC from 0.7 GPa up to 8.85 GPa. No other by-products were observed. The labels (*) and (+) are for Re reflections (gasket material) and LiF (pressure medium), respectively.

The cell was farther on compressed, in small steps, up to around 9 GPa. In the Figure 3.18, the XRDs patterns, collected between 0.7 and 8.85 GPa, are shown.

All the reflections in the XRD pattern could be interpreted on the basis of the spinel-type structure ($Fd\bar{3}m$, No. 227) and the LiF reflections. Up to a pressure of 9 GPa no changes were observed in the x-ray diffraction patterns. In Figure 3.18 the raw data of the measurement is presented, therefore the small shift of reflections towards higher d-spacing in the range between 2.14 and 5.07 GPa is due to zero shift.

Figure 3.19 exhibits the unit cell volume as a function of pressure *V(P)*, as measured for the spinel-structured gallium oxonitride. For fitting the data, the second-order Birch–Murnaghan equation EOS (K'= 4) was used (see Section 2.4.1). The fit yielded a bulk modulus K of 216(7) GPa and a volume at zero pressure V_0 of 552.9(5) $Å^3$.

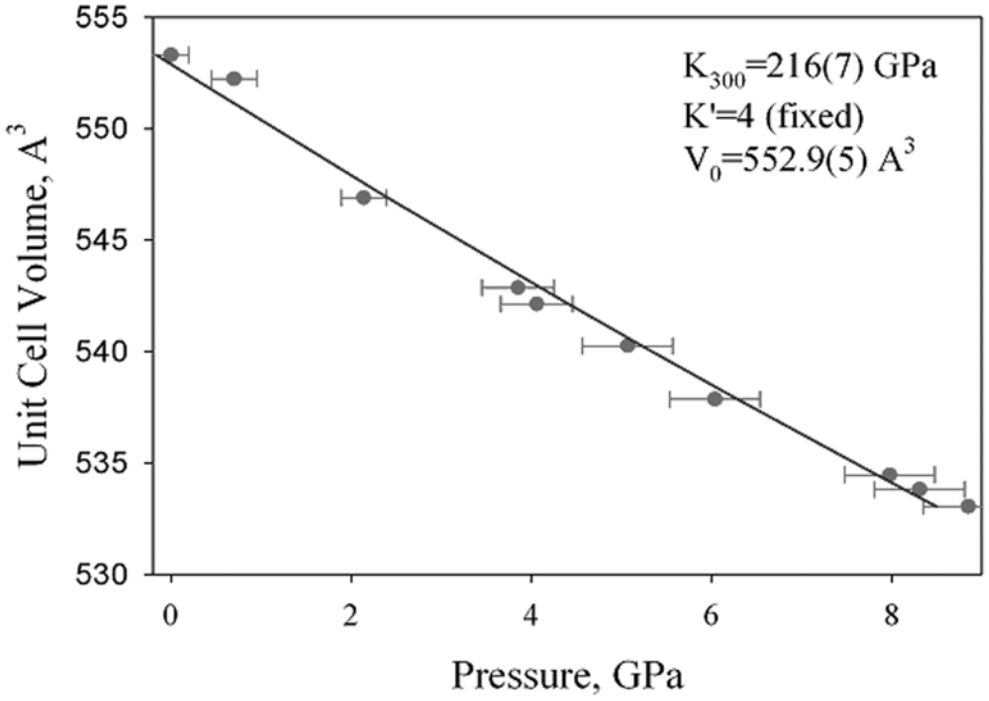

Figure 3.19 Unit cell volume of the spinel-type gallium oxonitride as a function of pressure. The experimental data are shown by solid circles. The error-bars of unit cell volume are within symbols. The solid line represents the least-squares fit of the second-order Birch-Murnaghan EOS (with K' fixed to 4) to the experimental data. The fit yielded K_{300} = 216(7) GPa.

The value for the bulk modulus determined in this work is in good agreement with the calculated and experimental values reported in the literature (see Table 3.10). However, the derived data have to be treated with caution, because different experimental conditions (like the pressure medium used) can have a considerable influence on the final evaluation of the bulk modulus. The use of a nearly hydrostatic pressure medium is of main importance for compressibility measurements [225].

Table 3.10 Experimental and calculated bulk modulus for the spinel-type gallium oxonitride.

Material	**$Ga_xO_yN_z$** (this work)	**Ga_3O_3N** cal.[133]	**Ga_3O_3N** exp [135]	**ALON** [20]	**γ-Si_3N_4** exp[226]	**Si_2AlON_3** cal. [227] normal/inversed
B_0 (GPa)	216(7)	232 (177) LDA(GGA)	234	208~234	302(6) (K'=4)	260 / 271

Even though a high bulk modulus doesn't automatically mean a high hardness [228], but if we compare the determined value of 216 GPa for gallium oxonitride with for example, that of 302(6) GPa (K' = 4) reported for γ-Si_3N_4 (H_v = 30-43 GPa) [226], it can be expected that the spinel-type gallium oxonitride exhibits also a considerable hardness.

3.3.2.2 Preliminary hardness tests

Preliminary micro and nano-hardness tests were done in collaboration with the Laboratory of Applied Mechanics, University of Rennes 1, France. The HP/HT spinel-structured gallium oxonitride was tested using the depth sensing (nano) indentation technique, since no pure gallium oxonitride was synthesised. w-GaN was always present in the high-pressure bulk to some extend. As weight loads were used as low as few mN, it was expected that the two phases could be identified from their different behaviour under load.

Two high-pressure samples were investigated, labelled in this work as $Ga_xO_yN_z$-1 and $Ga_xO_yN_z$-2. The samples were synthesised at 5 GPa and 1550 K in a multi anvil press from molar ratios GaN/Ga_2O_3 of 9/1 and 6/4, respectively. Figure 3.20 reveals the x-ray powder diffraction patterns of the two samples showing the presence of both, spinel gallium oxonitride and w-GaN. After the Rietveld refinement of both patterns, the nitride was found to make up ~60 fract.% and ~3 fract.% respectively. After mechanical polishing, the samples (~ 1 – 2 mm in diameter) were glued on a glass plate for the indentation tests.

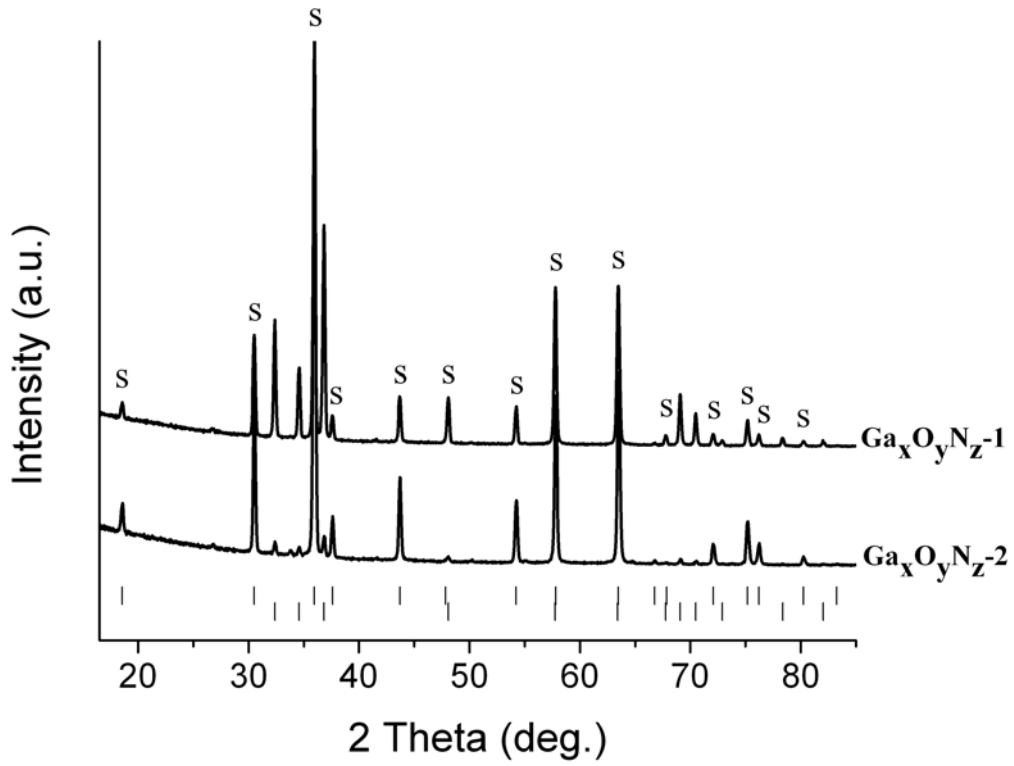

Figure 3.20 Powder XRD patterns (Cu-K_α = 1.540598 Å) from the two high-pressure samples ($Ga_xO_yN_z$-1 and $Ga_xO_yN_z$-2) used for the hardness tests. Both the samples show the presence of the spinel-type gallium oxonitride (s-the first row of Bragg reflections) and w-GaN (second row of Bragg reflections).

The first sample, $Ga_xO_yN_z$ -1, containing ~60 frac. % w-GaN, had a yellowish colour. During polishing and surface observation under the microscope the sample was found to have a high porosity. Polishing of the sample was difficult because it had a tendency to cleave unevenly. As discussed also in Section 2.4.2, high porosity and roughness are factors which substantially affect a hardness study. The second sample, $Ga_xO_yN_z$ -2, containing ~3 frac.% of GaN and having a dark grey colour, was much more compact, making possible to obtain a polished surface. From these observations it can be concluded that GaN was eliminated from the surface.

The experiments were performed using different loads (i.e. from 1 mN up to 2 N) corresponding to 64 - 2000 nm indentation depths. The typical load-displacement curve obtained by nanoindentation testing for stepwise loading is shown in Figure 3.21. The unloading steps were done after keeping the maximum load for one second and followed by unloading to half of the initial load. As can be observed in Figure 3.21, during unloading/reloading cycles the material exhibits distinct hysteresis loops

indicating the presence of a small reverse plasticity effect upon unloading. The reason for performing multiple loading-unloading was to make sure that the final unloading data used for analysis purposes were mostly elastic.

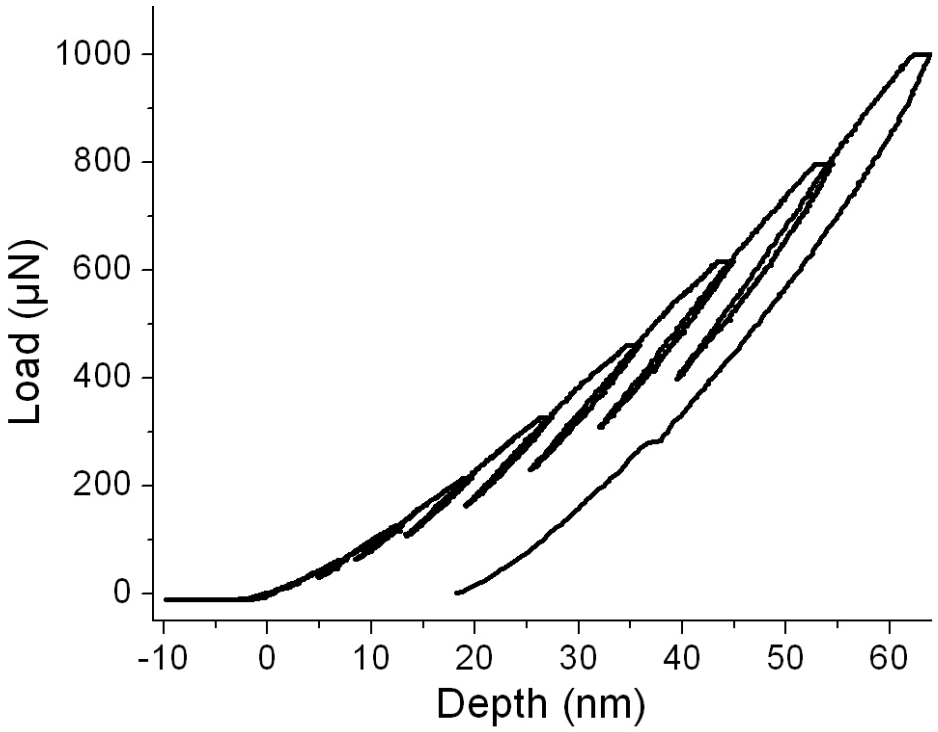

Figure 3.21 Typical load-displacement curve for $Ga_xO_yN_z$-1 measured by the nanoindentation technique.

The obtained curves were used to determine the nanoindentation hardness, H, and the reduced modulus, E_r, using the Oliver-Pharr method [202] (see Section 2.4.2.2).

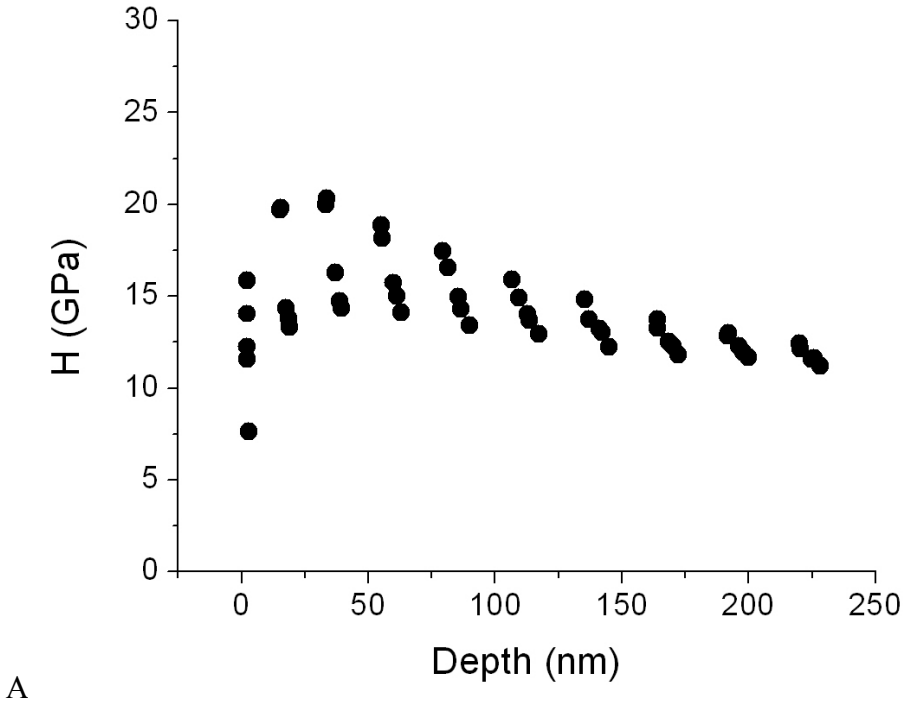

A

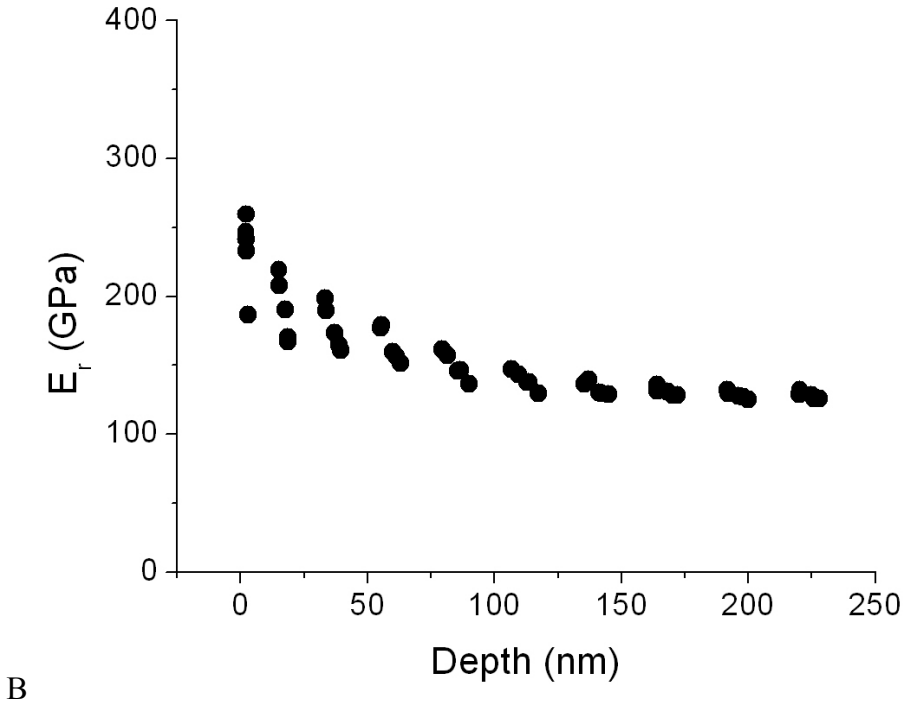

B

Figure 3.22 Nanoindentation hardness, H (A), and reduced elastic modulus, Er, (B) as a function of indentation depth, using Oliver-Pharr method. The measurements were performed on $Ga_xO_yN_z$-1 sample, using 1 mN maximum load.

For the $Ga_xO_yN_z$-1 sample, the nanoindentation hardness *H*, and the reduced elastic modulus E_r, values are shown as function of indentation depth in Figure 3.22. As discussed above, the surface of the $Ga_xO_yN_z$-1 was strongly affected by the mechanical polishing. The variations of both *H* and E_r with the indentation depth are

due to sample imperfections, i.e. the presence of pores beneath the indented area, or a layered microstructure.

To estimate a value for H and E_r from the obtained curves, only the range above 120 nm indentation depth was considered (where both parameters are only weakly dependent on indentation depth). From the data presented in Figure 3.22 an average indentation hardness of 12.3 GPa and a reduced elastic modulus of 128.34 GPa were determined.

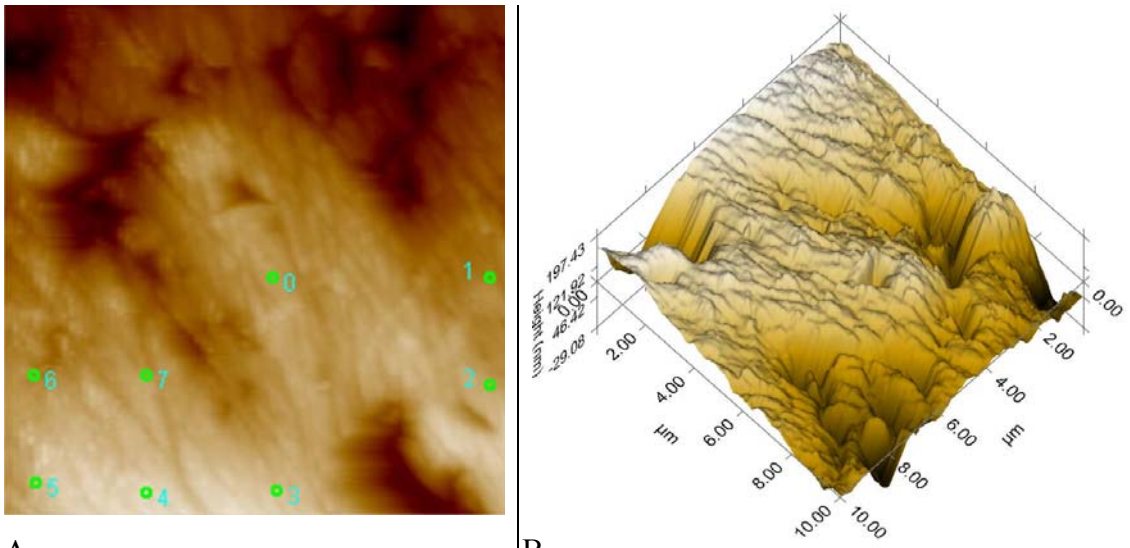

A B

Figure 3.23 Optical image of the investigated area (10 µm2) – zone 1 - from $Ga_xO_yN_z$-2 sample. 8 nanoindentations were made in the indicated points in Figure A. Figure B shows the same area, in 3D, indicating a surface roughness of ~200 nm.

In Figure 3.23 one of the investigated areas from $Ga_xO_yN_z$-2 is shown, zone 1, on which 8 indentations were performed using a loading force of 2 N. The area had a roughness of around 200 nm (see Figure 5.9 B). The indentations were done after careful observation of the surface, avoiding pores or other defects. The obtained hardness values for this area are given in Table 5.7, alongside the values from three other investigated areas. An average value for the hardness was calculated as 9.6 ± 1.8 GPa. Vickers hardness tests performed on the same sample, $Ga_xO_yN_z$-2, gave a hardness of 9.2 GPa, using a 300 mN load. Compared with the hardness value of w-GaN [229] (see Table 5.7), the hardness values determined in this work for $Ga_xO_yN_z$-2, are slightly lower. It should not be forgotten that nanoindentation hardness tests

performed in the present work were done on gallium oxonitride samples which also initially contained w-GaN (around 60 frac. % for $Ga_xO_yN_z$-1 and around 3 frac.% for $Ga_xO_yN_z$-2).

In Table 3.11 the nanoindentation hardness values obtained in this work are given for the two investigated gallium oxonitride samples. The w-GaN Vickers hardness is also given for comparison.

Table 3.11 Nanoindentation hardness, H, values determined from different areas from the two investigated samples, $Ga_xO_yN_z$-1 and $Ga_xO_yN_z$ -2. For $Ga_xO_yN_z$ -2, zone 1, eight indentations were made with the averaged hardness value given. Maximum loads used for $Ga_xO_yN_z$ -1 was 1mN and for $Ga_xO_yN_z$ -2, 2 N. Vickers hardness of w-GaN obtained at a load of 2 N is also shown for comparison.

Compound	H (GPa) for different zones				$\overline{H}$ (GPa)
	Zone 1	Zone 2	Zone 3	Zone 4	
$Ga_xO_yN_z$-1 (this work)					12.3
$Ga_xO_yN_z$-2 (this work)	11.4 ± 1.6	8.2 ± 1.8	9.3 ± 2.1	9.3 ± 1.5	9.6 ± 1.8
w-GaN [229]					12.00 ± 2.00

There are few theoretical studies of the elasto-mechanical properties of the spinel-type gallium oxonitride in the literature [133, 135]. Besides the bulk modulus, and shear modulus, Okeke *et al*. calculated also an elastic modulus E, for the spinel-structured gallium oxonitride, of 266 GPa (LDA) and 242 GPa (GGA) [133].

The results discussed in this section comprise the first attempt to measure the hardness of the spinel-type gallium oxonitride. As explained above, the available samples for these experiments were not sufficiently dense, at least for mechanical polishing. The presence of a second phase (w-GaN) in addition to the spinel gallium oxonitride, a reasonably high porosity and other possible sample imperfections allowed only preliminary elasto-mechanical properties tests to be made. Taking into account all of these issues, a hardness of around 10 GPa and reduced elastic modulus of around 130 GPa are considered as minimum values expected for the spinel-structured gallium oxonitride. Now that these problems are known, improved sample

preparation and a more systematic and detailed study are required as the next step for the accurate hardness and elastic modulus determination.

3.3.3 Thermal properties of the spinel-type gallium oxonitride

In addition to hardness and elastic moduli, there are some other important properties which can be important for potential technological applicaions. In particular, materials used as coatings for cutting tools, or as corrosion resistant layers should be thermally and chemically stable with a low thermal expansion coefficient. Therefore, the thermal expansion coefficient and the high-temperature oxidation stability of spinel-type gallium oxonitride have been investigated and are reported in the following section.

3.3.3.1 Thermal expansion

In order to obtain the thermal expansion coefficient of the spinel-structured gallium oxonitride, its x-ray powder diffraction patterns were collected on heating in air from room temperature (RT) up to 1170 K. The experiments were performed at ESRF, Grenoble at the high resolution XRD beamline (see Section 2.3.1.2). The sample used for the experiment was synthesised at 5 GPa and 1550 K in a multi anvil press. At room temperature a Rietveld refinement of the XRD patterned (Figure 5.10) showed the presence of the spinel gallium oxonitride (92.97(1.32) fract.%), w-GaN (0.72(0.04) fract.%) and α-Ga_2O_3 (6.32(0.86) fract.%).

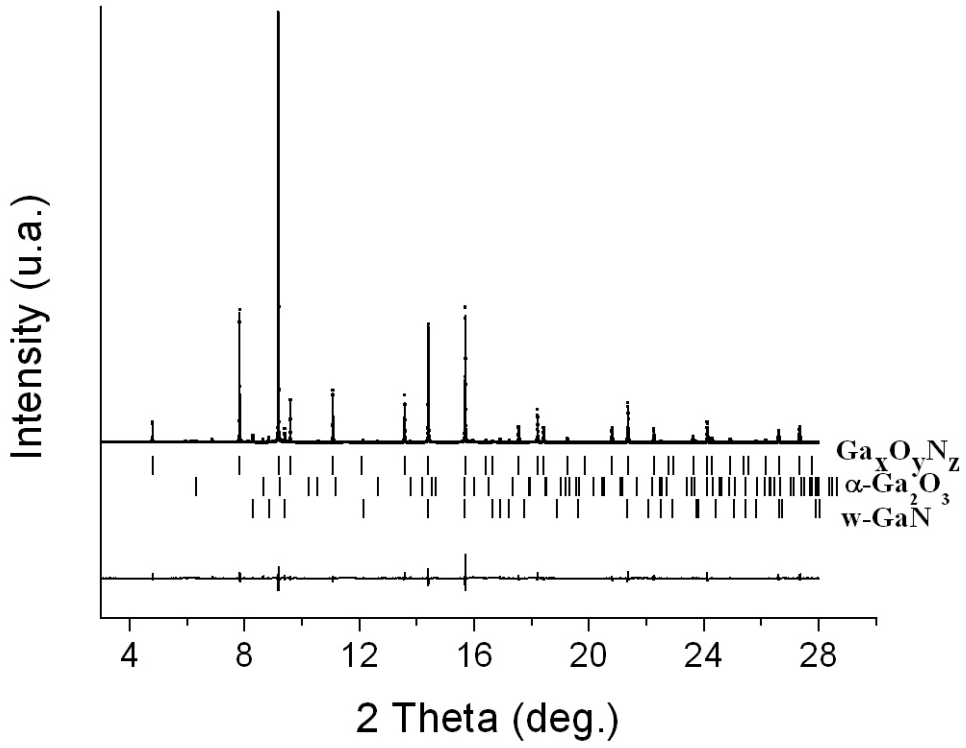

Figure 3.24 Rietveld refinement of the powder diffraction pattern (λ = 0.4 Å, RT) of the high-pressure sample used in the thermal expansion study. The experimental data points are shown as a dotted line and the fit to the data as a solid line.

The temperature was increased with 310 K/min up to around 1200 K, kept for 10 minutes and then decreased also with 310 K/min to room temperature. The lattice parameters of the spinel gallium oxonitride were determined using the profile matching mode of the Fullprof software [214].

Based on a literature research on spinel compounds (Si_3N_4) [230, 231], spinel-type oxonitrides (sialon, $Zr_{2.86}(O_{0.12}N_{0.88})_4$,) [232, 233], different polynomial functions were tried to fit the temperature dependence of the lattice parameters of the spinel-structured gallium oxonitride. A second order polynomial function was chosen due to better fitting and smaller standard deviations for the determined parameters:

$$a\,(T) = 8.27449 + 4.78378 \times 10^{-5}\,T + 1.76178 \times 10^{-8}\,T^2\ [\text{Å}] \qquad (5.1)$$

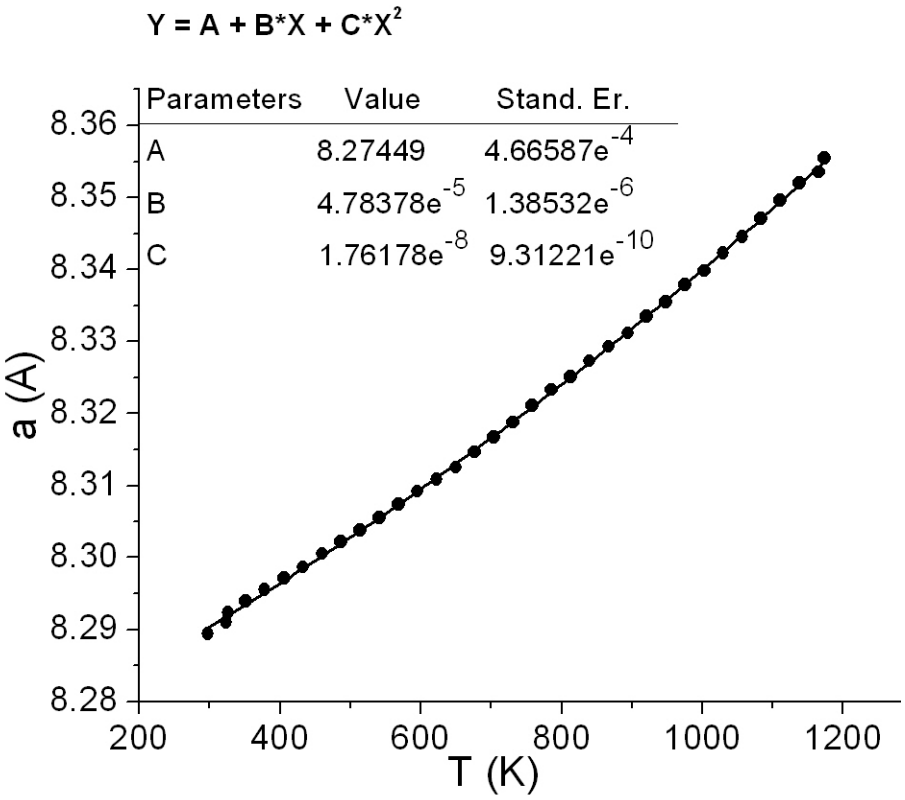

Figure 3.25 Lattice parameter of the spinel-type gallium oxonitride as a function of temperature. The experimental data points are given by solid circles. Solid line represents the least-square fit of the second order polynomial function (see inset) to the experimental data.

Two boundary conditions for the thermal expansion have to be taken into account, at T = 0 K the thermal expansion coefficient has to be zero and at high-temperatures has to tend to a constant value [234, 235]. To achieve these conditions the second coefficient in the *a(T)* function was omitted (inset Figure 3.26).

Applying the above *a(T)* relationship for the spinel gallium oxonitride the thermal expansion coefficient, defined as

$$\alpha\,(T) = \frac{1}{a(T)}\,\frac{\vartheta a(T)}{\vartheta T} \qquad (5.2),$$

was derived. The obtained α (T) is plotted in Figure 3.26.

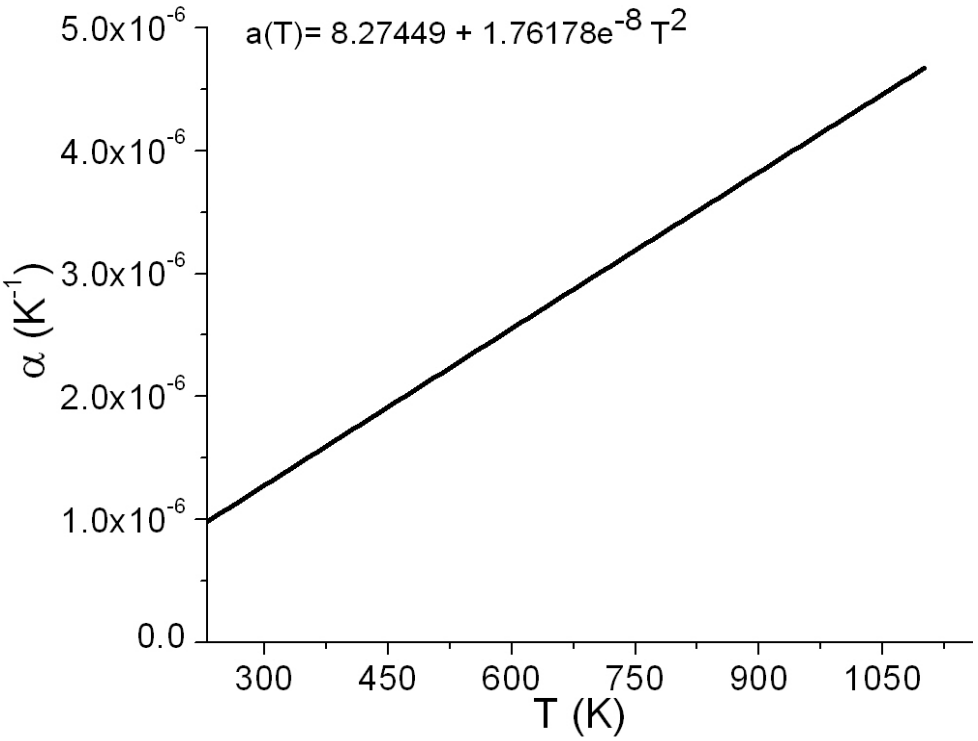

Figure 3.26 Linear thermal expansion α (K^{-1}) of the spinel-type gallium oxonitride as a function of temperature.

From Figure 3.26 it can be seen that the thermal expansion coefficient increases from 1.3 x 10^{-6} K^{-1} at 300 K to 4.7 x 10^{-6} K^{-1} at 1100 K. Compared with different other cubic compounds (see Table 3.12), nitrides and oxonitrides, spinel gallium oxonitride has a lower thermal expansion coefficient in the investigated temperature range.

Table 3.12 Thermal expansion coefficient for the spinel-type gallium oxonitride as measured in this work compared with different other cubic compounds. GaN and Ga_2O_3 are given, as further refferences.

Phase	**T (K)**	**α_a (x $10^{-6}K^{-1}$)**	**α_b (x $10^{-6}K^{-1}$)**	**α_c (x $10^{-6}K^{-1}$)**
$Ga_xO_yN_z$ (this work)	300	1.3	-	-
	1100	4.7	-	-
Sialon [232]	300	5.7	-	-
	1500	8.2	-	-
c-$Zr_{2.86}N_{4.88}O_{4.12}$ [233]	298	6.6	-	-
	873	14.2	-	-
c-Si_3N_4 [231]	300	3-4	-	-

	1100	6-7	-	-
w-GaN [236]	300	3.94	-	3.53
	900	5.40	-	4.71
	1200	5.52	-	4.79
β-Ga_2O_3 [237]	250	2.00	5.9	5.00

3.3.3.2 High-temperature oxidation stability

The thermal behaviour of the spinel-type gallium oxonitride was examined *via in situ* temperature-programmed x-ray powder diffraction [205]. The sample was synthesized from a mixture with the molar ratio w-GaN/β-Ga_2O_3 = 1/1 under high-pressure, high-temperature conditions of 4.5 GPa and 1550 K.

The *in-house* x-ray powder diffraction at RT revealed the presence of the spinel-structured gallium oxonitride, w-GaN (~15 %) and BN (from the crucible material). The powdered sample was heated up in air from RT to 1400 K in steps of 350 K/min. Cooling down the sample to room temperature was also done in steps of 350 K/min. Each temperature was kept constant for at least 10 min, before the measurements started. Figure 3.27 shows that successive heating of the product led to a shift of the reflections of the gallium oxonitride phase towards larger *d* values (larger cell volume) suggesting a positive thermal expansion (see Section 3.3.3.1). The reflections of w-GaN disappeared at a temperature of 1300 K. Since no extra reflections (i.e. Ga) appeared, this may have been due to movements of the sample in the capillary. No decomposition or cell distortions of the spinel-type gallium oxonitride could be observed up to a temperature of 1400 K.

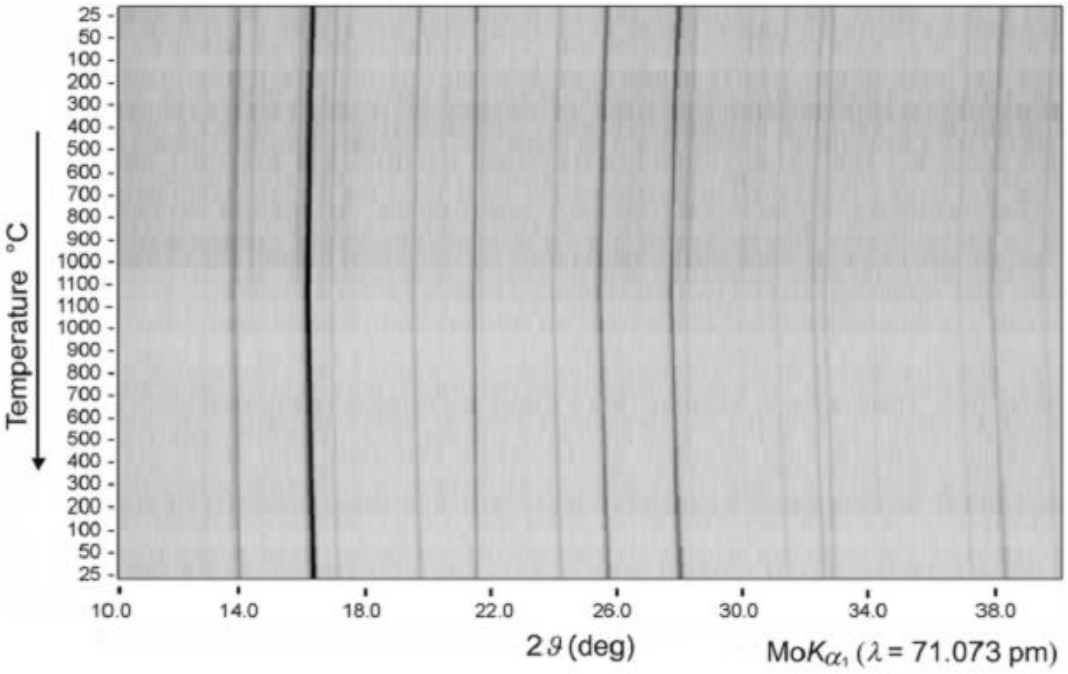

Figure 3.27 *In situ* temperature-programmed x-ray powder diffraction patterns showing the thermal behaviour of the spinel-type gallium oxonitride sample in air [205].

For the thermal expansion study of the spinel-type gallium oxonitride (see Section 3.3.3.1), the sample was heated up from room temperature to around 1200 K. The stability of the spinel phase was investigated using *in situ* XRD during the whole temperature range. The room temperature XRD pattern showed, in addition to tat of the spinel gallium oxonitride, the precence of w-GaN and that of the high-pressure phase of gallium oxide, α-Ga_2O_3 (see Figure 3.24). Within the investigated temperature range the spinel phase was stable with no cell distortions. GaN reflections were also present in the patterns up to the highest temperature. The α-Ga_2O_3 reflections were weak, and disappeared above 920 K. The disappearance of α-Ga_2O_3 reflections could not be due to sample movements since the powder was sealed in a completely full capillary. At ambient conditions α-Ga_2O_3 is a metastable phase and transforms 900 K into the stable phase β- Ga_2O_3 [66].

3.3.4 Experimental and theoretical band structure determination of the spinel-type gallium oxonitride

In this section the electronic structure and band gap determination for the spinel-type gallium oxonitride are discussed. Soft X-ray Spectroscopy (SXS) techniques combined with *ab initio* DFT (Density Functional Theory) will be shown to give clear and reliable insights on the crystal and electronic structure of the spinel phase. The investigations were focused on four high-pressure samples containing different amounts of the spinel-type gallium oxonitride. These results are subject of a collaboration with Profesor Alexander Moewes, from University of Saskatchewan, Canada. The experiments were performed at beamline 8.0.1 of the Advanced Light Source (ALS) at the Lawrence Berkeley National Laboratory, California, USA. Theoretical and technical aspects of these experiments can be found in Sections 2.3.1.2 (Synchrotron radiation) and 2.3.1.3 (Soft X-ray Spectroscopy).

3.3.4.1 Investigated high-pressure gallium oxonitride samples

This work is focused on four separate high-pressure samples which are labelled as $Ga_xO_yN_z$-3, $Ga_xO_yN_z$-4, $Ga_xO_yN_z$-5 and $Ga_xO_yN_z$-6. All four samples were synthesised from different w-GaN / β-Ga_2O_3 molar ratios, under different pressure and temperature conditions. The exact conditions for the syntheses are summarised in Table 3.13. In Figure 3.28 the x-ray diffraction patterns are shown from the four high-pressure samples, revealing the presence of spinel gallium oxonitride ($Fd\bar{3}m$, No. 227) and w-GaN as side product. There is no trace of β-Ga_2O_3 or α-Ga_2O_3 detected in these patterns. The amounts of each phase present in the final products are also listed in Table 3.13. These results were obtained from a Rietveld refinement of each x-ray diffraction patterns.

Table 3.13 HP/HT samples containing the spinel phase of gallium oxonitride. The starting materials, the experimental conditions (pressure, temperature) as well as the final products in mass percentage are given.

Sample	Initial molar ratio GaN / Ga_2O_3	P (GPa) / T(K)	Final products	Mass percentage
$Ga_xO_yN_z$-3	7 / 3	6 / 1500	s-GaON, w-GaN	39.82 (0.82) / 60.18 (2.16)
$Ga_xO_yN_z$-4	7 / 3	5 / 1500	s-GaON, w-GaN	57.70 (3.55) / 42.30 (3.95)
$Ga_xO_yN_z$-5	9 / 1	5 / 1550	s-GaON, w-GaN	89.96 (3.26) / 10.04 (0.62)
$Ga_xO_yN_z$-6	6 / 4	5 / 1550	s-GaON, w-GaN	99.31 (2.33) / 0.69 (0.12)

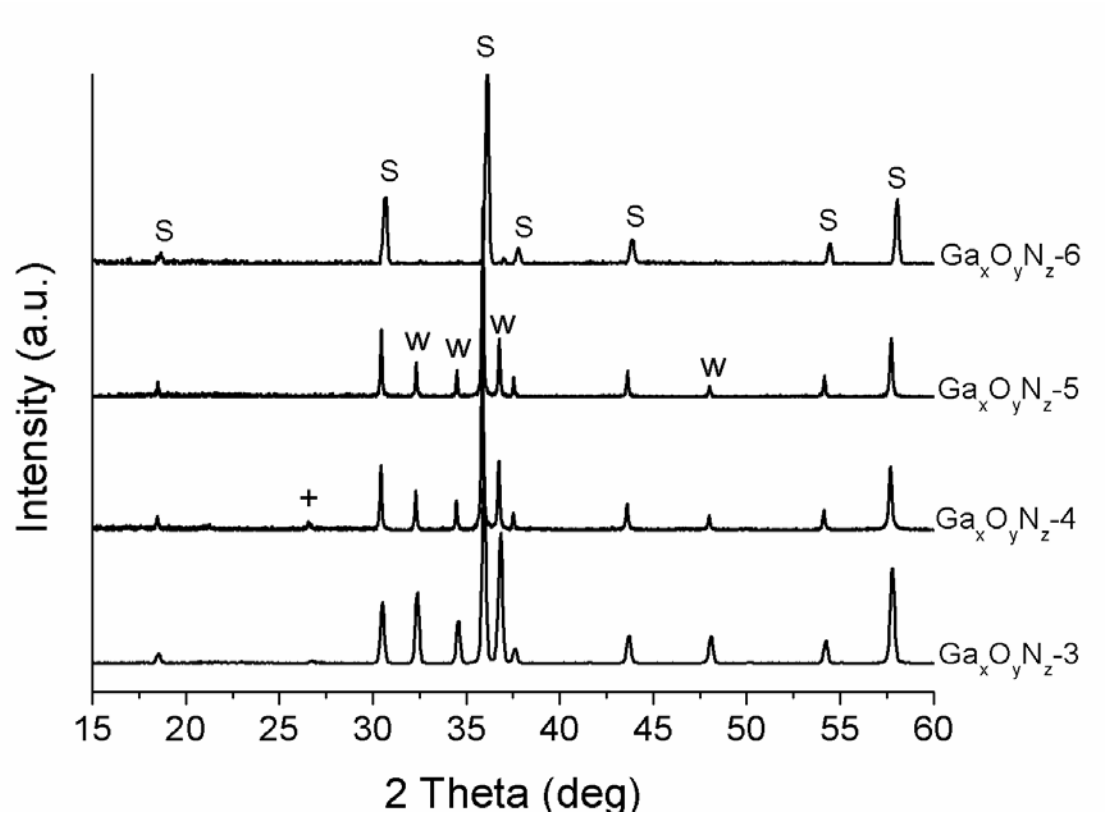

Figure 3.28 X-ray diffraction patterns of the four high-pressure investigated samples reviling the spinel phase gallium oxonitride (labelled with S) as well as w-GaN as side product (labelled with w). The + label indicates the presence of BN phase from the crucible material.

As discussed in Section 3.1.2.1.4, for a wide range of pressures (2.5 – 11.5 GPa) and temperatures (1300 – 1600 K), gallium nitride was always present in the final product

as well as the spinel gallium oxonitride. The β-Ga_2O_3 from the starting mixture either entirely transformed into the high-pressure phase, the corundum-type Ga_2O_3 (α-Ga_2O_3), or reacted totally to form the spinel gallium oxonitride (under certain conditions of pressure, temperature and ratios of the starting materials). As can be observed in Figure 3.28, the sample labelled $Ga_xO_yN_z$-6 is the purest one, containing only a small amount of GaN as side product. The other three samples were also investigated, as it was thought that the spinel gallium oxonitride present in these other samples would contain different amounts of nitrogen in the structure, which would be helpful for the analyses of the SXS spectra.

3.3.4.2 Experimental investigations using soft x-ray spectroscopy

Due to the contamination with GaN in all the probed samples (see Figure 3.28), the O K-edge was used (rather then nitrogen edge) to probe the electronic structure and determine the band gap for the spinel-type gallium oxonitride.

The O Kα XES and O 1s XANES spectra of w-GaN, β-Ga_2O_3 and the gallium oxonitride series are shown in Figure 3.29. The O 1s XANES may be split into two possible detection schemes, TFY and TEY (see Section 2.3.1.2). For all four probed materials, there are two prominent features in the O Kα XES spectra and three in the O 1s XANES spectra. The XES and XANES (TFY and TEY) spectra of the reference samples (gallium nitride and gallium oxide) are very similar in shape and energy position. This shows that the starting gallium nitride powder had a certain amount of oxygen incorporated into the structure. Previous investigations on oxidized GaN thin films have shown that gallium nitride can incorporate up to 15 % of oxygen in its lattice, whilst still maintaining the hexagonal structure [120]. Above this concentration the nitride becomes amorphous. More over, previous EELS measurements performed by our group also revealed the presence of some oxidized gallium nitride particles in the high-pressure bulk samples (spectrum not shown here). This aspect is taken into account later in this section for the interpretation of the spinel-type gallium oxonitride series spectra. Comparing the reference spectra with the spinel series ones, there are four key differences that need to be considered in the simulated spectra (see Figure 3.29).

1) Features *A* and *B* are shifted to lower energy in the gallium oxonitride series spectra then in the w-GaN one.

2) Features *C* and *D* have similar intensities in the gallium oxonitride O 1s TFY spectra while in the reference material (w-GaN) feature *C* has higher relative intensity than the feature *D*.

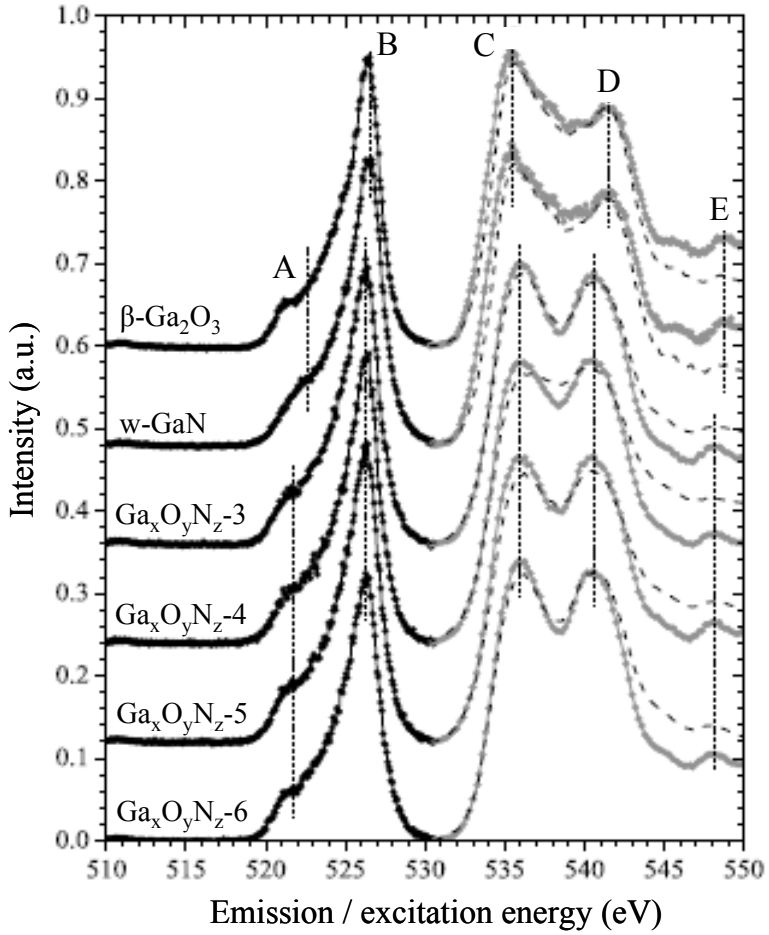

Figure 3.29 Measured O Kα XES (black scatter) and O 1s XANES in both, TFY (grey scatter) and TEY mode (dashed) spectra. The spectra are displayed offset and have been scaled to features A or C.

3) The peak separation between *C* and *D* is smaller in the gallium oxonitride spectra than in w-GaN, which is also reflected in the simulated ones.

4) The higher energy feature *E* is shifted to lower energy in gallium oxonitride spectra than in w-GaN spectrum.

The second key difference suggests that any contribution from the oxygen incorporated into gallium nitride would increase the intensity of *C* in the gallium oxonitride spectra and feature D should have higher intensity in the simulated

spectrum. These four criteria were used to evaluate which simulated spectra fitted best to the experimental results and will be discussed in the next section.

3.3.4.3 Theoretical studies of the electronic structure of the spinel-type gallium oxonitride

The x-ray diffraction technique revealed the high-pressure, high-temperature gallium oxonitride phase with a spinel-type structure, within the $Fd\bar{3}m$ (No.227) space group. Since XRD does not provide sufficient contrast to determine any oxygen or nitrogen site occupation preference, it was assumed that the anions are uniformly distributed within the *fcc* arrangement. This creates three distinct space groups, *Imm*2, *Ima*2 and *R*3*m*. There are key differences in the bond ordering of these structures even though they all evolve from the same $Fd\bar{3}m$ space group. The non-equivalent sites in each of the considered space groups will give different local bonding environments (see Table 3.14). As all three of them have Ga_4 as the nearest neighbour, the 2nd and 3rd nearest neighbour atom will play the decisive role in shaping the fine details of the spectra and giving the best fit between the simulations and experiment.

Table 3.14 Local bonding environments of anion sites in Ga_3O_3N.

Structure	Site	First NN	Second NN	Third NN
***Imm*2**	N_{4c}	Ga_4	O_2N	O_6
	$O_{4c\#1}$	Ga_4	O_3	O_4N_2
	$O_{4c\#2}$	Ga_4	O_3	O_2N_4
	O_{4d}	Ga_4	ON_2	O_6
***Ima*2**	N_{4b}	Ga_4	O_3	O_4N_2
	O_{4b}	Ga_4	O_2N	O_6
	O_{4c}	Ga_4	O_2N	O_4N_2
R*3*m	N_{2c}	Ga_4	O_3	O_6
	O_{6h}	Ga_4	O_2N	O_4N_2

Simulated spectra for the three considered symmetries were calculated and tried to fit the experimental ones. After careful examination, the *R*3*m* structure showed the best fit. Hence, for the *R*3*m* space group the simulated oxygen spectra are shown in Figure 3.30. The simulated O Kα XES and O 1s XANES spectra reproduce the measured

spectra very well and fit all the criteria laid out above. This structure minimised the oxygen clustering, as well as the nitrogen clustering with no oxygen near the nitrogen atoms up to the third coordination shell. Therefore this structure is shown to be the most appropriate to model the high-pressure phase of gallium oxonitride.

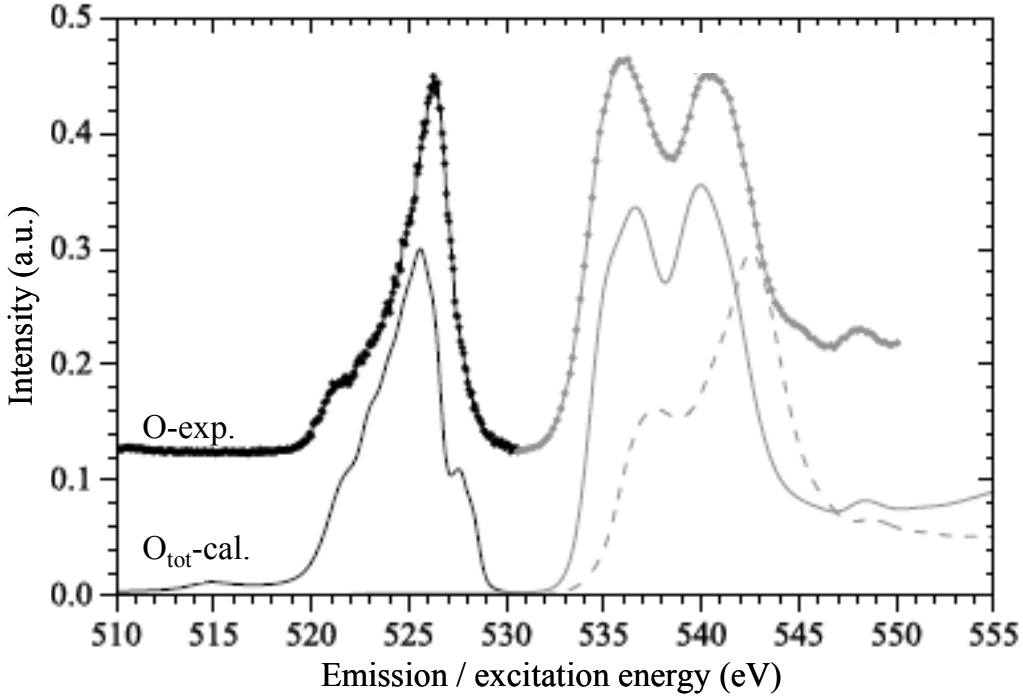

Figure 3.30 Experimental and calculated O Kα XES (black) and O 1s XANES (grey) spectra for the *R*3*m* space group. The dashed line shows the XANES spectra without the inclusion of the core hole in the final state.

*R*3*m* has also been found by Soignard *et al.* with the lowest equilibrium energy [135] and was considered to provide the ground-state configuration for their calculations.

3.3.4.3.1 Density of States

For the total electronic Density of States (DOS) and band structure calculations, the gallium oxonitride is considered to have a *R*3*m* symmetry. The results from ground state DFT calculations using the GGA exchange functional are shown in Figure 3.31. The calculated band structure showed a direct band gap for the gallium oxonitride phase of 1.14 eV.

Since the GGA method is well known to underestimate the band gap values by up to 50% [238], the calculated value can be considered as giving the lowest limit for the

energy gap. The bottom of the conduction band is predicted to be a single band making the inter-band gap transitions less likely, however the curvature is favourable to band gap transitions. The top of the valance band consists of a doubly degenerate highly curved band making the material a suitable candidate for optical devices.

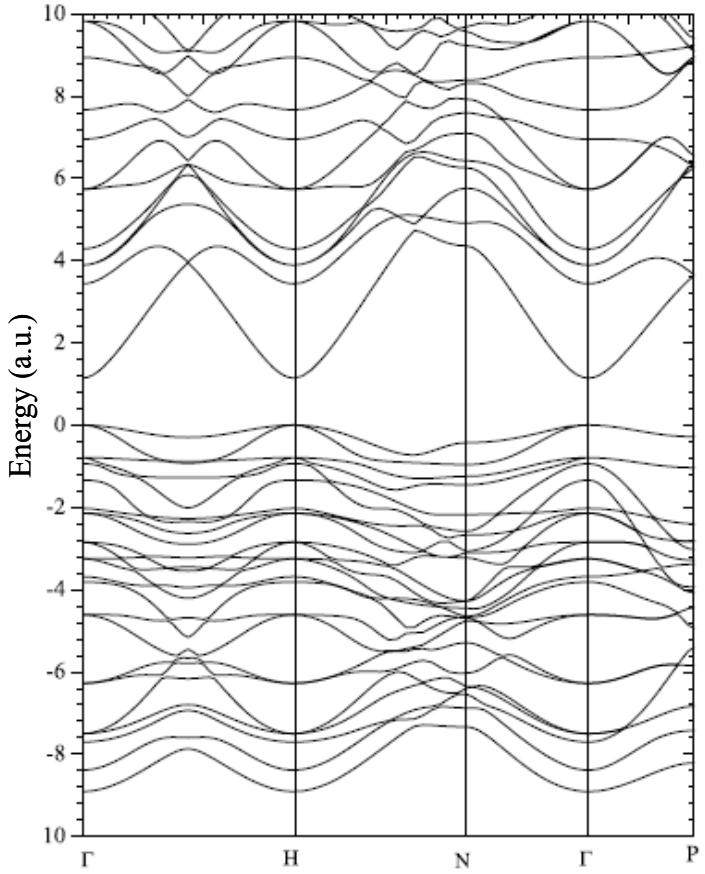

Figure 3.31 The calculated band structure of Ga_3O_3N with *R*3*m* symmetry.

The PDOS (Partial Density of States) is shown in Figure 3.32. The Ga 3d states at ~ -14 eV are almost completely filled and highly localized; there is less charge transfer from these states. The PDOS suggests that this material exhibits a large degree of covalent bonding. The localized d-states show a large degree of bonding with the nitrogen and oxygen s-states. The Ga_{1a} site has no nitrogen as nearest neigbour and is shifted to a higher binding energy due to its oxygen neighbours. There is Ga *d*-hybridization in both nitrogen and oxygen *s* and *p* bands. This creates Ga d-states in all three bands in this material. The nitrogen and oxygen *p*-states do show a large amount of occupied states, suggesting that there is some charge transfer from the gallium to the nitrogen and oxygen decreasing the nitrogen and oxygen unoccupied

states. The large amount of nitrogen and oxygen *p*-states near the Fermi level makes using the N K-edge or O K-edge the best candidate for band gap determination. In this work, the O K-edge was chosen over the N K-edge because of the GaN contamination of the samples, as stated at the beginning of this section.

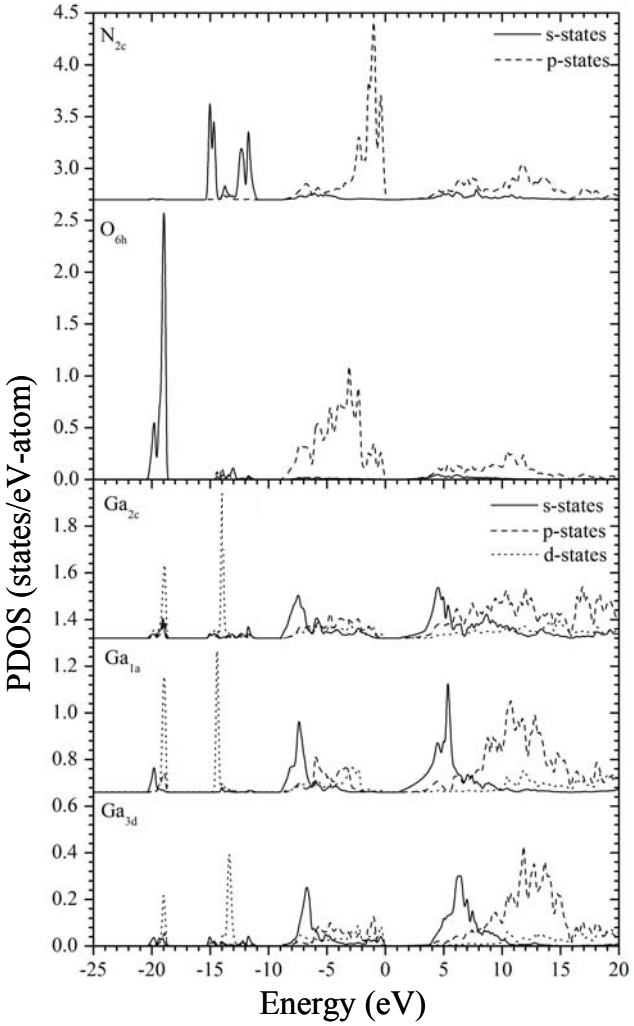

Figure 3.32 The calculated PDOS of Ga_3O_3N with *R*3*m* symmetry.

3.3.4.4 Band gap determination from the SXS spectra

Determining the band gap using the XES and XANES spectra requires several considerations: 1) determining the experimental minimum of the conduction band and maximum of the valence band, 2) correction of the core hole effect that is present in the final state of XANES measurements and 3) consideration of the site splitting or spin-orbit splitting that occurs in the measured spectrum.

The valence band and conduction band edges are also distorted by the oxygen contamination in the gallium nitride. Therefore careful analysis of the second derivative (SD) was performed and is discussed in the following. In Figure 3.33 the SD of the measured O Kα XES and O 1s XANES spectra are shown. The dashed lines indicate the top of the valence band and the bottom of the conduction band. The locations of the edges and the corresponding band gaps for the four investigated samples are listed in Table 3.15.

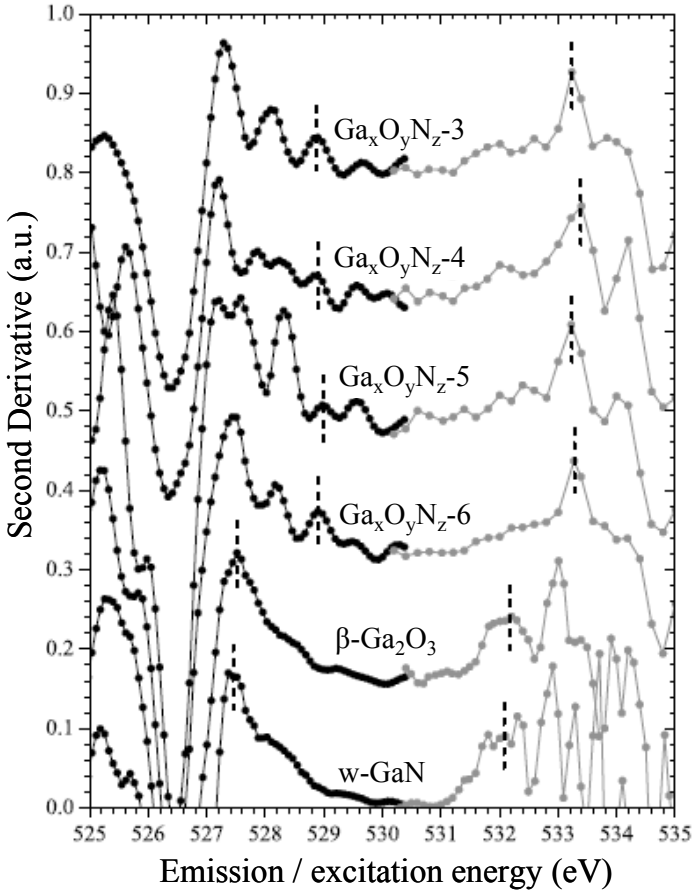

Figure 3.33 The second derivative (SD) of the measured O Kα XES (black) and O 1s XANES (grey) spectra. The dashed lines indicate the top of the valence band and the bottom of the conduction band.

The O K-edge spectra for the entire series are very similar and although there are slight differences in band gap values, this is only due to the limited precision in the XANES spectra (see Table 3.15). If it is assumed that there is a correlation between the nitrogen or oxygen concentration in the structure and the band gap value, it can be concluded that the investigated high-pressure spinel-type gallium oxonitride phases

have a similar chemical composition. Therefore, an average band gap of 4.39 ± 0.10 eV has been determined. The error associated with this value has been calculated from the precision of each measurement reading, as given in Table 3.15.

Table 3.15 Band gap values for the four investigated gallium oxonitride samples.

Sample	**E_{val}** ± 0.15 eV	**E_{cov}** ± 0.15 eV	**Band gap** ± 0.21 eV
$Ga_xO_yN_z$-3	528.90	533.25	4.4
$Ga_xO_yN_z$-4	528.90	533.40	4.5
$Ga_xO_yN_z$-5	528.95	533.25	4.3
$Ga_xO_yN_z$-6	528.90	533.30	4.4
Average band gap			**4.39 ± 0.10 eV**

In Table 3.16, the calculated and experimental band gap values for the spinel-type gallium oxonitride are compared with the reported ones in the literature. The calculated and experimental values for w-GaN and β-Ga_2O_3 are also given for comparison. A good agreement between the band gap values reported in this work and the previous reported ones can be observed. Referring to the corresponding nitride and oxide, it is noticeable that the band gap of the spinel gallium oxonitride is at an intermediary value, but closer to the gallium oxide band gap value. Lowther *et al.* also determined also an intermediary band gap value for the spinel gallium oxonitride between the two end members, but with a magnitude rather similar to that for wurtzite GaN [130]. Looking at the atomic coordinations for the three speciments, gallium nitride (w-GaN), monoclinic gallium oxide (β-Ga_2O_3) and spinel gallium oxonitride (Ga_3O_3N with or without a rhombohedral distortion), the following statements canbe made: all the Ga atoms in the wurtzite structure of GaN are tetrahedrally coordinated, while in the monoclinic β-Ga_2O_3 and spinel gallium oxonitride, Ga atoms are tetrahedrally and octahedrally coordinated. Based on this structural similarity, one would expect that the band gap for the high-pressure gallium oxonitride phase would be closer in magnitude to gallium oxide than to that of gallium nitride.

Table 3.16 Calculated and experimental band gap values for w-GaN, β-Ga_2O_3 compared with the ones for the experimental spinel-structured gallium oxonitride.

	Theoretical	**Experimental**
w-GaN	2.18 eV [130]	3.39 eV [25]
β-Ga_2O_3	2.63 eV [130]	4.7 eV [239]
Ga_3O_3N	2.16 eV (LDA)[130] 2.1 eV (LDA) [135] 1.72 eV; 1.37 eV (LDA; GGA) [133] 1.14 (GGA) (this work)	4.39 eV ± 0.10 (this work)

Lowther *et al.* discussed the dependence of the band gap with the oxygen concentration in $Si_{6-x}Al_xOxN_{8-x}$ systems [227]. It was shown that energy gap decreased from 4 eV for $x = 2$ to 3.1 eV for $x = 4$, the conduction band having a strong dependence on oxygen concentration. Based on this observation, it can be expected that the gallium oxonitride phases investigated in this work might have an increased amount of nitrogen in the structure, closer to the ideal stoichiometry, Ga_3O_3N. But the obtained band gap value is closer to the one for gallium oxide than for gallium nitride. Even though the spinel gallium oxonitride and spinel SiAlON phases are part of the same spinel oxonitride family, their electronic properties do not follow the same trend. This observation requires further investigation.

To conclude, in Section 3.3.4, it was reported and discussed the crystal and electronic structure of the high-pressure phase of gallium oxonitride. Four gallium oxonitride samples were synthesised under different high-pressure-high-temperature conditions, from different GaN / Ga_2O_3 molar ratios. The final products contained different amounts of the spinel gallium oxonitride phase, in addition to GaN from the starting material and, in smaller amounts, BN from the crucible material. Due to these contaminations, the electronic structure and band gap value of gallium oxonitride were determined by probing the O Kα XES and O 1s XANES. Independently, three different structures, *Imm*2, *Ima*2 and *R*3*m* were modelled and fitted to the experimental spectra. The structure which gave the best fit to the experimental spectra was found to be *R*3*m*. The DFT ground-state calculations found a direct band gap of 1.14 eV for the spinel-type gallium oxonitride, which is in good agreement with the previous reported values. The calculated PDOS suggested a large degree of covalent

character for the gallium oxonitride. The experimental band gap values for all four gallium oxonitride samples were very similar, the small differences being primarily due to the calibration precision. Therefore, the band gap of the spinel-type gallium oxonitride was determined to 4.39 ± 0.10 eV.

This was the first time that the band gap for the spinel gallium oxonitride has been determined experimentally. Being a wide band gap semiconductor, the spinel gallium oxonitride is a viable candidate for optoelectronic applications.

4 Conclusions and outlook

4.1 General conclusions

This work deals with the high-pressure, high-temperature syntheses and characterization of spinel-type of gallium oxonitride. The high-pressure phase of gallium oxonitride was fist obtained by Kinski *et al.* in 2005 [134] and independently by Soignard *et al.* [135]. Besides these experimental results, several theoretical studies have also been performed, which predict the formation of a new phase under pressure and temperature, and the resulting compounds have been predicted to present attractive mechanical and electronic properties [130-132, 135].
Following these published results, new goals and approaches were established for a new project on the high-pressure phase of gallium oxonitride. The new compounds were synthesised via the transformation of different starting materials by applying high-pressure, high-temperature conditions using various techniques (DAC, multi-anvil press, piston cylinder press).

Three different starting materials were used, which led to important insights about the pressure/temperature conditions for the syntheses of the gallium oxonitride phases. Using different molar ratios of GaN / Ga_2O_3, the spinel-structured gallium oxonitride formed in a diamond anvil cell at pressures as low as 3 GPa and temperatures around 1600 K. Increasing the pressure up to 20 GPa, the full transformation/recovery of the spinel phase could not be achieved. The multi anvil press device gave the target phase at pressures starting from 2.5 GPa to 11.5 GPa and temperatures above 1300 K. Molar ratios from 1/9 to 9/1 of the two end members gave oxonitride phases in a wide pressure-temperature range. In parallel to the DAC and the multi anvil press, a piston cylinder was also employed for high-pressure syntheses. None of these experiments showed any reactions between the loaded nitride and oxide. This may have been due to a problem with the sealing of the capsules, insufficient nitrogen loaded and/or the uni-axial pressure distribution in the sample assembly. Further iterations of this synthesis method may still lead to gallium oxonitride formation in future experiments.
A second starting material used for the high-pressure syntheses was a precursor-derived gallium oxonitride ceramic. As a first step, the syntheses of the precursors

were performed by heat treating gallium tris(t-butoxide) dimethylamine adduct, $Ga(O^tBu)_3.HNMe_2$, in a continuous ammonia flow at 650 K. Different runs of syntheses were performed, obtaining gallium oxonitride ceramics with different elemental compositions. In addition to this, the thermal stability of the ceramics was investigated. Above 1000 K the crystallisation of monoclinic β-Ga_2O_3 and in a lesser amount w-GaN, started to appear.

The *in-house* synthesised gallium oxonitride ceramics were further used in subsequent high-pressure, high-temperature syntheses in order to obtain the spinel-phase. The ceramics underwent a phase transition to the crystalline spinel phase at a pressure of 0.7 GPa in a diamond anvil cell. No by-products were observed in all the diamond anvil syntheses which had as the starting material the (GaON) ceramic. A Raman spectrum of the spinel phase has been obtained during one of the DAC synthesis. Compared with the spectrum previously reported by Soignard *et al.* [135], the Raman shifts are better defined. In order to obtain larger amounts of the spinel phase, a piston cylinder press was used. GaN was also found in the bulk product, but the spinel gallium oxonitride was possible to isolate having a darker colour and having a higher density than that of the nitride.

A third starting material used in the HP/HT syntheses was the cubic polymorph of gallium oxide, γ-Ga_2O_3. The oxide was loaded in a DAC with nitrogen and showed a transformation into a spinel structure at 4.2 GPa and temperatures between 1500-1800 K. This observation was supported by *in situ* Raman spectroscopy showing no nitrogen Raman active modes once the spinel phase appeared. The cubic γ-Ga_2O_3 which was loaded with neon instead of nitrogen in a DAC, gave no spinel phase under pressure or after laser heating, providing yet more evidence that the syntheses of the spinel-type gallium oxonitride were successful after γ-Ga_2O_3 reacted with nitrogen. In addition to this, the thermodynamically stable phase, β- Ga_2O_3, which was one of the starting materials for the gallium oxonitride syntheses, was also investigated under pressure and temperature. The phase transition β-to-α was reported to occur at 10.9 GPa and laser heated at around 2100 K. The experiment was done in a DAC with nitrogen as the pressure medium. During the experiments the incorporation of nitrogen into the gallium oxide structure was found.

The second part of this work was dedicated to the characterisation of the spinel-type gallium oxonitride phase obtained in large volume press devices.

Under high-pressure/high-temperature conditions of 5 GPa and 1250 °C, the cubic phase $Ga_{2.79}\square_{0.21}(O_{3.05}N_{0.76}\square_{0.19})$ ($\square$ = vacancy) was synthesized in a Walker-type multi anvil apparatus. For the first time, the crystal structure of a gallium oxonitride was determined on the basis of single crystal x-ray diffraction data. The cubic spinel-type gallium oxonitride crystallizes in the space group $Fd\bar{3}m$ (No. 227) with a lattice parameter a_0 = 8.2782 Å. The combination of energy-dispersive x-ray spectroscopy with electron energy-loss spectroscopy allowed the quantification of the relative amounts of nitrogen and oxygen for structural refinement. In the literature dealing with oxonitrides, crystal defects in spinel type materials are handled with different models, mainly the approximation of a constant anion model. The present results indicate that this model is questionable, and one should also take into account a model with both cation and anion vacancies. Furthermore, a linear relationship between the lattice parameters and the N/O ratio in the gallium oxonitrides is questionable. This conclusion is due to the assumption that the determined vacancies both in the cationic and anionic part of the structure have a noticeable impact on the size of the unit cell, reducing it to a smaller size than expected.

Compression–decompression runs were carried out in a DAC device in order to determine the bulk modulus of the spinel-type gallium oxonitride. A gallium oxonitride ceramic was loaded in a DAC with LiF as pressure medium and compressed up to around 9 GPa. A full phase transition to a spinel-structure was observed after applying 1 GPa. After fitting the compression–decompression runs data with the second-order Birch–Murnaghan equation EOS, a bulk modulus K of 216(7) GPa and a volume at zero pressure V_0 of 552.9(5) $Å^3$ were derived.

The first attempt to measure the hardness of the spinel phase by micro and nano-hardness tests is reported in this work. Two high-pressure samples obtained from a multi anvil synthesis were probed. The presence of a second phase (w-GaN) together with spinel gallium oxonitride, a reasonably high porosity and other possible sample imperfections allowed only preliminary studies of the elasto-mechanical properties.

Taking into account all of these issues, a hardness of around 10 GPa and reduced elastic modulus of around 130 GPa are considered as minimum values expected for the spinel-type of gallium oxonitride.

In order to obtain the coefficient of thermal expansion of the spinel-type gallium oxonitride, its powder XRD patterns were collected on heating in air from room temperature (RT) to 1170 K. It was found that the thermal expansion coefficient increases from 1.3 x 10^{-6} K^{-1} at 300 K to 4.7 x 10^{-6} K^{-1} at 1100 K. Within the investigated temperature range the spinel phase was stable with no cell distortions and decomposition. Compared with different other cubic compound, nitrides and oxonitrides, the spinel gallium oxonitride has a lower thermal expansion coefficient in the investigated temperature range.

The last point, but certainly not the least important, the electronic structure and band gap determination for the spinel-type gallium oxonitride were discussed. Four gallium oxonitride samples were synthesised under different high-pressure-high-temperature conditions, from different GaN / Ga_2O_3 molar ratios. The final products contained different amounts of the spinel gallium oxonitride phase, in addition to GaN from the starting material and, in smaller amounts, BN from the crucible material. Due to these contaminations, the electronic structure and band gap value of gallium oxonitride were determined by probing the O Kα XES and O 1s XANES. Independently, three different structures, *Imm*2, *Ima*2 and *R*3*m* were modelled and fitted to the experimental spectra. The structure which gave the best fit to the experimental spectra was found to be *R*3*m*. The DFT ground-state calculations found a direct band gap of 1.14 eV for the spinel-type gallium oxonitride, which is in good agreement with the previous reported values. The calculated PDOS suggested a large degree of covalent character for the gallium oxonitride. The experimental band gap values for all four gallium oxonitride samples were very similar, the small differences being primarily due to the calibration precision. Therefore, the band gap of the spinel-type gallium oxonitride was determined to 4.39 ± 0.10 eV. Being a wide band gap semiconductor, the spinel gallium oxonitride is a viable candidate for optoelectronic applications.

4.2 Outlook

One of the main goals of this work was to investigate the stability field of the spinel-type gallium oxonitride under high-pressure and high-temperature conditions. An intensive and systematic study, using w-GaN and β-Ga_2O_3 as starting materials, revealed a wide pressure-temperature-composition stability range for the spinel phase. For a complete determination of the phase equilibrium diagram, the experimental results obtained in this work should be complemented by theoretical calculations using thermodynamic data.

Using a molecular precursor-derived gallium oxonitride ceramic, the spinel phase was obtained at much lower pressures (below 1 GPa) than by using the two end members, the nitride and oxide. This result encourages further investigation to be made in order to decrease the necessary pressure and/or temperature for sample preparation as low as possible for industrial applications.

Another area which needs further investigation would be to systematically find the exact chemical composition of the synthesised spinel-type gallium oxonitride phases, especially the nitrogen and oxygen amounts. The method chosen in this work for the anion amount determination was EELS coupled with TEM. Due to a nitrogen loss in the high vacuum TEM column, it is difficult to quantify the exact amount of nitrogen using this method. Another commonly used method for chemical composition determination is Electron Probe Microanalysis (EPMA). This technique is based on the analysis of the characteristic x-ray fluorescence spectra from the sample excited by a focused high-energy electron beam. Due to similar experimental conditions between EPMA and EELS, EPMA was not chosen as an alternative for the elemental composition determination of the spinel-phase gallium oxonitride. The ideal choice for an elemental composition determination, especially when dealing with the presence of light elements is by using neutron diffraction methods. The reason for choosing neutrons over x-rays is because the neutron-nuclear scattering lengths vary irregularly among the isotopes due to their dependence on the details of the neutron-nuclear interaction potential. A drawback for using neutron diffraction is the need of a considerable amount of sample, which was not available for the work reported in this thesis. Nevertheless, as shown in this work, a piston cylinder was used successfully for the syntheses of the high-pressure phase, which can produce millimetre-size

samples in one run. Hence if several syntheses were performed using this high-pressure device, a sufficient amount of sample could be produced for neutron experiments.

Some of the properties of the spinel-phase gallium oxonitride were also investigated in this work. The main impediment for accurate determination of some of them (mechanical properties, electronic structure) was the lack of a phase pure sample of gallium oxonitride. This may be solved by having a better control over the experimental conditions. In the future, further hardness and elastic moduli investigations may be possible, when one succeeds in the synthesis of a larger amount of phase pure sample.

Acknowledgements

I am grateful to Prof. Dr. Dr. h. c. Ralf Riedel, my doctoral advisor, for giving me the opportunity to perform my PhD research in his group. His supervision, support and belief in my abilities helped me to overcome all my scientific and personal difficulties during the three years of my PhD.

I would also like to thank Prof. Leonid Dubrovinsky from Bayerisches Geoinstitut (BGI), Bayreuth, for introducing me to the high-pressure research field and providing me with access to all the high-pressure devices available in his group. This collaboration made much of the work in this thesis possible. Moreover, working in Prof. Dubrovinsky's high-pressure laboratory at BGI was one of the most enjoyable and scientifically satisfying experiences during my PhD. Special thanks also go to many of Prof. Dubrovinsky's co-workers: Evgeniya Zarechnaya, Olga Narygina, Alexander Kurnosov, Kostea Glazyrin and Slava Shcheka for all of their help with the diamond anvil cell and piston cylinder syntheses, but also for their friendliness which I will always remember fondly.

Many thanks go to Dr. Isabel Kinski (Fraunhofer-Institut für Keramische Technologien und Systeme, Dresden) for her great interest in this project, helpful advice and scientific discussions over the course of my PhD. Special thanks go to Prof. Hubert Huppertz (Leopold-Franzens-Universität Innsbruck, Austria) and Stefanie Hering (Ludwig-Maximilians-Universität München), with whom I worked with in a very productive collaboration on the high-pressure and high-temperature synthesis of the spinel-gallium oxonitride. Due to the successful multi-anvil syntheses done by Stefanie under the supervision of Prof. Huppertz, I was able to perform parts of the characterisation of the material reported in this work.

I am grateful to Gerhard Miehe for all of his help during TEM measurements and also concerning the Rietveld refinement method. I am thankful to Stefan Lauterbach for all the hours spent at the TEM and EELS. I would also like to acknowledge Prof. Alexander Möwes and Teak Boyko (at the University of Saskatchenwan, Canada) for the collaboration on understanding the band structure of spinel gallium oxonitride,

based on experiments performed at the ALS, Berkeley, US. I am thankful to Prof. Tanguy Rouxel, Ludovic Charleux, and Pathikumar Sellapan (Laboratory of Applied Mechanics, University of Rennes 1, France) for their help and support during the micro and nano-hardness measurements performed in Rennes.

In addition I would like to express my deepest gratitude to my colleagues from FG Disperse Feststoffe, FB Material- und Geowissenschaften, TU Darmstadt: Dima Dzivenko, Miria Andrade, Christoph Linck, Claudia Fasel, Emanuel Ionescu, Aleksander Gurlo, Rodrigue Ngoumeni Yappi, and Vassilios Siozios for their scientific help, moral support and friendship. Special thanks go to Dima for helpful discussions regarding a huge array of different scientific topics, but especially concerning my high-pressure experiments. I would also like to thank all my colleagues in the group at Darmstadt for providing a pleasant and friendly work atmosphere during my PhD.

A special thank you goes to Prof. Christina Roth, who provided me with helpful advice in writing my doctoral thesis, despite my PhD work being wholly independent of her. The level of support she gave me exceeded all expectations, and I hope she appreciates how grateful I am to her for her support.

Last but not least, I thank Andrew Walters from the bottom of my heart for all his corrections and advice with writing this thesis, our scientific discussions and most of all for his unconditional support and love during our time together.

I dedicate this thesis to my parents, Ioan and Violeta, and I am forever grateful to them for all their love, their belief in me and for their never-ending support.

Dedic această teză de doctorat părinților mei, Ioan şi Violeta. Vă sunt pe veci recunoscătoare pentru dragostea oferită şi încrederea pe care mi-ați acordat-o de-a lungul anilor mei de studiu.

References

1. Fuertes A., *Dalton Trans.* , 39, (2010), 5942-5948.
2. Shannon R. D., *Acta Crystallogr. A* 32, (1976), 751-767.
3. Marchand R., Pors F., Laurent Y., *Rev. Int. Hautes Temp. Refract.* , 23, (1986), 11-20.
4. Grins J., Käll P.O., Svensson G., *J. Solid State Chem.* , 117, (1995), 48-54.
5. Veith G.M., Greenblatt M., Croft M., Goodenough J.B., *Mater. Res. Bull.* , 36, (2001), 1521-1530.
6. Armytage D., Fender B.E.F., *Acta Craystallogr. B*, 30, (1974), 809-812.
7. Antoine P., Marchand R., Laurent Y., *Rev. Int. Hautes Temp. Refract.* , 24, (1987), 43-46.
8. Guyader J., Grekov F. F., Marchand R., Lang J., *Rev. Chim. Miner.*, 15, (1978), 431-438.
9. Pearson G. P., *Inorg. Chem.* , 30, (1991), 2856-2858.
10. "*Encyclopedia of Materials* " Vol. 7, 2001, Elsevier, Amsterdam. 6161.
11. Asahi R., Morikawa T., Ohwaki T., Aoki K., Taga Y., *Science*, 293, (2001), 269-271.
12. Hitoki G., Takata T., Kondo J. N., Hara M., Kobayashi H., Domen K., *Chem. Commun.* , 16, (2002), 1698-1699.
13. Jasen M., Letschert H.P., *Nature*, 404, (2000), 980-982.
14. Jorge A.B., Oro-Sole J., Bea A.M., Mufti N., Palstra T.T., Rodgers J.A., Attfield J.P., Fuertes A., *J. Am. Chem. Soc.* , 130, (2008), 12572-12573.
15. Kusmartseva A., Yang M., Oro-Sole J., Bea A.M., Fuertes A., Attfield J.P., *Appl. Phys. Lett.* , 95, (2009), 022110-022112.
16. Buchmann V., Ronda C., Oeckler O., Schnick W., Meijerink A., *Chem. Mater.* , 21, (2009), 316-325.
17. McCaulley J.W., Corbin N. D., *Army Materials and Mechanics research Center*, (1979), 476-479.
18. McCauley J.W., *J. Am. Ceram. Soc.*, 61, (1978), 372-373.
19. Corbin N. D., *J. Eur. Ceram. Soc.*, 5, (1989), 143-154.
20. McCauley J.W., Patel P., Chen M., Glide G., Strassburger E., Paliwal B., Dandekar D. P., *J. Europ. Ceram. Soc.*, 29, (2009), 223-236.
21. McCauley J.W., "*Encyclopedia of Materilas: Science and Technology*" 2001, Elsevier Science, NewYork.
22. Bray K. R., Weimer J., Wu R. L. C., Fries-Carr S., *CARTS USA* 3-6, (2006),
23. Jack K. H., *J. Mater. Sci.*, 11, (1976), 1135-1158.
24. Schwarz M., Zerr A., Kroke E., Miehe G., Chen I.-W., Heck M., Thybusch B., Poe B.T., Riedel R., *Angew. Chem. Int. Ed.* , 41, (2002), 789-793.
25. Maruska H. P., Tietjen J. J., *Appl. Phys. Lett.* , 15, (1969), 327-329.
26. Holt D.B., Yacobi B.G., "*Extended Defects in Semiconductors. Electronic Properties, Device Effects and Structures* " 2007, Cambridge University Press.
27. Ren F., Hong M., Chu S. N. G., Marcus M.A., Schurman M.J., Baca A., Pearton S.J., Abernathy C.R., *Appl. Phys. Lett.*, 73, (1998), 3893-3895.

28. Kaye&Laby, NPL, available from: http://www.kayelaby.npl.co.uk/general_physics/2_5/2_5_8.html.
29. Yoshikawa A., "*Development and Applications of Wide Bandgap Semiconductors"*, in *"Development and Applications of Wide Bandgap Semiconductors"*, Ed. Takahashi K., Yoshikawa A. and Sandhu A. 2007.
30. Nakamura S., Senoh M., Mukai T., *Jpn. J. Appl. Phys.*, 30, (1991), L1708.
31. Krukowski S., Bockowski M., Lucznik B., Grzegory I., Porowski S., Suski T., Romanowski Z., *J. Phys.: Condens. Matter.* , 13, (2001), 8881-8890.
32. Haines J., Leger J. M., Bocquillon G., *Annu. Rev. Mater. Res.* , 31, (2001), 1-23.
33. McMillan P. F., *Nature* 1, (2002), 19-25.
34. McMillan P. F., *High Pressure Research*, 23, (2003), 7-22.
35. Brazhkin V. V., Lypin A. G., Hemley R. J., *Phyl. Mag. A*, 82, (2002), 231-253.
36. Brazhkin V. V., *High Pressure Research*, 27, (2007), 333-351.
37. Riedel R., *Adv. Mater.*, 6, (1994), 549–560.
38. Hazen R. M., "*The Diamond Makers* " **1999**, Cambridge University Press, Cambridge.
39. Bundy F.P., Hall H. T., Strong H.M., Wentorf R. Jr., *Nature*, 176, (1955), 51-54.
40. Sigalas I., Caveney R. J., "*Diamond Materials and their Applications"*, in *"Diamond Materials and their Applications"*, Ed. Weinheim, 2000.
41. Wentorf R. Jr., *J. Chem. Phys.* , 26, (1957), 956-960
42. Solozhenko V. L., Andrault D., Fiquet G., Mezouar M., Rubie D.C., *Appl. Phys. Lett.* , 78, (2001), 1385-1387.
43. Zerr A., Miehe G., Seghiou G., Schwarz M., Kroke E., Riedel R., Fuess H., Kroll P., Boehler R., *Nature*, 400, (1999), 340-342.
44. Leger J. M., Haines J., Schmidt M., Petitet J. P., Pereira A. S., Jornada J. A. H., *Nature*, 383, (1996), 401.
45. Hubert H., Garvie L. A. J., Devouard B., Buseck P. R., Petuskey W. T., McMillan P. F., *Chem. Mater.* , 10, (1998), 1530-1537.
46. Dubrovinsky L., Dubrovinskaia N., Swamy V., Muscat J., Harrison N. M., Ahuja R., Holm B., Johansson B., *Nature*, 410, (2001), 653-654.
47. Tanaguchi T., Teraji T., Koizumi S., Watanabe K., Yamaoka S., *Jpn. J. Appl. Phys.*, 241, (2002), L109-L111.
48. Sumiya H., Toda N., Nishibayashi Y., Satoh S., *J. Cryst. Growth*, 178, (1997), 485-494.
49. Bockowski M., Wroblewski M., Lucznik B., Grzegory I., *Mater. Sci. Semicond. Process.*, 4, (2001), 543-548.
50. Leinenweber K., O'Keeffe M., Somayazulu M., Hubert H., McMillan P. F., Wolf G. H., *Chem. Eur. J.* , 5, (1999), 3076-3078.
51. Dong J., Sankey O. F., Deb S. K., Wolf G., McMillan P. F., *Phys. Rev. B*, 61, (2000), 11979-11992.
52. Soignard E., Somayazulu M., Mao H.-K., Dong J., Sankey O. F., McMillan P. F., *Solid State Commun.*, 120, (2001), 237-242.
53. Angus, Hayman, *Science*, 241, (1988), 913-921.
54. Carmalt C. J., *Abstr. Pap. Am. Chem. Soc.* , 219, (2000), 267.
55. Schmitz G., Gassmann P., Franchy R., *J. Appl. Phys.*, 83, (1998), 2533-2538.
56. Levin I., Brandon D., *J. Am. Ceram. Soc.*, 81, (1998), 1995-2012.
57. available from: http://www.reade.com.

58. Geller S., *J. Chem. Phys.* , 33, (1960), 676-684.
59. Ahman J., Svensson G., Albertsson J., *Acta Crystallogr.*, C52, (1996), 1336-1338.
60. Fleischer M., *J. Mater. Sci. Lett.* , 11, (1992), 1728-1731.
61. Passlack M., Schubert E. F., Hobson W. S., Hong M., Moriya N., Chu S. N. G., Konstandinidis K., Mannaerts J. P., Schnoes M. L., Zydzik, *J. Appl. Phys.*, 77, (1995), 686-693.
62. Aubay E., Gourier D., *Phys. Rev. B*, 47, (1993), 15023-15036.
63. Fleischer M., *Sens. Actuators B* 4, (1991), 437-441.
64. Passlack M., Hunt N. E. J., Schubert E. F., Zydzik, Hong M., Mannaerts J. P., Opila R. L., Fisher R. J., *Appl. Phys. Lett.*, 64, (1994), 2715-2717.
65. Choi C. Y., Kim W. S., Park Y. S., Lee S. M., Bae D. J., Lee Y. H., Park G.-S., Choi W. B., Lee N. S., Kim J. M., *Adv. Mater.*, 12, (2000), 746-750.
66. Roy R., Hill V. G., Osborn E. F., *J. Am. Chem. Soc.*, 74, (1952), 719-722.
67. Zinkevich M., Morales F. M., Nitche H., Ahrens M., Rühle M., Aldinger F., *Z. Metallkd.*, 95, (2004), 756-762.
68. Arean C. O., Bellan A. L., Mentruit M. P., Delgado M. R., Palomino G. T., *Microporous Mesoporous Mater.* , 40, (2000), 35-42.
69. Pohl K., *Naturwissenschaften*, 55, (1968), 82.
70. Nowak E., Quartararo J., Derouane E. G., Vedrine J. C., *Appl. Catal. A*, 251, (2003), 107-120.
71. Freeman D., Wells R. P. K., Hutchings J., *J. Catal.* , 205, (2002), 358-365.
72. Haneda M., Kintaichi Y., Mizushima T., Kakuta N., Hamada H., *Appl. Catal. B*, 31, (2001), 81-92.
73. Lavalley J. C., Daturi M., Montouillout V., Clet G., Arean C. O., Delgado M. R., Sahibed-dine A., *Phys. Chem. Chem. Phys.* , 5, (2003), 1301-1305.
74. Sohlberg K., Pennycook S. J., Pantelides S. T., *Chem. Eng. Comm.* , 181, (2000), 107-135.
75. Tu B., Cui Q., Xu P., Wang X., Gao W., Wang C., Liu J., Zou G., *J. Phys: Condens. Matter*, 14, (2002), 10627-10630.
76. Lipinska-Kalita K. E., Chen B., Kruger M. B., Ohki Y., Murowchick J., Gogol E. P., *Phys. Rev. B*, 68, (2003), 035209.
77. Grimsditch M., *Phys. Rev. Lett.*, 52, (1984), 2379-2381.
78. Meade C., Hemley R. J., Mao H. K., *Phys. Rev. Lett*, 69, (1992), 1387-1391.
79. Machon D., McMillan P. F., Xu B., Dong J., *Phys. Rev. B*, 73, (2006), 094125-1-9.
80. Kim H.-G., Kim W.-T., *J. Appl. Phys.*, 62, (1987), 2000-2002.
81. Akasaki I., Amano H., *Jpn. J. Appl. Phys.*, 36, (1997), 5393-5408.
82. Fasol G., *Science*, 278, (1997), 1902-1903.
83. Ponce F. A., Bour D.P., *Nature*, 386, (1997), 351-359.
84. Nelmes R. J., Mc Mahon M. I., "*High Pressure in Semiconductor Physics, Semiconductors and Semimetals*", ed. Suski T. and Paul W.Vol. 54, 1998 San Diego.
85. Shultz H., Theimann K. H., *Solid State Commun.* , 23, (1977), 815-918.
86. Baleva M., Mateeva E., *J. Phys: Condens. Matter*, 5, (1993), 7959-7970.
87. Kim J. G., Frenkel A. C., Liu H., Park R.M., *Appl. Phys. Lett.* , 65, (1994), 91-93.
88. Lin M. E., Xue G., Zhou G. L., Greene J. E., Morkoc H., *Appl. Phys. Lett.*, 63, (1993), 932-933.

89. Zhang C. G., Bian L. F., Chen W. D., Hsu C. C., *J. Cryst. Growth* 299, (2007), 268-271.
90. Rawat V., Zakharov D.N., Stach E.A., Sands T.D., *Phys. Rev. B*, 80, (2009), 024114-1-5.
91. Xu F., Xie Y., Zhang X., Zhang S., Shi L., *New J. Chem.* , 27, (2003), 565-567.
92. Xia H., Xia Q., Ruoff A. L., *Phys. Rev. B*, 47, (1993), 12925-12928.
93. Perlin P., Jauberthie-Carillon C., Itie J. P., San Miguel A., Grzegory I., Polian A., *Phys. Rev. B*, 45, (1992), 83-89.
94. Ueno M., Yoshida M., Onodera A., Shimomura O., Takemura K., *Phys. Rev. B*, 49, (1994), 14-21.
95. Ueno M., Onodera A., Shimomura O., Takemura K., *Phys. Rev. B*, 45, (1992), 10123-10126.
96. Besson J.M., *Jpn. J. Appl. Phys. Suppl.* , 32, (1993), 11.
97. Serrano J., Rubio A., Hernandez E., Munoz A., Mujica A., *Phys. Rev. B*, 62, (2000), 16612-16623.
98. Munoz A., Kunc K., *Phys. Rev. B*, 44, (1991), 10372-10373.
99. Christensen N. E., Gorezyca I., *Phys. Rev. B*, 50, (1994), 4397-4415.
100. Van Vachten J. A., *Phys. Rev.* , 182, (1969), 891-905.
101. Karpinski J., Jun J., Porowski S., *J. Cryst. Growth* 66, (1984), 1-10.
102. Yamane H., Shimada M., Clarke J., Disalvo F. J., *Chem. Mater.* , 57, (1997), 413-416.
103. Shin T. I., Yoon D. H., *Cryst. Res. Technol.*, 40, (2005), 827-831.
104. Rodewald D., Bill J., Beck U., Puchinger M., Wagner T., Greiner A., Aldinger F., *Adv. Mater.* , 11, (1999), 1502-1504.
105. Jegier J. A., McKernan S., Purdy A. P., Gladfelter W. L., *Chem. Mater.* , 12, (2000), 1003-1010.
106. Janik J. F., Wells R. L., Coffer J. L., St John J. V., Pennington W. T., Schimek G. L., *Chem. Mater.*, 10, (1998), 1613-1622.
107. Chaplais G., Kaskel S., *J. Mater. Chem.*, 14, (2004), 1017-1025.
108. Verdier P., Marchand R., *Rev. Chim. Miner.* , 13, (1976), 145.
109. Grekov F. F., Deminov D. M., Zykov A. M., *Zh. Prikl. Khim.* , 52(6), (1979), 1394.
110. Aleksandrov S. E., Zykov A. M., Kryakin V. A., Tsoi V. V., *Zh. Prikl. Khim.*, 61, (1988), 1454.
111. Shiota I., Miyamoto N., Nishizawa J.-I., *Surf. Sci.*, 86, (1979), 272-279.
112. Shiota I., Nishizawa J., *Surf. Interface Anal.* , 1, (1979), 185-188.
113. Tsuruoka T., Kawasaki M., Ushioda S., Franchy R., Naoi Y., Sugahara T., Sakai S., Shintani Y., *Surf. Sci.*, 427-428, (1999), 257-261.
114. Wolter S. D., DeLucca J. M., Mohney S. E., Kern R. S., Kuo C. P., *Thin Solid Films*, (2000), 153-160.
115. Puchinger M., Kisailus D. J., Lange F. F., Wagner T., *J. Cryst. Growth*, 245, (2002), 219-227.
116. Kerlau M., Merdrignac-Conanec O., Reichel P., RBarsan N., Weimar U., *Sens. Actuators B*, 115, (2006), 4-11.
117. Cailleaux X., Maria del Carmen Marco de Lucas, Merdrignac-Conanec O., Tessier F., Nagasaka K., Kikkawa S., *J. Phys. D*, 42, (2009), 045408-1-6.
118. Shanthi S., Hashimoto M., Zhou Y. K., Kimura S., Emura S., Hasegawa S., Hasuike N., Harima H., Asahi H., *Appl. Phys. Lett.*, 86, (2005), 092102-1-3.

119. Shanthi S., Hashimoto M., Zhou Y. K., Kimura S., Kim M.-S., Emura S., Hasuike N., Harima H., Hasegawa S., Ishimaru M., Hirotsu Y., Asahi H., *J. Appl. Phys.* , 98, (2005), 013526-1-8.
120. Budde F., Ruck B. J., Koo A., Granville S., Trodahl H. J., Bittar A., Williams G. V. M., Ariza M. J., Bonnet B., Jones D. J., Metson J. B., Rubanov S., Munroe P., *J. Appl. Phys.* , 98, (2005), 063514-1-4.
121. Sudhir G. S., Fujii H., Wong W. S., Kisielowski C., Newman N., Dieker C., Liliental-Weber Z., Rubin M. D., Weber E. R., *J. Electron. Mater.* , 27, (1998), 215-221.
122. Schmitz G., Eumann M., Stapel D., Franchy R., *Surf. Sci.*, 427-428, (1999), 91-96.
123. Cho S., Lee J., Park I.-Y., Kim S., *Mater. Lett.* , 57, (2002), 1004-1009.
124. Kikkawa S., Ohtaki S., Takeda T., Yoshiasa A., Sakurai T., Miyamoto Y., *J. Alloys Compd.*, 450, (2008), 152-156.
125. Kikkawa S., Nagasaka K., Takeda T., Bailey M., Sakurai T., Miyamoto N., *J. Solid State Chem.*, 180, (2007), 1984-1989.
126. Yamamoto S., Kikkawa S., Masubuchi Y., Takeda T., Wolff H., Dronskowski R., Yoshiasa A., *Solid State Commun.* , 147, (2008), 41-45.
127. Kinski I., Scheiba F., Riedel R., *Adv. Eng. Mater.*, 7, (2005), 921-927.
128. Kümmerle W., Grandmann U., *Solid State Commun.* , 24, (1977), 33-35.
129. Printz G. A., *Phys. Rev. Lett.* , 54, (1985), 1051-1055.
130. Lowther J. E., Wagner T., Kinski I., Riedel R., *J. Alloys Compd.*, 376, (2004), 1-4.
131. Kroll P., Dronskowski R., Martin M., *J. Mater. Chem.*, 15, (2005), 3296-3302.
132. Kroll P., *Phys. Rev. B*, 72, (2005), 144407-1-4.
133. Okeke O. U., Lowther J. E., *Phys. Rev. B*, 77, (2008), 094129-1-9.
134. Kinski I., Miehe G., Heymann G., Theissmann R., Riedel R., Huppertz H., *Z. Naturforsch.*, 60b, (2005), 831-836.
135. Soignard E., Machon D., McMillan P. F., Dong J., Xu B., Leinenweber K., *Chem. Mater.*, 17, (2005), 5465-5472.
136. Valet M., Hoffman D., *Chem. Mater.*, 13, (2001), 2135-2143.
137. Foley P., Zeldin M., *Inorg. Chem.* , 14, (1975), 2264-2267.
138. Nöth H., Konrad P., *Z. Naturforsch.* , 30b, (1975), 681-687.
139. Bridgman P. W., *Phys. Rev.* , 15, (1935), 825-847.
140. Eremets M. I., "*High Pressure Eperimental Methods*" 1996, Oxford University Press, Oxford.
141. Miletich R., Allan D. R., Kuhs W. F., *Rev. Mineral. Geochem.* , 41, (2000), 445.
142. Dunstan D. J., Scherrer W., *Rev. Sci. Inst.*, 59, (1988), 627-630.
143. Sung C. H., Goetze C., Mao H. K., *Rev. Sci. Instrum.*, 48, (1977), 1386-1391.
144. Kenichi T., *Phys. Rev. B*, 60, (1999), 6171-6174.
145. Chai M., Brown J. M., *Geophys. Res. Lett.* , 23, (1996), 3539-3542.
146. Sharma S. M., Gupta Y. M., *Phys. Rev. B*, 43, (1991), 879-893.
147. Decker D. L., Petersen S., Debray D., *Phys. Rev. B*, 19, (1979), 3552-3555.
148. Resel R., Oehzelt M., Shimizu K., Nakayama A., Takemura K., *Solid State Commun.*, 129, (2004), 103-106.
149. Machon D., Dmitriev V. P., Bouvier P., Timonin P. N., Shirokov V. B:, H.-P., *Phys. Rev. B*, 68, (2003), 144104-1-7.
150. Kurnosov A., Kantor I., Boffa-Ballaran T., Lindhardt S., Dubrovinsky L., Kunznetsov A., Zehnder B. H., *Rev. Sci. Inst.*, 79, (2008), 145110-1-5.

151. Barnett J.D., Block S., Piermarini G. J., *Rev. Sci. Instrum.* , 44, (1973), 1-9.
152. Piermarini G. J., Block S., Barnett J.D., Forman R. A., *J. Appl. Phys.* , 46, (1975), 2774-2780.
153. Hess N. J., Exarhos G. J., *High Pressure Research*, 2, (1989), 57-64.
154. Leger J. M., Chateau C., Lacam A., *J. Appl. Phys.* , 68, (1990), 2351-2354.
155. Birch F., *J. Geophys. Res.*, 91, (1986), 4949-4954.
156. Liu J., Dubrovinsky L., Ballaran T. B., Crichton W., *High Pressure Research*, 27, (2007), 483-489.
157. Schmidt M., Schiferl D., Zinn A.S., Ragan D.D., Moore D.S., *J. Appl. Phys.*, 69, (1991), 2793-2799.
158. Mao H. K., Bell P. M., *J. Geophys. Res.*, 91, (1986), 4673-4676.
159. Hemley R. J., Zha C. S., Jephcoat A. P., Mao H. K., Finger L. W., Cox D. E., *Phys. Rev. B*, 39, (1989), 11820-11827.
160. Zha C.-S., Boehler R., *Phys. Rev. B*, 31, (1985), 3199-3201.
161. Schiferl D., *Rev. Sci. Instrum.* , 58, (1987), 1316-1317.
162. Dubrovinskaia N., Dubrovinsky L., *Rev. Sci. Inst.*, 74, (2003), 3433-3437.
163. Dubrovinsky L., Saxena S. K., Lazor P., *Geophys. Res. Lett.*, 24, (1997), 1835-1838.
164. Zha C. S., Bassett W. A., *Rev. Sci. Instrum.*, 74, (2002), 1255-1262.
165. Dubrovinsky L., Glazyrin K., McCammon C., Narygina O., Greenberg E., Übelhack S., Chumakov A. I., Pascarelli S., Prakapenka V., Bock J., Dubrovinskaia N., *J. Synchrotron Rad.*, 16, (2009), 1-5.
166. Weathers M., Bassett W. A., *Phys. Chem. Minerals*, 15, (1987), 105-112.
167. Heinz D. L., Jeanloz R., "*Temperature measurementsin the laser-heated diamond anvil cell"*, in *"Temperature measurementsin the laser-heated diamond anvil cell"*, Ed. Manghnani M.H., Syono Y. and TERRAPUB Tokyo, 1987.
168. Hall H. T., *Rev. Sci. Inst.*, 31, (1960), 125-131.
169. Walker D., Carpenter M. A., Hitch C. M:, *Am. Mineral.*, 75, (1990), 1020-1028.
170. Walker D., *Am. Mineral.* , 76, (1991), 1092-1100.
171. Frost D.J., Poe B.T., Tronnes R.G., Liebske C., Duba A., Rubie D.C., *Phys. Earth Planetary Interiors*, 143-144, (2004), 507-514.
172. Boyd F. R., England J. L., *J. Geophys. Res.* , 65, (1960), 741-748.
173. Huppertz H., *Z. Kristallogr.*, 219, (2004), 330-338.
174. Rubie D.C., *Phase Transitions*, 68, (1999), 431-451.
175. Dubrovinsky L., Dubrovinskaia N., Kantor I., Nestola F., Gatta G. D., *High Pressure Research*, 26, (2006), 137-143.
176. Von Barth U., Grossmann G., *Phys. Rev. B*, 25, (1982), 5150-5179.
177. Krause M. O., Oliver J. H., *J. Phys. Chem. Ref. Data*, 8, (1979), 329-338.
178. Goodings D. A., Harris R., *J. Phys. C*, 2, (1969), 1808-1816.
179. available from: http://www-als.lbl.gov/als/.
180. available from: http://www-als.lbl.gov/als/.
181. Harris, *Journ. Phys. Pt. C Sol. Stat. Phys.*, 2, (1969), 1808
182. Oliver, *Journ. Phys. and Chem*, 8, (1979), 329
183. P. Blaha, ed. *WIEN2k An Augmented Plane Wave+Local Orbitals Program for Calculating Crystal Properties*. ed. Edition. 2008: Austria.
184. Blaha, *Comput. Mater. Sci.*, 28, (2003), 259.
185. K. Schwarz, *Comput. Phys. Commun.*, 147, (2002), 71.
186. J. Perdew, *Phys. Rev. Lett.*, 77, (1996), 3865

187. Williams D. B., Carter C.B., "*Transmission Electron Microscopy*" Vol. 1-4, 1996, Plenum press.
188. Krishnan R. S., Shankar R. K., *J. Raman Spectrosc.* , 10, (1981), 1-8.
189. Ferraro J. R., Nakamoto K., Brown C. W., "*Introductory Raman Spectroscopy*", ed. sec2003, Elsevier.
190. Loudon R., *Adv. Phys.* , 13, (1964), 423-480.
191. Soignard E., McMillan P. F., *Chem. Mater.*, 16, (2004), 3533-3542.
192. Murnaghan F. D., *Physics*, 30, (1944), 244-247.
193. Birch F., *Phys. Rev.*, 71, (1947), 809-824.
194. Vinet P., Rose J. H., Ferrante J., Smith J. R., *J. Phys.: Condens. Matter.*, 1, (1989), 1941-1963.
195. Holzapfel W. B., *High Pressure Research*, 16, (1998), 81-126.
196. Stacey F. D., *Geophys. J. Int.* , 143, (2000), 621-628.
197. Birch F., *J. Geophys. Res.*, 83, (1978), 1257-1268.
198. Brazhkin V. V., Lyapin A. G., Popova S. V., Klyuev Y. A., Naletov A. M., *J. Appl. Phys.* , 84, (1998), 219-226.
199. Szymanski A., Szymanski J. M., "*Hadness estimation of minerals, rocks and ceramic materials*" 1989, Elsevier, Amsterdam.
200. Riedel R. (ed), "*Handbook of Ceramic Hard Materials*" 2000, WILEY-VCH, Weinheim.
201. McColm I.J., "*Ceramic Hardness*" 1990, Plenum Press, New York.
202. Oliver W. C., Pharr G. M., *J. Mater. Res.* , 7, (1992), 1564-1583.
203. Fischer-Cripps A. C., "*Introduction to Contact Mechanics*" 2000, Springer, New-York.
204. Zvoriste C., Dubrovinsky L., Hering S. A., Huppertz H., Riedel R., Kinski I., *High Pressure Research*, 29, (2009), 389-395.
205. Hering S. A., Zvoriste C. E., Riedel R., Kinski I., Huppertz H., *Z. Naturforsch.* , 64b, (2009), 1115-1126.
206. Huppertz H., Hering S. A., Zvoriste C. E., Lauterbach S., Oeckler O., Riedel R., Kinski I., *Chem. Mater.*, 21, (2009), 2101-2107.
207. Kroll P., *J. Solid State Chem.* , 176, (2003), 530-537.
208. Deb S. K., Dong J., Huppertz H., McMillan P. F., Sankey O. F., *Solid State Commun.*, 114, (2000), 137-142.
209. McCaulley J.W., Patel P., Chen M., Glide G., Strassburger E., Paliwal B., Dandekar D. P., *J. Europ. Ceram. Soc.*, 29, (2009), 223-236.
210. Kroll P., *Personal Communication*.
211. Gurlo A., Personal communication.
212. Schiferl D., Cromer T., Ryan R. R., Larson A. C., Lesar R., Mills R. L., *Acta Cryst.*, C39, (1983), 1151-1153.
213. Rogriguez-Carvajal J., *Physica B*, 192, (1993), 55-69.
214. Rodriguez-Carvajal J., "*Short reference guide of the FullProf. prog.*" 2001, Laboratory Leon Brillouin (CEA-CNRS), Saclay.
215. Sheldrick G. M., *Shelxs-97 and Shelxl-97, Program suite for the solution and refinement of crystal structures* (1997), University of Göttingen, Göttingen, Germany.
216. Sheldrick G. M., *Acta Crystallogr.* , 64, (2008), 112-122.
217. O'Neill H. ST. C., Navrotsky A., *Am. Mineral.* , 68, (1983), 181-194.
218. McCaulley J.W., *J. Am. Ceram. Soc.*, 61, (1978), 372-373.
219. Adams I., AuCoin T. R., Wolff G. A., *J. Electrochem. Soc.* , 109, (1962), 1050-1054.

220. Lejus A. M., *Rev. Hautes Temp. Refract.* , 1, (1964), 53-95.
221. Fang C. M., Metselaar R., Hintzen H. T., Gijbertus de With, *J. Am. Ceram. Soc.*, 84, (2001), 2633-37.
222. Tabary P., Servant C., *J. Appl. Cryst.* , 32, (1999), 241-252.
223. Takano M., Onodera A., *Solid State & Mater. Sci.* , 2, (1997), 166-173.
224. Badding J. V., Meng J. F., Polvani D. A., *Chem. Mater.*, 10, (1998), 2889-2894.
225. Otto J. W., Vassilliou J. K., Frommeyer G., , *J. Synchrotron Rad.* , 4, (1997), 155-162.
226. Zerr A., Kempf M., Schwarz M., Kroke E., Riedel R., *J. Am. Ceram. Soc.* , 85, (2002), 86-90.
227. Lowther J. E., Schwarz M., Kroke E., Riedel R., *J. Solid State Chem.* , 176, (2003), 549-555.
228. Teter D.M., *MRS Bull.*, 23, (1998), 22-27.
229. Drory M.D., Ager J.W., Suski T., Grzegory I., Porowski S., *Appl. Phys. Lett.* , 69, (2009), 4044-4046.
230. Jiang J. Z., Lindelov H., Gerward L., Stahl K., Recio J. M., Mori-Sanchez P., Carlson S., Mezouar M., Dooryhee E., Fitch A., Frost D.J., *Phys. Rev. B*, 65, (2002), 161202-1-4.
231. Hintzen H. T., Hendrix M. R. M. M., Wondergem H., Fang C. M., Sekine T., With G., *J. Alloys Compd.* , 351, (2003), 40-42.
232. Gross T., Schwarz M., Knapp M., Kroke E., Fuess H., *J. Eur. Ceram. Soc.* , 27, (2007), 2163-2169.
233. Dzivenko D. A., *High-pressure synthesis, structure and properties of cubic zirconium(IV)- and hafnium(IV) nitrides*, (2008), PhD thesis (Technischen Universität Darmstadt).
234. Elliott S., "*The Physics and Chemistry of Solids*" 1998, John Wiley and Sons.
235. Kittel C., "*Introduction to solid state physics*" 6th ed1986, J. Wiley & Sons, New York.
236. Reeber R. R., Wang K., *J. Mater. Res.* , 15, (2000), 40-44.
237. Dohoy D., Gavarri J. R., *J. Solid State Chem.* , 49, (1983), 107-117.
238. Tran F., Blaha P., *Phys. Rev. Lett.* , 102, (2009), 226401-1-4.
239. Tippis H. H., *Phys. Rev. B*, 140, (1965), A316-A319.

Eidesstattliche Erklärung

Hiermit erkläre ich an Eides statt, dass ich die vorliegende Dissertation selbständig und nur mit den angegebenen Hilfsmiteln angefertigt habe. Von mir wurde weder an der Technischen Universität Darmstadt noch einer anderen Hochschule ein Promotionsversuch unternommen.

Darmstadt, 2011

Carmen Zvoriste

Curriculum Vitae

PERSONAL DATA:

Name: Carmen Zvoriste

Nationality: Romanian

Date and place of birth: 24.05.1980, Iasi, Romania

EDUCATION:

2011-present: Research assistant at Institute for Transuranium Elements, Karlsruhe, Germany.

2007-2010: PhD in Materials Science, Technical University of Darmstadt, Darmstadt, Germany.

2005-2006: Masters Degree in "Inorganic Chemistry of Nanosystems in Biology", University Paris XI, Orsay, France.

2004-2006: Masters Degree "The Dynamics and Analysis of Chemical Systems", University "Al.I.Cuza", Iasi, Romania.

2000-2004: Graduated: Faculty of Chemistry, Department "Chemistry-Physics", University "Al.I.Cuza", Iasi, Romania

List of publications:

1) Huppertz H., Hering S. A., Zvorişte C. E., Lauterbach S., Oeckler O., Riedel R., Kinski I., „*High-Pressure Synthesis, Electron Energy-Loss Spectroscopy Investigations, and Single Crystal Structure Determination of a Spinel-Type*

Gallium Oxonitride $Ga_{2.79}\square_{0.21}(O_{3.05}N_{0.76}\square_{0.19})$“, Chem. Mater., 21, (2009), 2101-2107.

2) Zvorişte C., Dubrovinsky L., Hering S. A., Huppertz H., Riedel R., Kinski I., „*Diamond Anvil Cell Synthesis and Compressibility Studies of the Spinel-Structured Gallium Oxonitride*“, High Pressure Research, 29, (2009), 389-395.
3) Hering S. A., Zvorişte C. E., Riedel R., Kinski I., Huppertz H., „*A Systematic Investigation of the Stability Field of Spinel-Type Gallium Oxonitrides*“, Z. Naturforsch. , 64b, (2009), 1115-1126.
4) Boyko T.D., Zvorişte C.E., Moewes A., Hering S.A., Huppertz H., Riedel R., Kinski I., „*Experimental and Theoretical Determination of the Band Gap and Structure of Spinel-Type Gallium Oxonitride*“, in preparation.